A STUDY OF RELATIVE K X-RAY INTENSITIES AND OF HIGH Z K-FLUORESCENCE YIELDS

A THESIS

Presented to

The Faculty of the Division of Graduate Studies and Research

by

John Steven Hansen

In Partial Fulfillment

of the Requirements for the Degree

Doctor of Philosophy

in the School of Nuclear Engineering

Georgia Institute of Technology

March, 1971

In presenting the dissertation as a partial fulfillment of the requirements for an advanced degree from the Georgia Institute of Technology, I agree that the Library of the Institute shall make it available for inspection and circulation in accordance with its regulations governing materials of this type. I agree that permission to copy from, or to publish from, this dissertation may be granted by the professor under whose direction it was written, or, in his absence, by the Dean of the Graduate Division when such copying or publication is solely for scholarly purposes and does not involve potential financial gain. It is understood that any copying from, or publication of, this dissertation which involves potential financial gain will not be allowed without written permission.

[redacted]

7/25/66 [redacted]

A STUDY OF RELATIVE K X-RAY INTENSITIES AND OF HIGH Z K-FLUORESCENCE YIELDS

Approved: [redacted]

Date approved by Chairman: March 12, 1971

To My Parents

So I triumphed ere my passion sweeping
    through me left me dry,
Left me with the palsied heart, and left
    me with the jaundiced eye;

Eye, to which all order festers, all
    things here are out of joint;
Science moves, but slowly, slowly, creeping
    on from point to point;

from "Locksley Hall"
by Alfred, Lord Tennyson
(1842)

ACKNOWLEDGMENTS

It is a pleasure to recognize the many persons whose support made this research possible.

I wish to express my sincere appreciation to my thesis advisor, Professor R. W. Fink, who suggested the research project and repeatedly served as a source of guidance, motivation and inspiration. Professors D. S. Harmer and G. G. Eichholz, who served on the reading committee, provided valuable suggestions in their review of the manuscript. To Professor Eichholz a special thanks is extended for the continued encouragement and interest shown throughout the course of this study.

Dr. H. U. Freund provided invaluable advice and assistance in the preliminary stages of this work, for which I am most appreciative. A large amount of credit is due Dr. J. C. McGeorge, who not only served as technical advisor in a postdoctoral capacity but also as friend and co-worker. Many of the ideas in this work evolved from our discussions and collaborative laboratory work. Dr. W. D. Schmidt-Ott, who, to my misfortune, arrived only in the latter stages of this work, has nevertheless aided in several technical aspects. Both Dr. Schmidt-Ott and Dr. McGeorge carefully reviewed this manuscript and supplied helpful suggestions.

Professors P. Venugopala Rao, R. E. Wood and J. M. Palms of Emory University kindly permitted the use of their electron detection system, for which I am most grateful. Professor Wood and Mr. H. O. Puckett, also of Emory, went out of their way to provide special assistance and instruction in the use of this equipment.

Professor D. J. Kennedy of Georgia Tech and Professor S. T. Manson of Georgia State University provided valuable theoretical calculations prior to publication. In addition, their advice on particularly elusive theoretical aspects was especially useful and very much appreciated. Dr. Manson, along with Professors R. F. Borkman and R. H. Felton were kind enough to review an early draft of this thesis.

Mr. D. N. Nix provided helpful aid in radioactive source preparation and Mr. F. Tolea furnished an urgently needed Russian translation. Mr. J. M. Burke of the reactor shop was always willing and able to provide assistance.

This research project was supported by AEC Contract AT(40-1)-3346. Personal financial support was provided by a U. S. Public Health Service Fellowship, a U. S. Atomic Energy Commission Traineeship, and a Georgia Tech Research Assistantship.

The one person who should be most easily acknowledged is at the same time most difficult, since this dissertation

from beginning to end has been as much a part of her as of me. Her dedication, pride, interest and faith have led her to suffer the same joys and agonies as myself; to my wife, Cora, I extend my warmest and unbounded thanks and praise.

Finally, to my parents, who instilled in me the strength and spirit to persist and overcome, I express my deepest appreciation and fondest memory.

TABLE OF CONTENTS

TABLE OF CONTENTS (Concluded)

LIST OF TABLES

LIST OF ILLUSTRATIONS

LIST OF ILLUSTRATIONS (Concluded)

SUMMARY

This research project involves an experimental study of the relative K x-ray intensities and of high Z K-fluorescence yields. The present study of the atomic transition rates is important because:

(1) The relative simplicity of the K x-ray spectra permits more accurate interpretation of experimental results than is, in general, possible for higher shells.

(2) The experimental results may be compared to recent refined theoretical predictions.

(3) Preliminary investigation showed that older experimental results were in disagreement with the theoretical predictions and the source of these discrepancies could be investigated by new and more accurate experimental techniques.

The study of the K x-ray intensity ratios includes measurements of the K_β/K_α intensity ratios over an extended range in atomic number, $17 \leq Z \leq 96$. Results of measurements for the $K_{\alpha_2}/K_{\alpha_1}$, $K'_{\beta_1}/K_{\alpha_1}$, $K'_{\beta_2}/K_{\alpha_1}$ ratios at $Z = 81$, 82 and 96 are also given.

Comparison of the above measured ratios to corresponding theoretical predictions allowed the following major conclusions to be drawn:

(1) The most refined present-day theoretical predictions employing wave functions as given by the relativistic Hartree-Fock-Slater model and also relativistic wave functions of the "Burns" screened hydrogenic type are in excellent agreement but show systematic differences with the experimental findings.

(2) The above discrepancies suggest, in a general sense, that the theoretical screening of M and higher shells is overestimated.

(3) The discrepancies between the theoretical predictions and experimental findings at low Z are probably related to chemical bonding effects and ionization of the 3p electrons.

(4) The general agreement between the two above theoretical approaches over essentially the entire range of Z may imply that the Slater exchange approximation introduces very little error into the Hartree-Fock-Slater calculations of atomic transition rates.

(5) The effects of relativity on the K_β/K_α intensity ratios are generally small, suggesting that further theoretical studies can be carried out in the electric dipole approximation using nonrelativistic wave functions.

This experimental study of the relative K x-ray intensity ratios involved the use of semiconductor radiation detectors selected for their generally good resolution and

and high efficiency in the K x-ray region, i.e. $E \lesssim 150$ keV. A comprehensive study of the efficiencies of Ge(Li) and Si(Li) detectors in the K x-ray energy region was necessary in order to eliminate systematic error in the evaluation of the experimental results. The findings of this study are presented in terms of a semi-empirical model of detection efficiency. In general, it can be stated that quite large errors (10% - 20%) in the efficiencies of semiconductor detectors may arise from cursory experimental estimates of these efficiencies in the K x-ray energy region.

Measurements of the K-fluorescence yields (ω_K) in the present work give $\omega_K(Z=78) = 0.967 \pm 0.008$ and $\omega_K(Z=82) = 0.972 \pm 0.008$. These results are found to be in reasonable agreement with relativistic Hartree-Fock-Slater predictions and with the most reliable semi-empirical predictions. The present results are not in agreement with older measurements of ω_K at $Z = 80$.

CHAPTER I

INTRODUCTION

When an atom is ionized in an inner shell, it may deexcite either by emission of an x ray or by the ejection of an outer-shell electron. The latter is known as the Auger effect (Auger[1], 1925).

These two modes of deexcitation have in recent years been a topic of great interest, primarily for two reasons: (1) the advent of high-speed computers permits sophisticated numerical approaches to theoretical problems of atomic transition rates that were formerly prohibitive, and (2) experimental techniques, with advanced electronics and detection devices, can now provide a sensitive test of the range and validity of the theoretical approximations. The present experimental study with high-resolution, semiconductor detectors represents an effort to test the validity of theoretical predictions of atomic transition probabilities involving the K shell.

In the present work, measurement of the relative intensities of the K_α and K_β x-ray groups was made over an extended range in atomic number ($17 \leq Z \leq 96$). In addition, at high Z ($Z \geq 81$), the energy separation of the L_2 and L_3

subshells and the M and N shells is sufficient to determine the relative transition probabilities of the K_{α_1}, K_{α_2}, K'_{β_1}, and K'_{β_2} x rays. The nonradiative width has been deduced at Z = 78 and 82 from K-fluorescence yield measurements. Recent and current theoretical studies[2,3,4,5] of atomic transition rates make the experimental work timely and significant.

1.1. Historical Background

Just seventy-five years ago the first x rays were observed by Röntgen[6] (1895), who used a simple electron bombardment technique and a fluorescent screen. Because of the unknown character of these penetrating radiations, they became known as "x rays". Further studies of the properties of x rays by Haga and Wind[7] (1899) and C. G. Barkla[8] (1908) showed that the radiation was of the same nature as visible light, except that its wave length was several orders of magnitude shorter.

The first systematic studies of characteristic x-ray energies, carried out by Moseley[9] (1913) and interpreted on the basis the the Bohr[10] (1913) theory of the atom, confirmed that the characteristic x rays arise from within the atom. Although x-ray energies could be calculated by the empirical rules set forth by Moseley[9], a consistent theoretical framework, in which the transition rates of x-ray lines could be predicted, was not available until the development of

quantum mechanics by Heisenberg[11] (1925), Schrödinger[12] (1926) and Dirac[13] (1926).

Early experimental studies by Meyer[14] (1929) with photographic plates and Williams[15] (1933) with ionization chambers stimulated theoretical calculation of the relative K x-ray rates. A later more extensive investigation of the relative K x-ray line intensities was made by Beckman[16] (1955) with a transmission-type, curved crystal spectrometer.

In cloud chamber measurements of the track-length of photoelectrons resulting from x-ray bombardment of noble gases, Auger[1] (1925) observed a curious phenomenon. In addition to the photoelectron track of length dependent upon the impinging x-ray energy, a second track of length independent of the energy of the bombarding x rays was observed from some of the ionized atoms. This mode of deexcitation, involving the ejection of an atomic electron rather than the emission of an electromagnetic quantum was described by Auger[1] as a radiationless transition. Because of the conclusive nature of his findings, this deexcitation process is known as the Auger effect. That the radiationless transfer of ionization energy can occur between atomic subshells within a major shell was confirmed experimentally by Coster and Kronig[17] (1935) in a study of satellite lines in x-ray emission spectra. Early theoretical attempts

to calculate[18,19] the Auger transition rates could not be adequately tested, because of the limited number of transitions calculated and the experimental difficulties associated with high-resolution spectroscopy of low-energy electrons. A review of early experimental and theoretical attempts to study the Auger effect and other radiationless transitions has been given by Burhop[20] (1952).

The application of beta spectrometers, curved crystal spectrometers and semiconductor detectors to high-resolution studies of Auger-electron and x-ray spectra has provided impetus for a more detailed investigation of the processes involved in atomic deexcitation. A summary of the more recent studies related to atomic inner shell deexcitations is given below.

1.2. Recent Studies of Atomic Inner Shell Processes

In the past few years many experimental measurements of the relative K x-ray intensities have been made[21-28]. Comparison of these findings with the most refined theoretical calculations[2,3,29,30] have disclosed discrepancies, particularly at low and high z, with each of the theoretical predictions. The nature and magnitude of these discrepancies is considered in Chapters V and VI. The 1969 experimental measurements by Nelson, John and Saunders[31] of the natural line width of the K_{α_1} and K_{α_2} x-ray transitions provide evidence that theoretical predictions of the total

radiative widths of the K shell agree with the measured widths within experimental uncertainty.

Relative Auger electron intensities for the K-LL group have been measured in the range of Z = 9 to Z = 94. Relative intensities of lines within the K-LM Auger group have been determined in isolated experimental studies from Z = 47 to Z = 83, but no attempts to determine the relative intensities of the lines comprising the K-XY group have been published. A summary of the above experimental results is given by Ramsdale; in addition, he has calculated theoretical absolute and relative intensities of lines comprising the K-LL and K-LX groups predicted by the relativistic Hartree-Fock-Slater model.

Fink, et al.[32] and Bambynek, et al.[33] have given comprehensive reviews of the measurements and theoretical calculations of K, L, and M fluorescence yields and Coster-Kronig transition probabilities. The relationship of the K-fluorescence yield to the radiative and nonradiative K-shell width is discussed in Chapter II.

1.3. Brief Outline of the Atomic Deexcitation Process

A vacancy in the K shell may be created in many ways, e.g. by the photoelectric effect, electron capture, charged-particle bombardment, or internal conversion. Within 10^{-17} to 10^{-14} seconds, the vacancy is filled by an outer shell electron and the excess energy is carried off by one of two

processes: K x-ray emission or K-Auger electron emission.

Radiative (K x-ray) deexcitation results from the filling of a K vacancy by an outer-shell electron with the emission of a photon of energy equal to the difference in the binding energies of the K shell and the subshell to which the vacancy is transferred. The spectroscopic notation used in describing x-ray transitions is due to M. Siegbahn[34] and is described in Fig. 1 for the K shell. The individual lines (transitions) arranged in the order of decreasing intensity are as follows: K_{α_1}, K_{α_2}, K_{β_1}, K_{β_3}, K_{β_2}, K_{β_5}, and K_{β_4}. Because of the limited resolution of semiconductor detectors, separate lines can not be resolved at low Z and are grouped accordingly into the resolved K_α and K_β x-ray groups. At high Z, where the separation of the L_2 and L_3 subshells is greater than 1 keV and that of the M and N shells even larger, the K_{α_1}, K_{α_2}, K'_{β_1} and K'_{β_2} x-ray groups can be resolved by Si(Li) and Ge(Li) cooled semiconductor x-ray detectors. Typical K x-ray spectra at low, medium and high Z are shown in Fig. 2.

The alternate means of K-shell deexcitation, the Auger effect, involves the ejection of an outer-shell electron. The ejected Auger electrons are classified according to the initial and final vacancy distribution, $K\text{-}X_pY_q$, where the original vacancy is viewed as being shifted to the X_p shell with the Y_q electron being ejected.

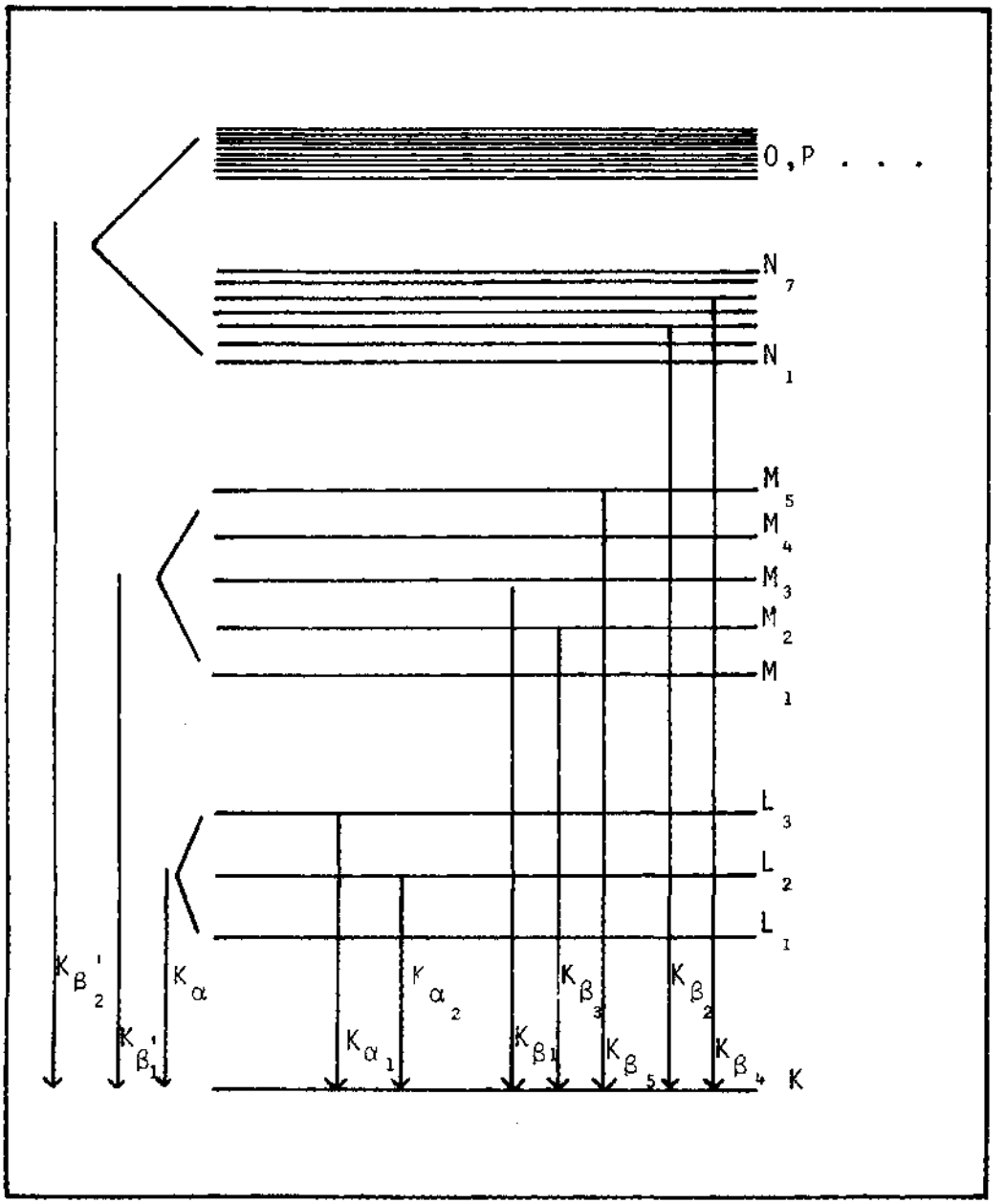

Fig. 1. Siegbahn Notation For The K Shell (K_{β_2}, K_{β_4} and K_{β_5} refer to $K\text{-}N_{2,3}$, $K\text{-}N_{4,5}$, and $K\text{-}M_{4,5}$, respectively.)

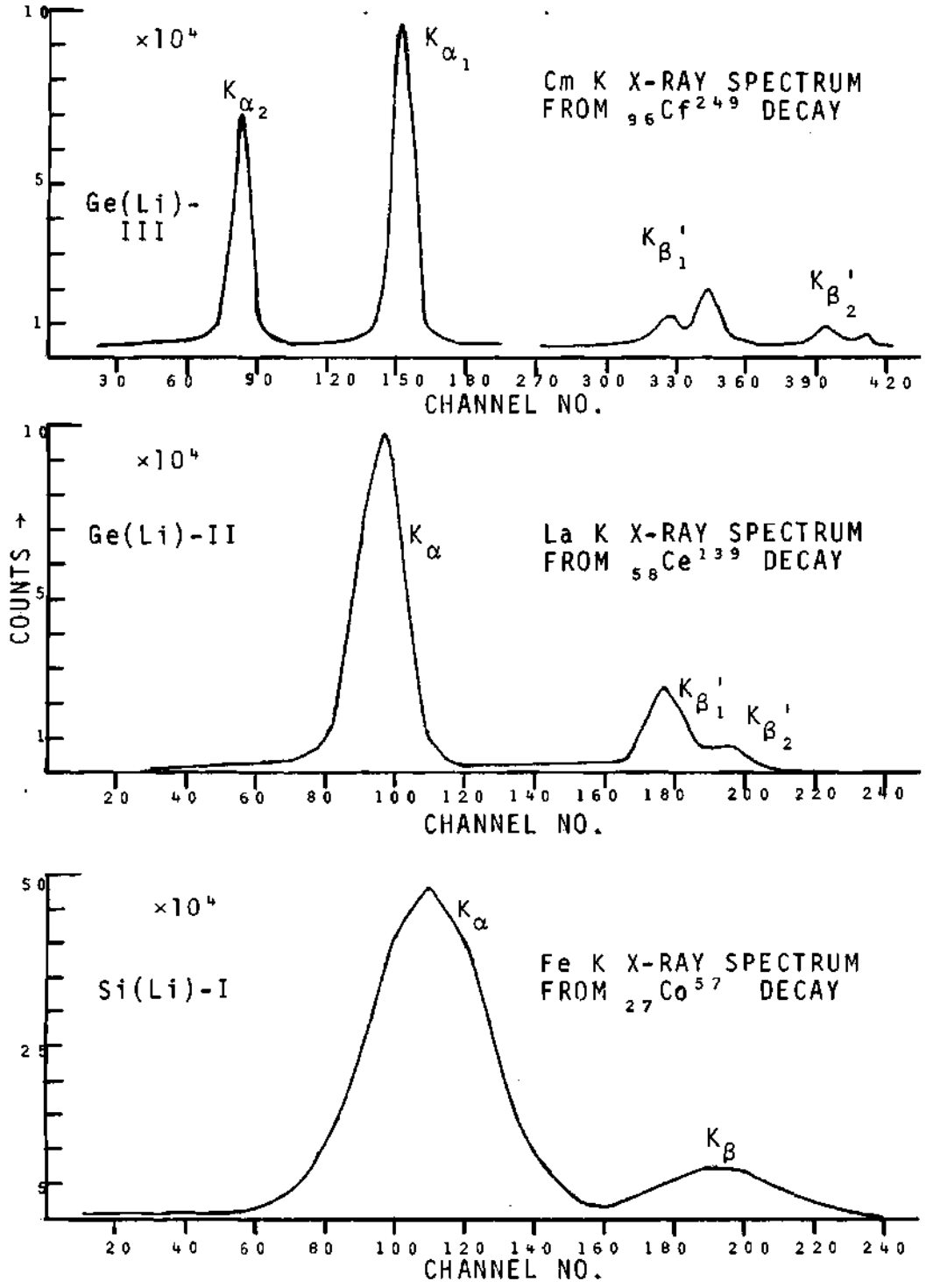

Fig. 2. Typical K X-ray Spectra With Cooled Semiconductor Detectors. (Large Peak/Continuum results from use of carrier-free radioactive sources.)

Energetically, the transitions K-X_pY_q and K-Y_qX_p are indistinguishable, thus associated with each Auger electron energy is a given pair of equivalent transitions, e.g. K-L_1L_2, K-L_2L_1. The K-Auger spectra is divided energetically into three major groups, K-LL, K-LX and K-XY, where X and Y refer exclusively to M and higher shells. The K-LL group is composed of six lines in the jj-coupling scheme which is predominant at high Z: K-L_1L_1, K-L_1L_2, K-L_1L_3, K-L_2L_2, K-L_2L_3, K-L_3L_3. The minor perturbation on the energy levels introduced by L-S coupling splits the K-LL spectra into nine lines in the medium to high Z region and is observed only with the highest resolution beta-spectrometers[35,36].

The energy of the emitted electron is not only dependent on the initial and final vacancy distributions, but also is to a lesser extent affected by the rapidly changing Coulomb field resulting from the introduction of vacancies into the atomic structure. To a close approximation, the energy of the emitted K-Auger electron is therefore

$$E(\text{Auger}) = E_K - E_{X_p} - E_{Y_q} \qquad (1\text{-}1)$$

where the binding energies E_K, E_{X_p} and E_{Y_q} are those of the neutral atom. The approximation yields K-LL Auger energies that are slightly higher[4] (≈0.5% at Z = 30) than observed experimentally.

The subsequent rearrangement processes which result from shifting the original K vacancy to higher subshells are further complicated by the presence of radiative and nonradiative processes between subshells of the same principal quantum number. Such Coster-Kronig[17] events are discussed in detail by Fink, et al[32] and Karttunen[37].

1.4. Motivation and Objectives

The general area of atomic transition probabilities envelopes many different fields of endeavor which include studies of optical transition probabilities, relative and absolute Auger transition probabilities, and relative and absolute inner-shell radiative transition probabilities.

The present work is confined to the K shell for several important reasons:

(1) The relative simplicity of the K x-ray spectra permits interpretation of experimental results often difficult or impossible in higher shells owing to poorly defined vacancy distributions within the atomic subshells.

(2) Since each K shell transition involves the wave functions of less energetic levels, the interpretation of K spectra does not limit itself to one particular shell or level.

(3) Certain effects, such as relativity and finite nuclear size, are more important in the K shell than in any of the higher shells.

(4) The experimental results may be compared to theory. This is in contrast to studies of transition probabilities and fluorescence yields for higher levels where complete theoretical studies of the transition probabilities and fluorescence yields are not yet available.

(5) Semiconductor detectors are particularly suited for the study of K x rays over a wide range of atomic number whereas experimentally, one is limited in L- and higher-shell spectra to studies at middle and very high Z.

(6) Preliminary investigations revealed that older experimental results[14,15,16] were not in agreement with the most recent theoretical calculations[2,3] and the cause of the discrepancies was not known.

The objective of this work was to study the relative K-shell x-ray intensities and high Z K-shell fluorescence yields in order to determine the limitations of the most refined theoretical studies now available. In order to reveal the inherent accuracies of these predictions, comparisons of the experimental results were made with theoretical predictions of a less sophisticated nature. Moreover, through a comparison of the experimental findings and the theoretical predictions, particular regions of theoretical inadequacy may be pointed out, suggesting limitations in the approximations involved in the theoretical studies.

1.5. Applications of This Study

The study of relative K x-ray intensities and K-fluorescence yields finds major applications in the area of x-ray fluorescence analysis where the identification of individual elements may be made nondestructively by analysis of the x-ray emission spectra. The most intense group in the K x-ray emission spectrum is K_α; thus only by knowledge of the fractional contribution of K_α to the total K x-ray emission spectrum can one determine accurately low-intensity emission lines or interpret complex spectral groups. In recent years compact x-ray fluorescence spectrometers have been developed for geological exploration, designed for field use. Rock samples from the surface of the moon have also been analysed using an electron microprobe to produce fluorescence x rays[38].

For the accurate determination of buildup factors in thick radiation shields, one must have knowledge of the fluorescence yields and relative K x-ray intensities. The dose rate in a medium after many mean free paths of the incident radiation is particularly dependent on the energy deposition of secondary fluorescence radiation.

The study of the detection characteristics of semiconductor detectors (Chapter III) is directly applicable to other similar detection apparatus. In studies involving the determination of intensities of gamma or x rays in the

region below 100 keV, knowledge of the detection efficiency is essential.

CHAPTER II

THEORETICAL BACKGROUND

The two competing processes in atomic deexcitation, x-ray and Auger electron emission, result from basically different interactions, as described below (Secs. 2.1 and 2.2). Since each process can be studied theoretically and experimentally independent of the other, each is normally approached, particularly in a theoretical sense, exclusive of the other. Experimental and theoretical studies of the K-fluorescence yield and the width (energy) of the K level are exceptions to this statement and involve a combination of results of both studies; for this reason it is pertinent to the present experimental determination of ω_K at high Z to investigate the interrelationship of the two processes.

The following formula (Eqn. 2-1), in a general sense, predicts the time rate of decay of an atomic state, including the decay rates associated with the Auger effect and K x-ray emission, and thus serves as a beginning for a discussion of the transition probabilities involving the K shell. The transition probability per unit time from an initial state i to a final state f is given by a formula from

time-dependent perturbation theory (Fermi's Golden Rule[39]):

$$\Gamma_{fi} = \frac{2\pi}{\hbar}|\langle f|H'|i\rangle|^2 \rho(E_f) \qquad (2\text{-}1)$$

where $\langle f|H'|i\rangle$ is the matrix element of the interaction Hamiltonian H' and $\rho(E_f)$ is the density of the final states at an energy E_f, satisfying conservation of energy. The matrix element $\langle f|H'|i\rangle$ is defined as

$$\langle f|H'|i\rangle \equiv \int_\tau \psi_f^* H' \psi_i \, d\tau \qquad (2\text{-}2)$$

where ψ_i is the initial state wave function and ψ_f^* is the complex conjugate of the final state wave function and the integration is carried out over all spatial coordinates τ. The total transition probability per unit time Γ is found by summing Eqn. 2-1 over all final states.

It has been shown[40] that the total probability distribution (time-independent) as a function of energy, has a maximum at an energy of exactly the difference in energies $E_i - E_f$, i.e. the most probable energy of the emitted particle is $E_i - E_f$. The probability is decreased by a factor of two when the emitted particle differs from $E_i - E_f$ by an amount $(\frac{1}{2}\hbar\Gamma)$, hence, one commonly speaks in terms of the width, ΔE, of an excited state expressed by:

$$\Delta E = \hbar \Gamma \qquad (2\text{-}3)$$

A vacancy in the K shell of an atom is representative of an excited atomic state for which two separate modes of deexcitation are available; therefore:

$$\Gamma_K = \Gamma_{KR} + \Gamma_{KN} \qquad (2\text{-}4)$$

where Γ_{KR} and Γ_{KN} are defined as the K-shell radiative and nonradiative transition probability (decay) rates, respectively, and Γ_K is the total decay rate for the excited state, as represented by a K-shell vacancy. The radiative decay rate, Γ_{KR}, has components Γ^i_{KR} which are the decay rates for individual K x-ray transitions, e.g. K_{α_2}, K_{β_1}, etc; similarly, Γ_{KN} has components Γ^i_{KN} which are the decay rates for individual K-Auger electron transitions, e. g. $K\text{-}L_1L_2$, $K\text{-}L_2L_3$, etc. Radiative and nonradiative decay rates, Γ^i_{KR} and Γ^i_{KN}, respectively, are sensitive to the detailed nature of the atomic wave functions; thus experimental and theoretical studies of the ratios of the radiative components, Γ^i_{KR}, and of the nonradiative components, Γ^i_{KN}, may lead to useful information concerning the nature of the potential in which the transitions occur.

The transition probability rates Γ_{KR} and Γ_{KN} are related through the experimentally measurable K-fluorescence

yield which is defined as[41]

$$\omega_K \equiv \frac{\Gamma_{KR}}{\Gamma_{KR} + \Gamma_{KN}} = \frac{\Gamma_{KR}}{\Gamma_K} \qquad (2\text{-}5)$$

Thus, ω_K represents the probability of decay by K x-ray emission for a single atom with a vacancy in the K shell or for a large number of atoms of the same type with single vacancies in the K shell it represents the fraction of these atoms which decay by K x-ray emission.

The decay of a vacancy in the K shell leads to an energy spread or width of the state from the uncertainty principle. The total K-shell width, $\Gamma_K \hbar$ at Z = 50 is[2] of the order of 10 eV ($\Gamma_K = 1.5\times10^{16}\text{sec}^{-1}$) and increases to 90 eV at Z ≈ 90. This uncertainty in energy manifests itself as a broadening of emitted K x-ray and K-Auger lines. High-resolution (0.15%) measurements[31] of the natural line width of K_{α_1} and K_{α_2} x rays have been made, from which the total K-shell width is deduced. As is apparent from Eqn. 2-5, the primary source of line broadening for large values of ω_K, which occur at high Z, is the uncertainty in the radiative component Γ_{KR}; conversely, for small values of ω_K which occur at low Z, the primary source of line broadening is in the uncertainty in the nonradiative component Γ_{KN}.

In the following sections dealing with the radiative (Sec. 2.1) and nonradiative (Sec. 2.2) processes, a brief description is given of the nature of the respective processes, followed by a review of the more significant theoretical work. Section 2.3 involves a discussion of the theoretical calculations of K-fluorescence yields based on the above processes. The final section summarizes the present theoretical status in the area of atomic transition rates.

2.1. Radiative Transition Probabilities

A detailed treatment involving the theory of quantum electrodynamics is required to derive relativistic expressions for the radiative transition probability used in the most sophisticated of present-day calculations. Derivations of the relativistic interaction Hamiltonian, H' in Eqn. 2-1, have been given[42,43]. The form of the Dirac type electronic wave functions employed in relativistic calculations of the radiative transition probabilities are described in several treatises on the subject[44,45,46].

The nonrelativistic expression for the probability of a radiative transition to a K shell vacancy can be expanded in multipoles; the leading terms are[47]:

$$\Gamma_{KR} = \sum_{f} \frac{16\pi^2 \nu_{if}^3}{3c^3\hbar} \left[|\langle f|e\underset{\sim}{r}|i\rangle|^2 + |\langle f|\frac{e}{2mc}\,\underset{\sim}{r}\times\underset{\sim}{p}|i\rangle|^2 + \frac{3}{10}\pi^3 \frac{\nu_{if}^2}{c^2} |\langle f|e\underset{\sim}{\underset{\sim}{r}}\underset{\sim}{r}|i\rangle|^2 \right] \tag{2-6}$$

The terms between the brackets relate to transitions arising from electric dipole, magnetic dipole and electric quadrupole interactions, respectively. The quantity ν_{if} is the frequency of the emitted radiation; e, the electronic charge; $\hbar$, Planck's constant divided by 2π; and c, the speed of light. The quantities $\underset{\sim}{r}$ and $\underset{\sim}{p}$ are the position and momentum vectors of the electron involved in the transition. Contributions from higher-order multipole radiations, e.g. E3, M2, etc., neglected in this expression, are less than 1 percent[2]. In the long wave-length approximation, i. e. assuming the wave length of the emitted radiation is much greater than characteristic atomic dimensions (optical region), it can be shown[48] that the contributions from the second and third terms (M1 and E2) in Eqn. 2-6 are $\simeq 10^{-5}$ times that arising from the electric dipole interaction. Even for K x-ray energies of the order of 100 keV ($Z \simeq 92$), the electric dipole contribution to the total K x-ray emission rate is approximately 99 percent and increases to approximately 99.9 percent at $Z = 50$.

The predominant contribution of electric dipole transitions in x-ray spectra has led to the well-known allowed (E1) selection rules[49]

$$\Delta\ell = 1 \qquad \Delta j = 0, \pm 1 \qquad \text{for electric dipole radiation} \tag{2-8}$$

where $\Delta\ell = |\ell_i - \ell_f|$ and $\Delta j = |j_i - j_f|$; where ℓ_i and ℓ_f are the orbital angular momentum quantum numbers of the initial and final states, respectively; and j_i and j_f are the initial and final total angular momentum quantum numbers of the initial and final states.

Electromagnetic radiation is normally classified by multipole orders L according to the angular momentum L (in units of h) carried off by each quantum. For each multipole order there are two possible classes of radiation: electric 2^L pole (EL) and magnetic 2^L pole (ML) which differ with respect to parity. The conservation of angular momentum and parity for the system of atom plus x rays imposes general selection rules[50] on the possible multipolarities of an x-ray transition between two states of specified angular momentum (j_i, j_f) and parities (π_i, π_f):

$$|j_i - j_f| \leq L \leq j_i + j_f \qquad \Delta\pi = (-1)^L \text{ for EL radiation} \tag{2-9}$$

$$\Delta\pi = (-1)^{L-1} \text{ for ML radiation} \tag{2-10}$$

where $\Delta\pi = +1$ denotes no parity change and $\Delta\pi = -1$ denotes parity change.

It is seen that the above rules restrict the emission of radiation resulting from a radiative filling of the K shell ($1s_{\frac{1}{2}}$) to a maximum of two orders of multipole radiation, i.e. $j_f + \frac{1}{2}$ and $j_f - \frac{1}{2}$, where j_f represents the total angular momentum quantum number of the final state vacancy. These rules are most general and suggest that the emission of magnetic dipole radiation (M1) between the $2s_{\frac{1}{2}}$ and $1s_{\frac{1}{2}}$ states is possible, in direct contrast to the nonrelativistic prediction which prohibits the emission of electromagnetic radiation of any form between L_1 (2s) and K (1s) shells. Theoretical predictions of the intensity of the ("K_{α_3}") radiation have been made[2,3,51] in addition to experimental observations[16].

The emission of electric dipole radiation, resulting from the radiative filling of a K vacancy is restricted to a final state with a vacancy in a p subshell. The simplest theories employing unscreened hydrogenic wave functions predict that $\Gamma_{KR} \propto Z^4$. On these grounds, Callan[52] computed radiative K level widths semiempirically using the equation

$$\Gamma_{KR} = Z^4 \sum_n A_n \qquad (2\text{-}11)$$

where A_n are empirical coefficients proportional to the relative intensities of the various dipole radiations associated with the np-1s transitions. The results agree[53] within ±5% with experimental results and compare favorably with more sophisticated calculations[2,3].

Relativistic calculations of K x-ray emission rates have been carried out by Massey and Burhop[54], Laskar[55,56], Payne and Levinger[57], Taylor and Payne[58] and Babushkin[29]. All of the above calculations are based on a Coulomb potential. The latter calculation, by Babushkin, introduced the use of screening parameters[59] derived from Hartree-Fock wave functions and are in good agreement with present-day experimental results for the K x-ray emission rates. The other calculations are less successful in the prediction of the K x-ray emission rates, primarily owing to the approximate fashion in which the effects of atomic screening were accounted for.

Recently, comprehensive treatments of the problem of radiative transition rates have been made by Scofield[2] and by Rosner and Bhalla[3]. Scofield has computed the total radiative decay rates for vacancies in the K and L shells, in addition to a number of x-ray lines for selected atomic numbers between $12 \leq Z \leq 92$. The atomic electrons were assumed to be in single-particle states in a central potential given by the Hartree-Fock-Slater model, as

prescribed by Herman and Skillman[60] and modified by Liebermann, Waber and Cromer[61] to include relativistic effects. All multipoles of the radiation field and all transitions from occupied states were included. The electrons were treated relativistically and the effect of retardation was included.

The calculation by Rosner and Bhalla[3] is very similar to Scofield's; a small effect[62] arising from the finite nuclear size is accounted for and all transitions up to and including the N shell were computed. Total emission rates for ten different atomic numbers between $Z = 21$ and $Z = 93$ were included for the K, L, and M shells. The major x-ray components involved in the radiative filling for the K and L shells were listed[3]. The results of Scofield and of Rosner and Bhalla agree to three significant figures in all cases.

2.2. Nonradiative Transition Probabilities

The first explanation of nonradiative emission of electrons in atomic decay was given by Auger[1], who explained the process as an internal photoelectric effect with characteristic K x rays in the atom. Wentzel[63] showed that in the limit of nonrelativistic theory, a nonradiative transition is caused by the Coulomb interaction of the two electrons participating in the transition. Eqn. 2-1 for the nonradiative transition probability per

unit time, in the nonrelativistic approximation, takes the form[53]

$$\Gamma_{if} = \frac{2\pi}{\hbar}|D - E|^2 \qquad (2\text{-}12)$$

Here $D = \iint \psi_f^*(1)\psi_f^*(2)\ \frac{e^2}{r_{12}}\psi_i(1)\psi_i(2)d\tau_1 d\tau_2$

where $\psi_f^*(1)$ and $\psi_f^*(2)$ are the complex conjugates of the final state electrons 1 and 2, respectively, and $\psi_i(1)$ and $\psi_i(2)$ are the initial state wave functions of the electrons 1 and 2, respectively. The initial states of both electrons and the final state of one electron are described in terms of bound-state wave functions, whereas the wave function of the ejected electron must be described in terms of a continuum (Coulomb)[64] wave function. The exchange element E, found by an interchange of the labels 1 and 2 in the initial state, results from the indistinguishability of certain pairs of transitions, e.g. K-L_1L_3 and K-L_3L_1. A thorough account of the nonrelativistic approach to the Auger effect has been given by Kostroun, Chen and Crasemann[53].

In the relativistic theory, no simple explanation of the Auger effect can be given. The relativistic two-electron interaction is described only by a rigorous quantum electrodynamical treatment of the retarded interaction between the

two electrons. Here the perturbation is caused by the radiation field created by one electron in filling the initial vacancy and acting upon the second electron, ejecting it from the atom[65,4].

Certain selection rules† can be deduced from the nonrelativistic theory by inspection of the nonzero matrix elements. The initial state is given by the two-electron configuration $(n_1\ell_1, n_2\ell_2)$ with quantum numbers L_i, S_i, J_i and parity Π_i. The final state is given by the electron configuration $(n_3\ell_3, E\ell)$ with quantum numbers L_f, S_f and J_f. Here $E\ell$ refers to the ejected electron in the continuum with positive energy E and orbital angular momentum ℓ. The selection rules[65] state

$$\Delta L = \Delta S = \Delta J = 0, \quad \Pi_i = \Pi_f \tag{2-13}$$

i.e. transitions are allowed only if the initial and final states have identical symmetries, L, S, J, and parity Π. Under these selection rules the Auger transition $K\text{-}L_1L_1$ is permitted, whereas the $K\text{-}L_1L_1$ transition would be essentially forbidden if the Auger effect was treated as an internal

†The existence of metastable atomic transitions violate these selection rules but the intensity of such transitions is less than approximately 10^{-6}, the intensity of transitions permitted by the selection rules. [Private communication from S. T. Manson. See, for example, S. T. Manson, Phys Rev. A3, 147 (1971)].

photoelectric process because of the low intensity of the L_1-K ("K_{α_3}") radiative transition (see Sec. 2.1).

The early work by Wentzel[63] contained no quantitative calculations but showed that if screening is neglected, the K-Auger electron transition probabilities are essentially independent of Z. The first quantitative results were provided by Pincherle[18], who used pure nonrelativistic hydrogenic wave functions. The first relativistic calculations were made by Massey and Burhop[66], using Slater[67] screened hydrogenic wave functions. Their study, restricted to only three transitions, indicated that relativistic effects increased the K-L_1L_2 and K-L_1L_3 transition probabilities but decreased the K-L_1L_1 transition probability.

Recent attempts have been made to predict accurately the intensities of the individual K-Auger lines and rather large differences in the predicted K-Auger electron intensities have been found from the various theoretical approaches, as summarized below. These calculations may be roughly divided into categories with regard to the type of potential assumed and as to whether relativistic effects were included. Callan[52] calculated the individual K-LL Auger lines for forty-two Z values from Z = 12 to Z = 80 in the LS (Russell-Saunders[68]) coupling scheme (residual Coulomb interaction large) using nonrelativistic hydrogenic

wave functions with screening constants from Hartree-Fock self-consistent field functions. Callan[52] found rather large departures from the experimentally measured† relative K-Auger electron intensities for $Z < 60$ as a result of the neglect of relativistic effects in the calculation.

Asaad[69] calculated the relativistic K-LL transition probabilities at $Z = 80$ using a Hartree[70] self-consistent field potential. Calculations were made using the jj (strong spin-orbit interaction) scheme. Asaad's results indicate that all of the K-LL transition probabilities are increased as the result of relativistic effects, in contrast to the earlier predictions of Massey and Burhop[66]. The Asaad predictions agree within ±10% with the more rigorous relativistic Hartree-Fock-Slater calculations.

Asaad[71] and Melhorn and Asaad[72] have made nonrelativistic calculations in the intermediate coupling scheme including configuration interaction in an attempt to resolve discrepancies at low atomic numbers between experimental and theoretical K-LL Auger electron intensities. The effects of configuration interaction were seen to decrease the $K\text{-}L_1L_1$ transition probability at low Z, thus reconciling differences between experimental and calculated values of the relative K-Auger electron intensities in the low Z region.

†The experimental results for the K-Auger electron intensities referred to in this section have been taken from the summary given in Ref. 4.

The first calculations using a relativistic, self-consistent Hartree-Fock-Slater potential were made recently by Ramsdale and Bhalla[73,74,75,76] and a general agreement between experiment and the calculated K-Auger electron line intensities was found. In this work, not only were the probabilities of the six lines in the jj-coupled, K-LL Auger spectrum computed for several atomic numbers between $Z = 13$ and $Z = 93$, but several of the major transitions in the K-LM and L-MM were reported at $Z = 48$, 70, 80, and 93. The results of this work were combined with a relativistic Hartree-Fock-Slater calculation[3] of the radiative transition probabilities in the K shell, in order to compute the K-fluorescence yield[5] for selected values of Z between $13 \leq Z \leq 93$ (see Sec. 2.3).

2.3. K-fluorescence Yield

A theoretical determination of the K-fluorescence yield ω_K (Eqn. 2-5) requires the calculation of the absolute radiative transition probability Γ_{KR} and of the absolute nonradiative transition probability Γ_{KN}. The immense problem of calculating <u>all</u> of the quantities Γ_{KR} and Γ_{KN} has demanded, until recently, that corrections - often large - be applied to the theoretical findings in order that they might be compared directly to experimentally measured values of ω_K. The brief review below indicates some of the assumptions inherent in past theoretical

determinations of the K-fluorescence yield.

Wentzel[63] first suggested that the K-fluorescence yield could be expressed in the following manner:

$$\omega_K = (1 + \alpha/Z^4)^{-1} \qquad (2\text{-}14)$$

where the empirical constant, $\alpha \approx 10^6$. The simple form of this expression relies upon two approximations: (1) the radiative decay probability increases proportionately as Z^4, which is the approximate dependence for electric dipole (E1) radiation and (2) the nonradiative transition probability is constant with atomic number. These two assumptions arise from interpretation based on the use of pure hydrogenic wave functions.

Burhop[77] later attempted to account for the effects of screening and relativity by proposing the following formula:

$$\left(\frac{\omega_K}{1 - \omega_K}\right)^{\frac{1}{4}} = -A + BZ - CZ^3 \qquad (2\text{-}15)$$

where the terms $-A$ and $-CZ^3$ account for the screening effect and relativistic effects, respectively.

The simple dependence with Z suggested for the screening term and the relativistic correction, in addition to the neglect of any K x radiation other than E1,

indicates that Eqn. 2-15 is only a rough approximation for the Z dependence of the K-fluorescence yield. The theoretical findings of Ramsdale[4] also indicate that the K-LL transition probability increases by a factor of approximately 4 from Z = 21 to Z = 93, thus Γ_{KA} is not constant with Z, as implied[79] in Eqn. 2-15.

Until the past year, the most complete set of calculated values of ω_K were from the semitheoretical work of Callan[52]. In this study, Callan calculated theoretical values of the (K-LX)/(K-LL) and the (K-XY)/(K-LL) ratios and the radiative transition probabilities calculated by Geffrion and Nadeau[78], in order to compute ω_K. In a later paper[79] Callan used radiation widths which were computed empirically from the quasi-hydrogenic approximation $\Gamma_{KR} = Z^4 \sum_n A_n$, where the empirical coefficients A_n are averaged values of the radiative transition probabilities (Sec. 2.1) from the p-subshells to the K shell.

A similar attempt to estimate the K-fluorescence yield at Z = 65, 81, and 92 was made by Listengarten[80]; as in the case of Callan[79], he found it necessary to correct the calculated K-LL transition probabilities for the K-LX and K-XY transitions. The radiative transition probabilities were obtained by using Asaad's[81] relativistic calculation of the K_α transition probability and correcting it using the relative K x-ray intensity ratios

(K_β/K_α) compiled by Wapstra[82].

In the past year considerable effort[5,53,83] has been made to calculate K-fluorescence yields that need not include large corrections for theoretically undetermined transitions. The theoretical approach of each of these calculations is significantly different and is outlined below.

Kostroun, Chen and Crasemann[53] have calculated selected values for ω_K from $Z = 10$ to $Z = 70$, employing nonrelativistic screened hydrogenic wave functions and including all K-Auger electron transitions. The screening parameters used were derived from Hartree-Fock wave functions and the radiative transition probabilities were taken from the relativistic Hartree-Slater calculations by Scofield.[2] The authors suggest that their values of ω_K are probably too high above $Z \lesssim 50$ because of the neglect of relativistic effects in the calculation of the K-Auger transition rates.

McGuire[83] has calculated values for ω_K between $Z = 4$ and $Z = 54$ by approximating the nonrelativistic Hartree-Fock-Slater potential such that it leads to an exactly solvable Schrödinger equation. Both the radiative and nonradiative transition probabilities are calculated, leading to values for ω_K which agree well with experimental findings although both the radiative and nonradiative K-level

widths are approximately 20 percent higher than the more rigorous determinations of Scofield[2] and Ramsdale[4] respectively.

K-fluorescence yields have also been calculated by Bhalla, Ramsdale and Rosner[5] using a fully relativistic Hartree-Fock-Slater model. Values for the K-fluorescence yield were obtained for Z over a wide range in atomic number ($21 \leq Z \leq 93$). The determination of the K-shell radiative widths included contributions from all subshells, whereas the nonradiative K-shell widths included only the K-LL and K-LM contributions. The effect of including all possible radiative transitions, but including only the nonradiative contributions from the K-LL and K-LM Auger groups would lead to values of ω_K that are systematically high unless correction is made for the unaccounted for K-Auger electrons. The relative error in ω_K due to this approximation may be as large as 15 percent at low Z ($Z < 30$) but is small at $Z \gtrsim 80$ ($\approx 0.3\%$). This point is further discussed in evaluating the significance of the present work (Sec. 5.2.2).

2.4. Present Theoretical Status in the Area of Inner-shell Atomic Transition Rates

At present, the electronic structure of free atoms and ions is generally best described in terms of the relativistic Hartree-Fock-Slater model. Although, in principle, the more

rigorous Hartree-Fock model more accurately describes the atomic potential, Hartree-Fock wave functions have been obtained thus far for only a limited number of atoms and ions, therefore preventing a full-scale investigation of the atomic transition rates as has been made with the less involved Hartree-Fock-Slater model.

In addition to the self-consistent field approach, viz. Hartree-Fock-Slater model,to the problem of estimating the effects of atomic screening, a second, less direct approach has also proven successful in the prediction of atomic transition rates. The use of screening coefficients which are derived from a direct comparison of hydrogen-like wave functions with rigorous Hartree-Fock wave functions, has enabled workers to calculate both radiative[29] and non-radiative[53] transition rates using wave functions expressed in closed form. This particular approach, applied to the problem of atomic transition rates, has proven to be comparable in accuracy to the Hartree-Fock-Slater method and has the added advantage of being adaptable to computers of limited storage and speed.

In view of the uncertainty of the theoretical predictions of the atomic transition rates and the need for more precise experimental data to help evaluate the validity of existing calculations, it was decided to measure certain K x-ray intensity ratios over a wide range in atomic number

and to measure the K-fluorescence yield at high Z.

The experimental measurements of the relative K x-ray intensities and the high Z K-fluorescence yields are discussed in Chapters III and IV, respectively.

CHAPTER III

RELATIVE K X-RAY INTENSITIES

In measurements of the relative K x-ray intensities, by earlier workers, based on fluorescent excitation of thick targets and the use of ionization chambers[15] or high resolution curved crystal spectrometers[16], major corrections for the continuum and for self-absorption were necessary. The present method of using carrier-free radioactive sources and Ge(Li) and Si(Li) x-ray detectors does not require large corrections for self-absorption, nor is the uncertainty in the continuum under the K x-ray peaks a major problem owing to very high peak-to-continuum ratios. Furthermore in the present method, the low intensity lines β_5 (K-$M_{4,5}$), β_4 (K-$N_{4,5}$) and K-$O_{2,3}$ are not resolved from the more intense group, so that the problem of determining accurate intensities at very low peak-to-continuum ratios is avoided.

In the present work, measurement of the relative intensities of the major K_α and K_β groups was made to approximately 2 percent accuracy over an extended range in Z and values were obtained at Z = 81, 82 and 96 of the $K_{\alpha_2}/K_{\alpha_1}$, $K'_{\beta_1}/K_{\alpha_1}$ and $K'_{\beta_2}/K_{\alpha_1}$ x-ray intensity ratios. Also, measurements of the K_β/K_α ratios were made in the

lanthanide region where previously it was necessary to use values interpolated from older work[15,16].

3.1. Basis of the Method

The present method of measuring relative K x-ray intensities using high-resolution semiconductor detectors involves a determination of the areas, in the output spectrum, of each well-resolved K x-ray group (Fig. 1); in addition, differing detection efficiencies of the compared K x-ray groups must be taken into account.

The area of the peaks in the output spectra, in principle, can be measured by graphical integration; in the present work, it was found that for well-resolved K x-ray groups that numerical peak integration, following subtraction of the continuum under the peaks, was in general a more consistent means of determining the peak areas. The measurement of the relative intensity ratio of two specific lines or groups in a particular K x-ray spectrum thereby constitutes a comparison of the two measured counting rates and applying suitable corrections for the differing detection efficiencies.

The ratio of intensities, I_{K_i}/I_{K_j}, for two K x-ray peaks, K_i and K_j may therefore be expressed as:

$$I_{K_i}/I_{K_j} = \frac{C_{K_i}/\varepsilon(K_i,\Omega)}{C_{K_j}/\varepsilon(K_j,\Omega)} \qquad (3\text{-}1)$$

where the quantities C_{K_i} and C_{K_j} are the measured counting rates, and $\varepsilon(K_i,\Omega)$ and $\varepsilon(K_j,\Omega)$ are the detection efficiencies for a specific geometry. The geometry in this context is determined by the solid angle, Ω, originating at the geometric center of the source and subtending the detector face.

The detector efficiency $\varepsilon(E,\Omega)$ for a peak of energy, E, is related to the "relative (photon) efficiency, $\varepsilon_R(E,\Omega)$" as follows:

$$\varepsilon(E,\Omega) = \varepsilon_R(E,\Omega)\ \frac{\Omega}{4\pi} \qquad (3\text{-}2)$$

therefore Eqn. 3-1 can also be expressed in terms of the relative efficiencies:

$$I_{K_i}/I_{K_j} = \frac{C_{K_i}/\varepsilon_R(K_i,\Omega)}{C_{K_j}/\varepsilon_R(K_j,\Omega)} \qquad (3\text{-}3)$$

For peaks of approximately equal energies the relative efficiencies will normally be very nearly the same, thus only small corrections for differing relative efficiencies need be applied i.e. $\varepsilon_R(K_i,\Omega)/\varepsilon_R(K_j,\Omega) \simeq 1$. In the present work, preliminary attempts were made to determine the intensities of K x-ray peaks which are close in energy, as for example, K'_{β_1} and K'_{β_2} from Ce^{139} decay (Fig. 2).

These attempts were unsuccessful owing to large uncertainties associated with unfolding the overlapped multiplets; consequently, the present reported results only include ratios of peaks or multiplets well resolved from one another. For this reason, although no uncertainty in the present work arises from spectrum unfolding, the assumption $\varepsilon_R(K_i\Omega)/\varepsilon_R(K_j\Omega) \simeq 1$ is, in general, not valid and corrections for differing detection efficiencies must be taken into account. This point is further discussed in Sec. 3.2.4.

3.2. Experimental Equipment and Measurements

3.2.1. Radioactive Sources

The sources used in the measurements of the relative K x-ray intensities were mounted on thin Mylar film in order to minimize Compton scattering. By the use of carrier-free liquid solutions, source thicknesses of less than 100 $\mu g/cm^2$ were obtained, thus eliminating self-absorption of K x-rays. Each source was covered with a Krylon spray coating of approximately 100 $\mu g/cm^2$ to prevent loss of activity due to sublimation.

Each of the absolutely calibrated radioactive gamma standardized sources, provided by the International Atomic Energy Agency, Vienna, (IAEA), was sandwiched between two 17.5 mg/cm^2 polyethylene discs. Absorption corrections were negligible except in the case of (Cr, Fe) K x rays from Mn^{54} and Co^{57} decays. The error in the

disintegration rates of each of the IAEA standardization sources is ±1% to ±2%; the quoted error in the intensities of the x rays or gamma rays emitted varied between 1% and 10%, depending on uncertainties in the decay schemes, conversion coefficients or fluorescence yields. Table 1 lists the standardization sources used; references to the emission rates and uncertainties are supplied in the footnotes.

The source-to-detector distance was never greater than 3.5 cm to minimize air absorption; corrections for air attenuation were negligible above 10 keV. The sources used to measure the K x-ray intensities were mounted in the same geometry as the standardization sources used to calibrate the detectors.

3.2.2. Detectors and Electronics

In order to obtain a suitable compromise of detector efficiency and resolution over the entire K x-ray energy range, lithium-drifted semiconductor detectors were used. The detectors used in the study of the relative K x-ray intensity ratios are described in Table 2. The relative efficiencies of these detectors are each normalized to unity at the maximum in the measured efficiency curves.

The detectors, Ge(Li)-I, Ge(Li)-II, Ge(Li)-III and Si(Li)-I were fitted with beryllium windows of 0.25 mm, 0.25 mm, 0.13 mm and 0.05 mm, respectively. Absorption in

Table 1. Standardization Sources

Nuclide	Daughter	Photon Energy (keV)	Photons Emitted Per Decay
$_{95}Am^{241}$	$_{93}Np^{237}$	13.9	0.135 ±0.003 (a)
		17.8	0.184 ±0.004 (b)
		20.8	0.050 ±0.001
		26.4	0.025 ±0.002
		59.54	0.359 ±0.006
$_{27}Co^{57}$	$_{26}Fe^{57}$	6.4	0.558 ±0.012 (c)
		14.36	0.095 ±0.002
		121.97	0.856 ±0.003
		136.33	0.1075±0.003
$_{80}Hg^{203}$	$_{81}Tl^{203}$	72.873	0.0977±0.005 (d)
		82.5	0.0273±0.002 (d)
		279.191	0.8155±0.015
$_{55}Cs^{137}$	$_{56}Ba^{137}$	32.1	0.0566±0.002 (d)
		36.5	0.0134±0.001 (d)
		661.635	0.851 ±0.004
$_{25}Mn^{54}$	$_{24}Cr^{54}$	834.81	1.000
		5.9	0.250 ±0.002 (e)
$_{39}Y^{88}$	$_{38}Sr^{88}$	14.4	0.616 ±0.002 (f)
		511.006	0.004 ±0.002
		898.04	0.914 ±0.007
		1836.0	0.994 ±0.001
$_{27}Co^{60}$	$_{28}Ni^{60}$	1173.23	0.9974±0.0005
		1332.49	0.9985±0.0003
$_{11}Na^{22}$	$_{10}Ne^{22}$	511.006	1.797 ±0.008
		1274.55	0.9995±0.0002

(continued)

Table 1. Standardization Sources (Concluded)

Nuclide	Daughter	Photon Energy (keV)	Photons Emitted Per Decay	
$_{73}Ta^{182}$	$_{74}W^{182}$	100.1	100[g]	(100)[h]
		113.7	14	(14.2)
		116.4	3.2	(3.17)
		152.4	51	(51.9)
		156.4	20	(19.6)
		179.4	23	(23.6)
		198.4	11	(10.7)
		222.1	56	(55.2)
		229.3	28	(29.0)
		264.1	27	(25.9)

(a) All values other than those footnoted are as given by IAEA, Vienna.

(b) This intensity has been determined in the present work to be incorrect as given by IAEA, Vienna. The measured intensity found in the present work was 0.202±0.004.

(c) From - H. U. Freund and J. C. McGeorge, Z. Physik 238, 6 (1970).

(d) The original values as supplied by IAEA, Vienna, have been corrected for the K_α/K_β intensity ratio measured in the present work.

(e) Computed using an average value of $P_K\omega_K = 0.250\pm0.002$.

(f) Private communication from J. C. McGeorge.

(g) These values normalized to 100 at 100 keV; taken from W. F. Edwards, F. Boehm, J. Rogers and E. J. Seppi, Nucl. Phys. 63, 97 (1965).

(h) Measured in the present work to approximately 5%.

Table 2. Characteristics of Detectors Used in Present Study

Detectors	Nominal Dimensions[a] Depth × Area	Resolution [FWHM][b] 6.4 keV	122 keV	Relative Efficiency[b] 14.4 keV	122 keV
Ge(Li)-I	5.0 mm × 50 mm^2	440 eV	730 eV	0.77	0.41
Ge(Li)-II	5.0 mm × 50 mm^2	440 eV	730 eV	0.62	0.31
Ge(Li)-III	5.5 mm × 50 mm^2	325 eV	560 eV	0.74	0.32
Si(Li)-I	3.0 mm × 30 mm^2	260 eV	640 eV	1.0	0.0096
Si(Li)-II	2.0 mm × 30 mm^2	440 eV	800 eV[c]	1.0	0.0055

[a] As supplied by manufacturers

[b] Measured values normalized to maximum in measured efficiency curves.

[c] Measured at 75 keV

the beryllium windows is essentially negligible above 10 keV.

The output from the detectors was passed to preamplifiers which are an integral part of each detector system. Pulse shaping and further amplification was provided by conventional active-filter spectroscopic main amplifiers. The output of the main amplifier was normally passed directly to a multichannel pulse height analyser except in those cases where a biased amplifier was required for a more detailed inspection of a specific energy region.

3.2.3. Preliminary Studies of Equipment

Preliminary investigations of two of the germanium detectors [Ge(Li)-I and Ge(Li)-II] and the Si(Li) detector revealed that Ge(Li)-I had a thick ≃5000Å gold layer and a 15000Å-thick dead layer of germanium on the front face of the detector. The gold layers of Ge(Li)-II and Si(Li)-I were found to be less than 300Å and 300Å respectively. In order to avoid large corrections for absorption in the detector window, Ge(Li)-I was not used in the measurements of the relative K x-ray intensities.

The results of preliminary experimental measurements of the efficiencies of the supposedly identical detectors, Ge(Li)-I and Ge(Li)-II, showed decided differences. Furthermore, the efficiency curve supplied by the

manufacturer† was found to be only a very crude estimate of the efficiency curves for these detectors. Fig. 3 shows that curve and an experimental determination of the relative efficiencies, ε_R, for the two detectors. It is seen that the usable energy range was in fact narrower than anticipated on the basis of manufacturer specifications.

In order to determine the effective sensitive volume of two of the detectors, Ge(Li)-II and Si(Li)-I, each was scanned with a 1.3 mm collimated Co^{57} beam and the relative count rates plotted as a function of position along one coordinate (Fig. 4). Results were plotted for two of the lines of Co^{57} at 14.4 and 122 keV. The presence of an outer dead ring on the front face of the detectors, suggested by the manufacturers, was confirmed in the scanning studies.

Since the study of the relative K x-ray intensities involved the use of several different detectors and electronic equipment, selected by considerations‡ of resolution and efficiency, preliminary consistency checks were made to ensure that various combinations of electronic units yielded identical results (within the statistical counting

†ORTEC, Inc., Oak Ridge, Tenn.

‡The higher resolution Si(Li) detector was particularly suited to the study of low-energy K x rays but because of significantly lower efficiency than the germanium detectors, was not used above approximately 50 keV for K x-ray measurements. The germanium detectors on the other hand were not suited to measurements below approximately 15 keV because of the presence of the discontinuity in efficiency due to K x-ray escape (Sec. 3.3.1).

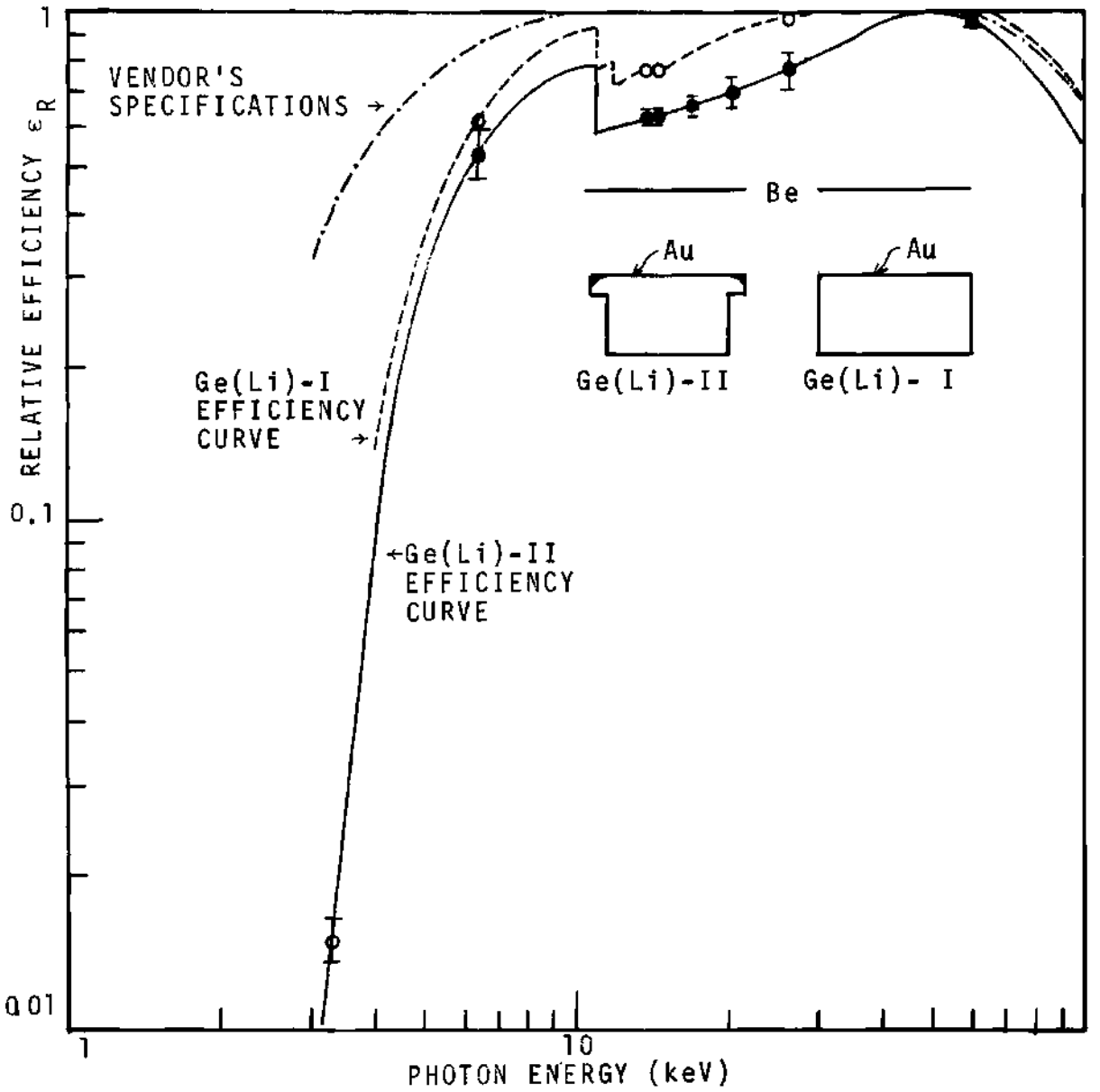

Fig. 3. Relative Efficiency Curves For Two Ge(Li) Detectors With Identical Nominal Specifications. (Source to detector distance = 35 ± 2 mm.)

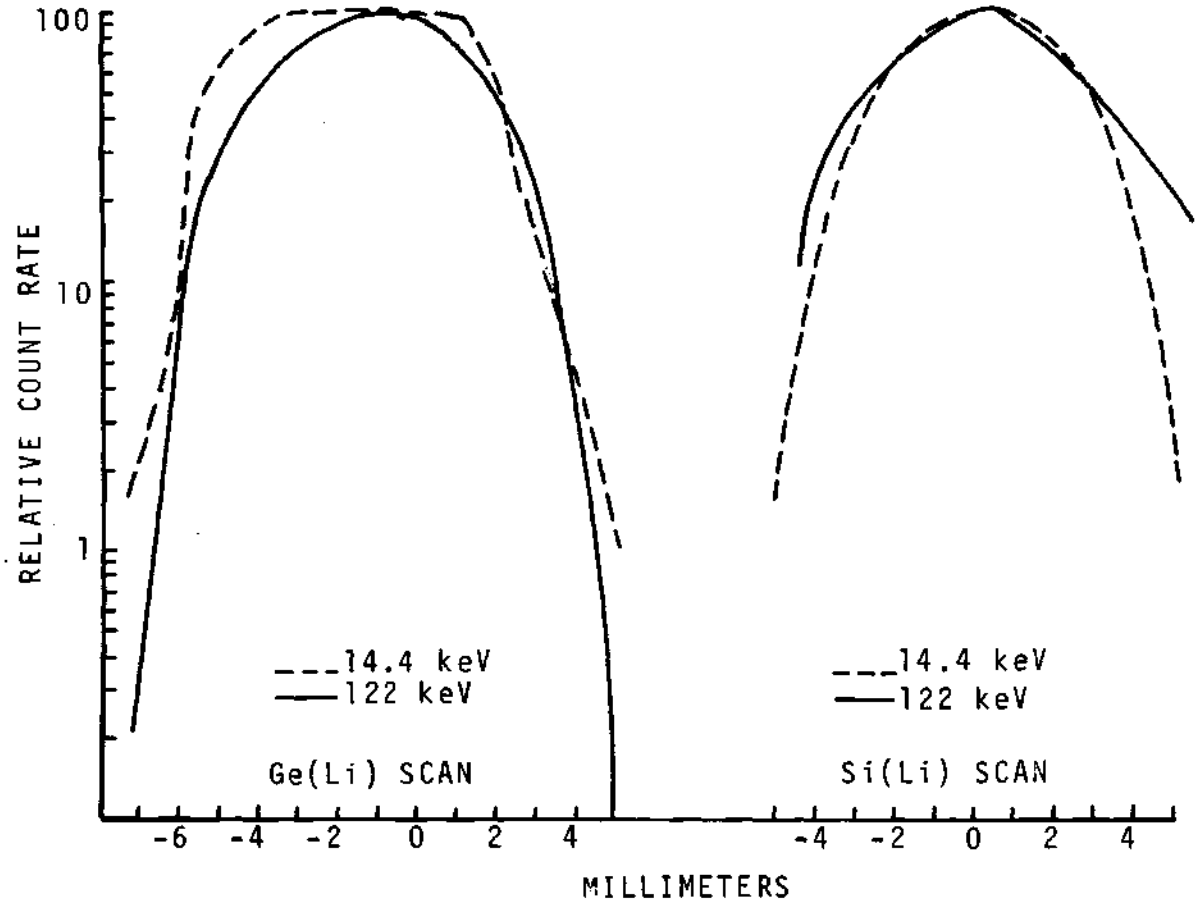

Fig. 4. Detector Scans With Collimated Photon Beam. (Radial asymmetry arises probably from the presence of weak field zones and dead regions.)

error) under identical conditions. Studies of the full energy peak-to-tail ratio were carried out to further determine the most suitable main amplifier time constants and detector bias. The results of these studies are shown in Fig. 5. The gradual rise of the peak-to-tail ratio with decreasing photon energy is probably due to an increased charge collection efficiency for photons interacting near the front face of the detector. The peak-to-tail ratio decreases rather abruptly in Ge(Li)-I and Ge(Li)-II below a detector bias of approximately 400 volts as the result of the ineffectiveness of the weakened field in collecting the charge. The germanium detectors were normally operated at 900 volts, well above the threshold for this effect. The decrease in the peak-to-tail ratio with short main amplifier time constants results from clipping of the slower pulses in the main amplifier, hence causing them to fall in the low-energy degradation tail. Main amplifier time constants of approximately 2 μsec, well above the threshold of this effect, were used throughout the course of this work.

3.2.4. Detection Efficiency

A few preliminary measurements of the relative K x-ray intensities disclosed rather large discrepancies from previous measurements[15,16] and in addition suggested a systematic difference between the present results and the

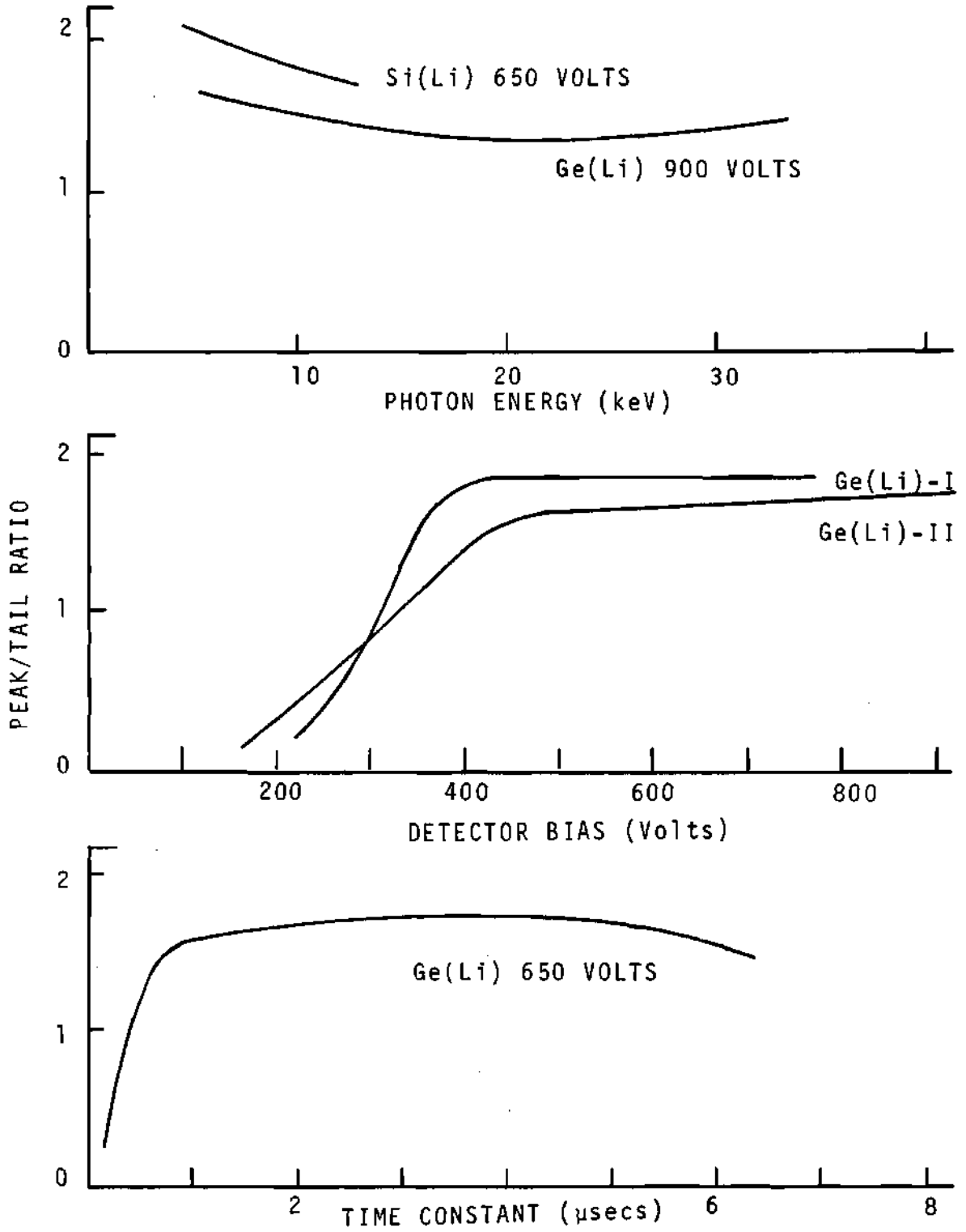

Fig. 5. Peak/Tail Ratios For Low-energy Photons In Ge(Li) and Si(Li) Detectors. (See discussion in text (Sec. 3.2.3)

theoretically predicted values[2]. Prior to an extended investigation of the relative K x-ray transition rates, a comprehensive study of the factors involved in the detection efficiency was necessary for the following reasons: (1) the disagreement in the experimental efficiency curves of Ge(Li)-I and Ge(Li)-II could not be resolved by simply accounting for the thick Au layer and germanium dead layer on the face of Ge(Li)-I; (2) the scarcity of sources with accurately-known gamma- and x-ray emission rates required interpolation between experimental values, each subject to its own error and often widely separated in energy; for example, no reliable experimental values are available between 30 and 60 keV, an energy region spanning the entire rare-earth K x-ray region; (3) the assumption that an interpolation can be carried out using a simple description of the efficiency curve is evidently fallacious, considering the major discrepancies between the experimental efficiency curves and those supplied by the manufacturers, see Figs. 3 and 6; (4) the relative K x-ray intensity ratios depend on the relative efficiency (Eqn. 3-2) thus the overall success of the study of these ratios appeared to rely on an accurate estimate of the relative efficiencies of the detectors.

To clarify this issue, the results of a study of the efficiencies of semiconductor detectors are presented in the

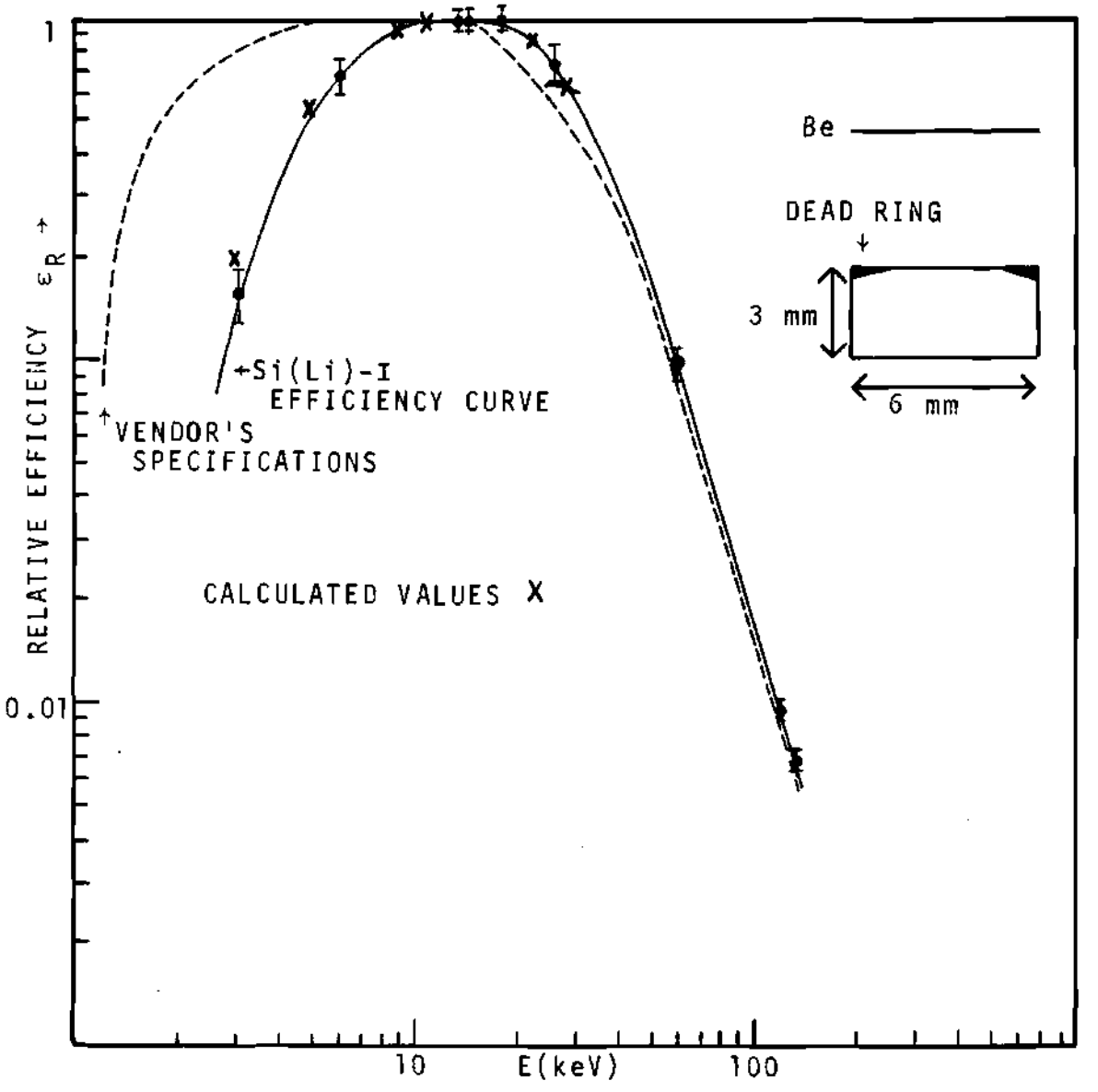

Fig. 6. Relative Efficiency Curve for Si(Li)-I. (Annular dead ring was disclosed by scanning this detector with a collimated photon beam. See Fig. 4. Source to detector distance = 35mm.)

form of a semi-empirical model. Some of the aspects of the model e.g. the effects of K x-ray escape, attenuation in the sensitive volume, may be applied to other similar devices as used in this study; whereas certain other aspects such as charge collection efficiency, collimation effects and window absorption may vary significantly between nominal detectors. Because of these many factors affecting the efficiency of semiconductor detectors below 100 keV, no two detectors will ordinarily have identical efficiency curves, even if their nominal specifications are identical. For this reason efficiency curves of semiconductor detectors in the energy region below 100 keV must be determined experimentally for each detector.

3.3. Semi-empirical Model of the Detection Efficiency of Semiconductor Radiation Detectors

The relative detection efficiency of a semiconductor detector may be described by[84]

$$\varepsilon_R = \varepsilon_a \, f_a \, f_{Au} \, f_d \, f_e \, f_c \, \varepsilon_s \qquad (3\text{-}4)$$

where ε_a is the intrinsic efficiency of the sensitive volume of the detector, assuming 100 percent charge collection; f_a is a correction factor for attenuation in materials external to the detector face; f_{Au} is the correction for attenuation in the thin Au layer on the

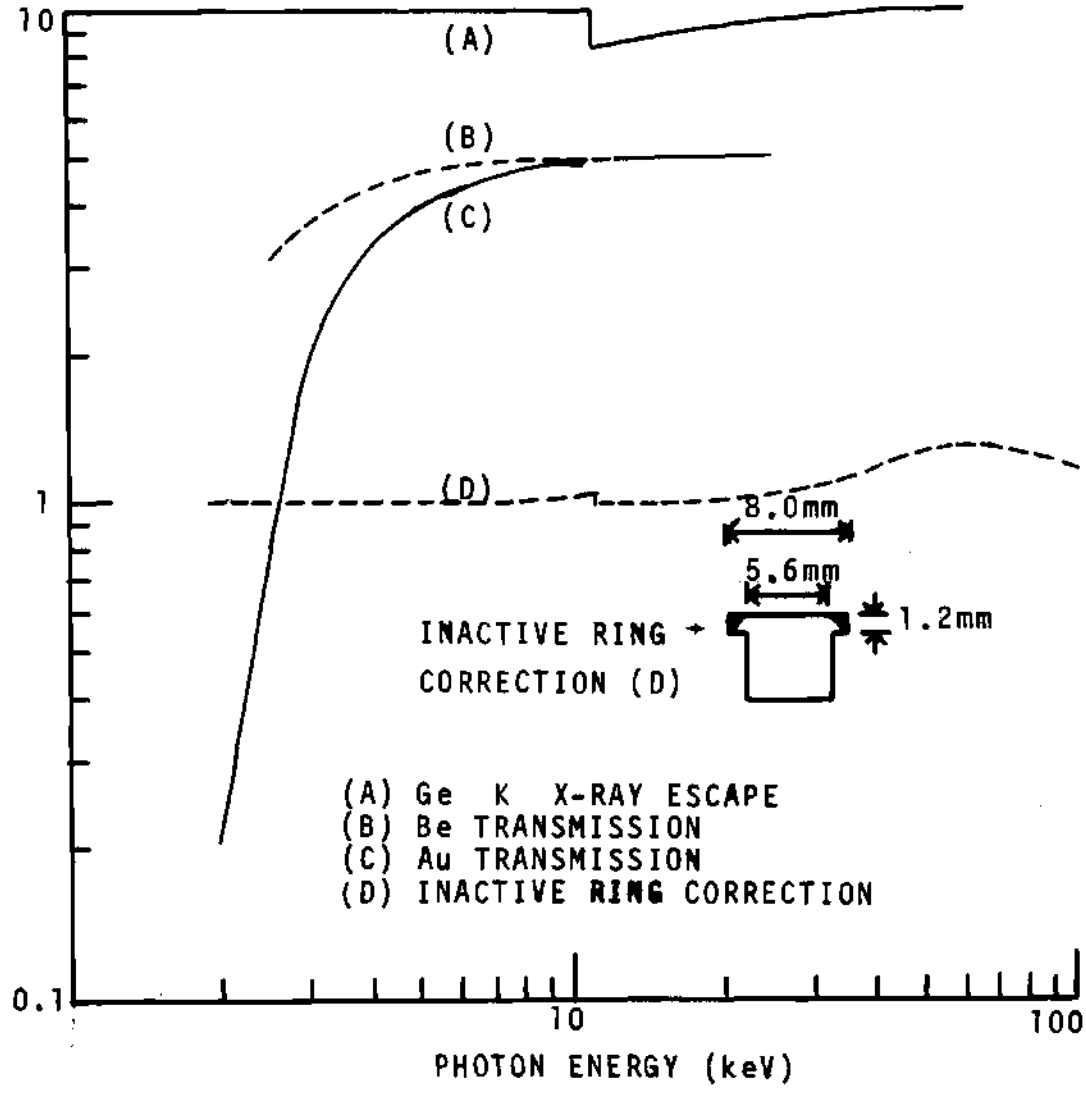

Fig. 7. Relative Factors Affecting the Efficiency Calculation For Ge(Li)-II

detector face; f_d is the correction for attenuation in the uniform dead layer between the Au and sensitive volume; f_e is a correction for escape of K x rays from the sensitive volume; f_c is a correction for the effects, if any, of collimation; and finally, ε_s is the efficiency of total charge collection. If ε_s is less than 100 percent, this implies incomplete charge collection and hence a decrease in signal amplitude. This means that the event will appear to have a reduced energy and it will fall into the low-energy tail of the corresponding peak in the energy spectrum. A summary of the factors f_a (beryllium only), f_{Au}, f_e and f_c for Ge(Li)-II is given in Fig. 7 as a function of energy.

Because of the competing nature of the processes (photoelectric, Compton, and pair production) leading to full-energy pulses at high energy, as opposed to the dominance of the photoelectric effect at low energy, the ensuing discussion is divided in the following manner: $(\sigma_{ph}/\sigma_{sc}) > 10$ and $(\sigma_{ph}/\sigma_{sc}) \leq 10$, where σ_{ph} is the cross-section for the photoelectric effect and σ_{sc} the cross-section for competing effects, e.g. Compton scattering, Rayleigh scattering, etc. In germanium and silicon, the ratio $(\sigma_{ph}/\sigma_{sc}) = 10$ occurs at approximately 60 keV and 25 keV, respectively.

3.3.1. Low Energy Region Where $\sigma_{ph}/\sigma_{sc} > 10$

In this energy region, the intrinsic efficiency

for normal incidence is given by

$$\varepsilon_a = 1 - e^{-\mu_t d} \qquad (3\text{-}5)$$

where μ_t is the total attenuation coefficient and d is the true depletion depth as obtained from the slope of the curve through the high-energy experimental points. The correction factor f_a which accounts for attenuation between source and detector face, excluding source self-absorption, is given by

$$f_a = \sum_i e^{-\mu_i x_i} \qquad (3\text{-}6)$$

where μ_i and x_i are the total attenuation coefficient and thickness of any absorber between source and detector. At low energies, air and Be absorption may be significant, being 41% and 17.5% for 1 cm air and 0.10 mm (2 mil) Be at 3 keV, respectively.

The correction f_{Au} for absorption of the incident photons in the Au layer evaporated on the detector face can be calculated from Eqn. 3-6, once the Au thickness has been determined. The average Au thickness was determined in the present study by measuring the ratio of the counting rate of fluorescent Au L_α x rays to the counting rate of the 14.4 keV line from the decay of Co^{57}. The average Au

thickness was determined from the following equation:

$$\frac{C_{L_\alpha}}{C_{14.4}} = \frac{\varepsilon_{L_\alpha} F_{L_\alpha} \omega_3 X_{Au}}{2\varepsilon_{14.4}} \left[\mu_1 (f_{13} + f_{12} f_{23}) + \mu_2 f_{23} + \mu_3 \right] \qquad (3\text{-}7)$$

where C_{L_α} and $C_{14.4}$ are the respective counting rates of the Au-L_α x rays and the 14.4 keV gamma ray from the decay of Co^{57}, respectively; the quantity F_{L_α} represents the fraction of radiatively-filled L_3 vacancies which give rise to the emission of an L_α x ray[2] ($F_{L_\alpha} = 0.80$); $\varepsilon_{L_\alpha}/\varepsilon_{14.4}$ is the ratio of the respective Au-L_α x-ray (9.7 keV) and 14.4 keV gamma-ray efficiencies; $\omega_3 = 0.31$ is the fluorescence yield of the L_3 subshell at $Z = 79$[85]; the Au thickness, $X_{Au}^{(cm)}$ has to be determined; the quantities μ_1, μ_2 and μ_3 are the linear photoelectric[86] absorption coefficients (cm^{-1}) of the L_1, L_2 and L_3 subshells of gold; the Coster Kronig transition probabilities f_{12}, f_{13} and f_{23} are 0.56, 0.14 and 0.17, respectively[85]. The minimum detectable Au thickness, which is primarily a function of the peak-to-continuum ratio for the 14.4 keV line is found in the present work to be approximately 300 Å. The Au layer thickness of each of the detectors was measured by this method, and it was found that only in the case of Ge(Li)-I was the Au thickness greater than 300 Å: in fact, for this detector the measured thickness of the gold layer

was determined to be 4900 Å.

In the case of Ge(Li)-I, another check was made by comparing the intensities of fluorescently-excited selenium K_α and K_β x rays which straddle the Au L_3 edge with the same intensity ratio in the Si(Li) detector where the Au thickness is less than 300 Å. The results of this experiment gave a 5100 Å thickness for the gold layer, confirming the previous findings.

The factor f_d, the correction for absorption in the dead layer on the front surface of the detector was found for germanium experimentally by fluorescent excitation of the characteristic K x rays of germanium, again using the 14.4 keV gamma ray from Co^{57} decay. The germanium dead layer thickness is given by

$$\frac{C_{K_\alpha}}{C_{14.4}} = \frac{\mu_K \, X_{Ge} \, \omega_K}{2} \left(\frac{\varepsilon_K}{\varepsilon_{14.4}} \right) \left(\frac{1}{1 + K_\beta/K_\alpha} \right) \tag{3-8}$$

where C_{K_α} and $C_{14.4}$ are the respective counting rates of Ge K_α x rays and the 14.4 keV gamma ray from Co^{57} decay; the quantity μ_K is the total K-shell photoelectric absorption coefficient (cm^{-1}) at 14.4 keV; X_{Ge} is the thickness of the germanium dead layer; the K-fluorescence yield of germanium[87] is $\omega_K = 0.570 \pm 0.003$; the ratio of the detection efficiency of Ge-K_α x rays (9.9 keV) and the

detection efficiency for the 14.4 keV gamma ray is given by the ratio $\varepsilon_K/\varepsilon_{14.4}$; the ratio $\frac{1}{1 + K_\beta/K_\alpha}$ corrects for the contribution from K_β x rays of germanium, which are not counted. The minimum detectable germanium dead thickness in the present study was approximately 3000 Å. The germanium dead layer thickness of the two detectors Ge(Li)-II and Ge(Li)-III was measured using this technique and the dead germanium thickness found to be less than 3000 Å.

A second estimate of the germanium dead layer thickness was made by straddling the Ge K edge (11.1 keV) with the K_α and K_β x-ray doublet from Se^{75} decay. The application of this technique to the measurement of the germanium dead layer thickness is described in Ref. 84. The germanium dead layer of Ge(Li)-I was measured by this technique and found to be 15000 Å (1.5 microns). In each of the measurements of the gold layer thickness and the germanium dead layer thickness, the Co^{57} source was collimated to a beam diameter of approximately 6 mm, in order to avoid fluorescent excitation of gold or germanium which is not on the front face of the detector. An accurate determination of the Si dead layer thickness by fluorescent excitation is not possible because of the low value of the K-fluorescence yield[33], $\omega_K = 0.0458 \pm 0.005$ (see Eqn. 3-8) and the low energy of the emitted Si K x rays ($\approx$1.74 keV). A technique involving the measurement

of the energy degradation of alpha particles in passing through the silicon dead layer has been described by Price[88]. In principle, this method should be quite sensitive but suffers from the disadvantage of having to situate the alpha source in juxtaposition with the detector face, which is not possible for detectors mounted within sealed vacuum cryostats. The magnitude of the effect of photon absorption in the silicon dead layer is small except at very low energies (<4 keV), assuming a 10^4 Å-thick silicon dead layer. At an incident photon energy of 2.0 keV, the absorption in one micron (10^4Å) of Si is 50 percent; for very low energy work, absorption in the dead silicon layer may contribute significantly to the rapid drop-off in photon efficiency.

The factor f_e is a correction for the escape of characteristic K x rays from the sensitive volume, and is related to the fraction of K x rays escaping from the sensitive volume by

$$f_e = 1 - \frac{I_e}{I_\gamma} \qquad (3\text{-}9)$$

where I_e is the intensity of the K x-ray escape peak and I_γ the intensity of the incident gamma rays, and the fraction of K x rays escaping from the sensitive volume is given by:

$$\frac{I_e}{I_\gamma} = \frac{\mu(K)\omega_K}{2\mu_\gamma} K_\alpha \left[1 + \frac{\mu_{K_\alpha}}{\mu_\gamma} \ell n \left(\frac{\mu_{K_\alpha}}{\mu_{K_\alpha} + \mu_\gamma} \right) \right] + \frac{\mu(K)\omega_K}{2\mu_\gamma} K_\beta \left[1 + \frac{\mu_{K_\beta}}{\mu_\gamma} \ell n \left(\frac{\mu_{K_\beta}}{\mu_{K_\beta} + \mu_\gamma} \right) \right] \quad (3\text{-}10)$$

where ω_K is the K-fluorescence yield of the bulk detector material (Ge or Si). The quantities $\mu(K)$ and μ_γ are the linear K-shell photoelectric coefficient and total γ-ray linear attenuation coefficient, respectively. The quantities K_α and K_β are the fractions of the total K x-rays in the K_α and K_β groups, respectively, and μ_{K_α} and μ_{K_β} are the respective total linear attenuation coefficients of the K x rays emitted by the detector material. The computed ratio I_e/I_γ is given in Fig. 8 for silicon and germanium, together with experimentally measured values for germanium. A derivation of Eqn. 3-10 is given in Appendix A.

The factor f_c is a correction for any collimation which limits the beam diameter to less than the radial dimensions of the sensitive volume of the detector. Dead edges and weak field zones at the detector periphery are common in semiconductor x-ray detectors and act as effective collimators at low energies. Figs. 3 and 6 approximately describe this geometric asymmetry of the sensitive volumes for Ge(Li)-II and for Si(Li)-I. These two detectors were investigated with a collimated beam and

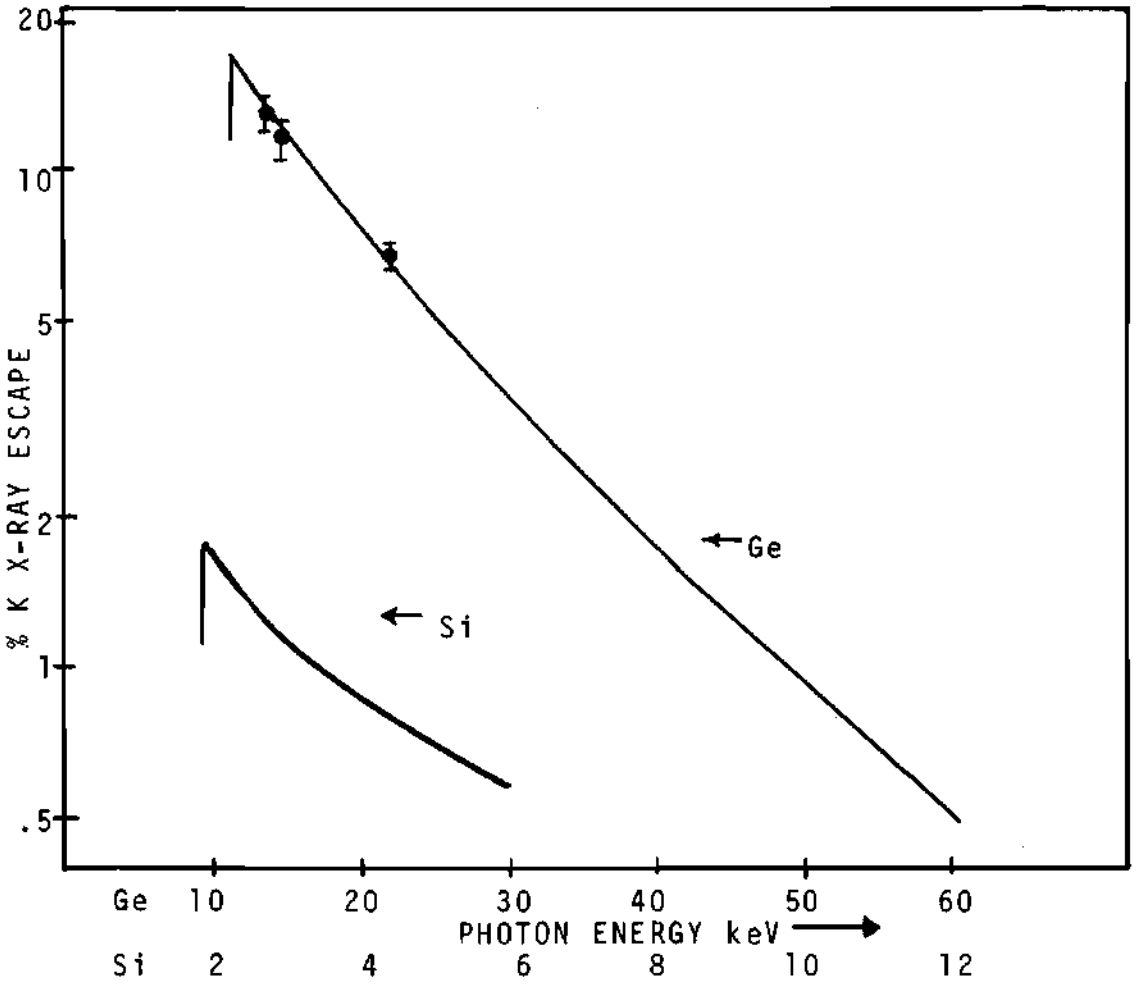

Fig. 8. K X-ray Escape Probability. (See Appendix A for a derivation of the expression used to calculate these curves.)

the resultant cross-sections are given in Fig. 4. Because of the inherent dead edges and weak field zones at the detector periphery, detector manufacturers often use a collimator in order to screen off this partially sensitive volume at the detector edges. Regardless of the type of collimator, added or effective, with some photon energy, the collimation tends to become transparent, giving rise to a larger sensitive solid angle than at lower energies. The effect of such shadow collimation is to give an abrupt increase in the detector efficiency, often large (≈25% in the case of Ge(Li)-II, Fig. 3). Because of the irresolvable problems associated with the probing of a small device with a collimated photon microbeam, it is essential that the manufacturers specify precisely any added collimation which may be present in the detection system if an accurate determination of the low-energy efficiency is to be made.

The effective collimation of Ge(Li)-II, Fig. 3, gives rise to a correction factor f_c as displayed in Fig. 7 and results in the steady increase in efficiency (Fig. 3) in the region from approximately 20 keV to 50 keV. The analogous effect in the case of Ge(Li)-I was not observed; in the case of Si(Li)-I the effect was small in magnitude and prevailed only at energies less than 6 keV; and in the case of Ge(Li)-III, which has added aluminum collimation, the factor f_c was easily evaluated.

The factor ε_s results from the manifestation of incomplete charge collection in semiconductor detectors. The study of the peak-to-tail ratio as a function of amplifier time-constant. indicated the presence of slow pulses from full energy events which, at short time constants, fell into the degradation tail as the result of clipping in the main amplifier. This tailing, although constant above some certain time constant (see Fig. 5), is generally not negligible and suggests the presence of carrier trapping in the sensitive volume. The magnitude of this effect was measured in the case of Ge(Li)-III by integrating the degradation tail from zero to the full peak energy and comparing the result to the integrated full energy peak, care being taken to correct for Compton events in the degradation tail. The magnitude of the effect,

$\frac{C_{tail}}{C_{tail} + C_{peak}}$ was found to be approximately 50 percent;

where C_{tail} and C_{peak} are the counting rates in the tail and peak, as described above. In principle, the energy dependence of this ratio need not be constant and may give rise to variations (slow) in the relative detection efficiency (ε_R). Attempts to measure the energy dependence of this ratio were inconclusive because of the overriding presence of the Compton effect in the degradation tail at higher energies, hence the factor f_s was assumed to be energy independent.

3.3.2. High Energy Region Where $\sigma_{ph}/\sigma_{sc} \leq 10$

The region in which $\sigma_{ph}/\sigma_{sc} \leq 10$ occurs at energies greater than 60 keV for germanium and greater than 25 keV for silicon. The relative efficiency ε_R as defined in Eqn. 3-4 then reduces to the form

$$\varepsilon_R \simeq \varepsilon_a \varepsilon_s \tag{3-11}$$

where ε_a is the intrinsic efficiency of the sensitive volume of the detector and ε_s is the charge collection efficiency. This approximation assumes that absorption in windows and sources is negligible and that the quantity f_c reduces to unity at high energies.

Unlike the analytical approach which is successful in describing the quantity ε_a at low energies, the presence of multiple events leading to full energy pulses requires that for normal photon incidence

$$\varepsilon_a = 1 - e^{-\mu(E)d} \tag{3-12}$$

where d is the true sensitive depth of the assumed planar semiconductor detector and the cross-section $\mu(E)$ may be described as follows:

$$\mu(E) = \mu^{ph} + a(E)\mu^{C} + b(E)\mu^{P} \tag{3-13}$$

where μ^{ph}, μ^{C} and μ^{P} are the photoelectric, Compton and pair-production attenuation coefficients, respectively. For energies below the pair production threshold (1.022 MeV), the factor b(E), multiplying the pair production attenuation coefficient μ^{P}, is zero. The quantity a(E), multiplying the Compton attenuation coefficient μ^{C}, is interpreted as follows: assume that a Compton event occurs within the sensitive volume of the detector; then a(E) is the probability that the full energy of the initial photon is absorbed in the sensitive volume. The exact form of a(E) is dependent upon energy as well as detector design. Because of the stochastic nature of the Compton effect, expressions for a(E) must be determined empirically[89] or by the application of the Monte Carlo method[90].

A quantitative attempt was not made to compare the experimentally-found efficiency at high energies to that from Monte Carlo calculations, since the measurement of K x-ray intensities was restricted to an energy region below 150 keV. At low incident photon energies electron binding effects tend to decrease[91] the Compton cross-section, thus application of the free-electron Klein-Nishina formula normally used[90,92] at higher energies is no longer suited to accurate calculation of detection efficiency.

3.3.3. Comparison of Calculated and Measured Efficiencies

The calculated efficiencies of Ge(Li)-II and Si(Li)-I

are compared to experimentally determined values in Fig. 9 and Fig. 6. For comparitive purposes, the predicted curves are also given, based on a simple model which accounts only for absorption in the beryllium windows and for the attenuation in the sensitive volume. The solid curves drawn through the experimental points were used in the present work to determine the efficiencies for the various K x-ray groups. The Ge(Li)-II curve in Fig. 9 is identical to the Ge(Li)-II curve in Fig. 3, other than being expanded over a larger energy range.

The model is valuable in understanding the energy dependence of the efficiency which is not possible using a simpler model including only Be absorption and the intrinsic efficiency as defined in Eqn. 3-4. In the region below 10 keV, the rapid decline in efficiency is due not only to the attenuation in the beryllium but also to attenuation in the gold and germanium dead layer. In silicon the arch-shaped dead layer also tends to effectively decrease the sensitive area of the detector face, giving rise to a steep decent in efficiency below 6 keV. The discontinuity in the efficiency at the K binding energy of the detector material is the result of the sharp increase in the photoelectric cross-section at energies slightly above the K-shell ionization energy. This increased cross section results in an abrupt discontinuity in efficiency due to increased K

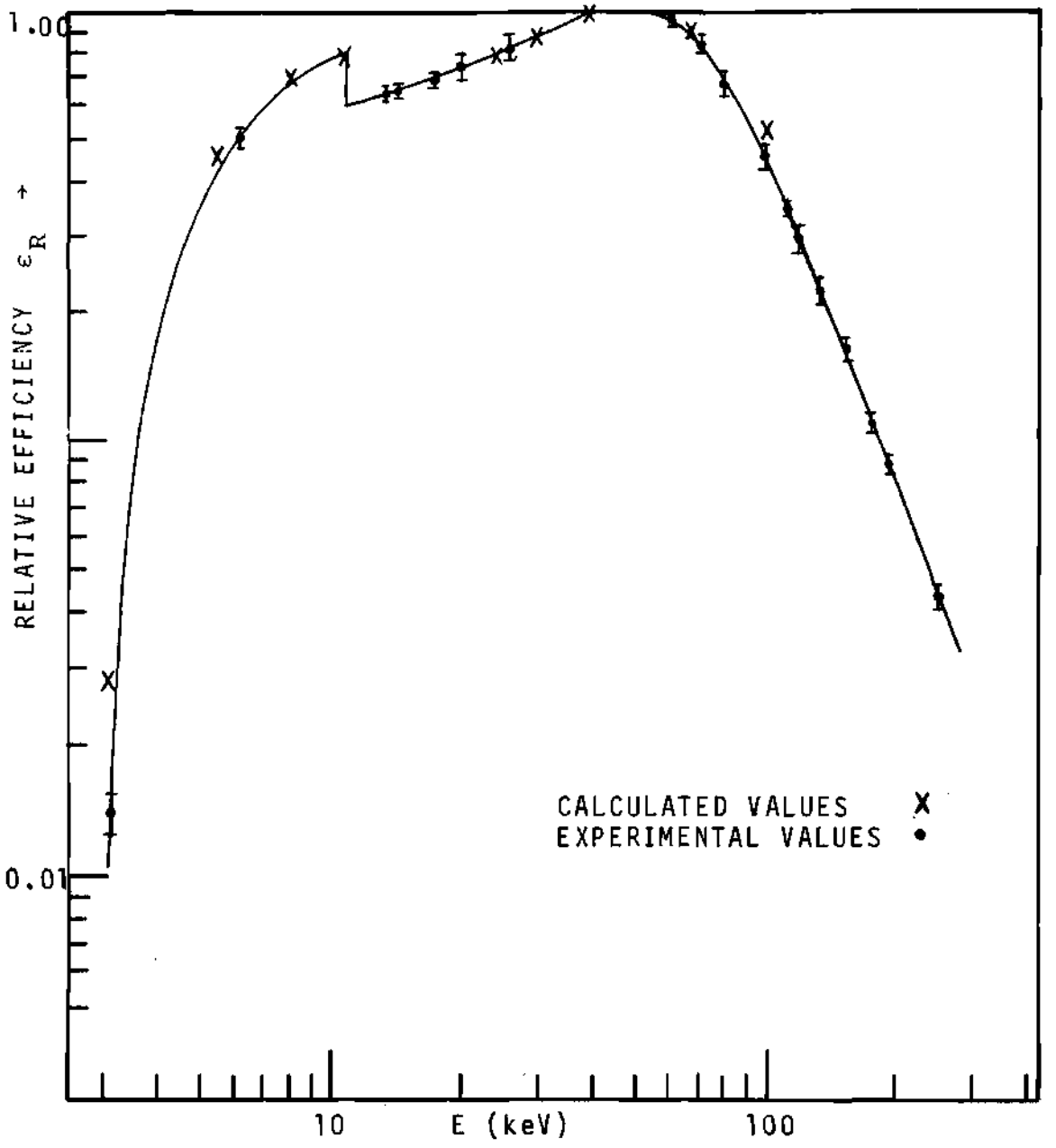

Fig. 9. Comparison of Calculated and Experimental Efficiencies for Ge(Li)-II. (Solid circles represent experimental values; crosses are calculated values from the semi-empirical model discussed in Sec. 3.4. Source to detector distance 35 ± 2 mm.)

x-ray escape in addition to the attenuation in the detector dead layers, whether uniform or arch-shaped. In the region above the K edge, the efficiency increases as the attenuation in the detector window and the probability of K x-ray escape decreases. Finally, at still higher energies the efficiency curve attains a maximum and then decreases monotonically as the probability for radiation to penetrate the entire thickness of the detector increases.

For Si(Li) detectors in the region of about 3 to 100 kev the relative efficiency over narrow energy regions can be determined to approximately 1% per 10 keV. This approximation is not strictly valid for large differences in energies, tending to overestimate the uncertainty e.g. between 10 and 100 keV for the above approximation, it implies an estimated error of 9 percent, whereas the error in relative efficiency may be kept as small as 2%-5% by careful experimental efficiency calibration. Furthermore, to a certain extent the relative efficiency is dependent upon the nearness (in energy) of accurately known calibration points i.e. the uncertainty in the relative efficiency between two experimental calibration points, regardless of the energy differences, is of the order of the combined errors of the two (calibration) points. Similar accuracies in the relative efficiency can be obtained for Ge(Li) detectors in energy regions where no discontinuities exist.

In the region of the Ge K edge (11.1 keV), the accuracy is much higher with Si(Li) than with Ge(Li) detectors.

The absolute efficiencies can be determined in principle with an uncertainty approximately equal to the combined error of the relative efficiencies and the error in the absolute calibration sources. Considering also error in source positioning i.e. error in the solid angle, the absolute efficiencies of Si(Li) and Ge(Li) detectors in the energy regions below 100 keV can be determined with an uncertainty of approximately 1 percent plus the error in the relative efficiencies.

3.4. Correction for Chance Summing and Coincidence Summing

Consideration of summing effects must be made in an experimental determination of the relative K x-ray intensities, since $E_{K_\beta} = E_{K_\alpha} + E_L$ where E_{K_β}, E_{K_α} and E_L are the respective energies of the K_α, K_β and L x rays for a specific atomic number. The rate of occurrence of this summing effect is obviously related to the probability for both K_α and L x rays to deposit their entire energy simultaneously within the sensitive volume of the detector.

Two individual types of summing may have effects upon the K_β/K_α ratios. The first of these, chance summings, is a function of the counting rates and is defined by the equation:

$$C_{12} = C_1 C_2 \, 2\tau \qquad (3\text{-}14)$$

where C_1 and C_2 are the individual counting rates of the two peaks in question and τ is the effective resolving time of the system. It can be seen that the fractional losses to K_α and to K_β are identical in all cases except summing of K_α and L x rays, which yields a sum peak of energy equal to K_β. In the present experiment, count rates for K_α and L x rays were maintained such that chance summing was negligible (<0.1%).

The second type of summing, coincidence summing, is count rate independent and occurs between L x rays in actual time-coincidence with K_α x rays. The relative error ζ, introduced by sum coincidences between L and K_α x rays is given by

$$\zeta = \frac{\omega_{KL} \, \epsilon_L \, (1 + C_{K_\alpha}/C_{K_\beta})}{1 - \omega_{KL}\epsilon_L} \qquad (3\text{-}15)$$

where C_{K_α} and C_{K_β} are the counting rates of the K_α and K_β x rays; ϵ_L is the average L x-ray detection efficiency and ω_{KL} the probability of L x-ray emission following a K_α x-ray emission. The correction at $Z = 96$ is approximately 0.7 percent. For lower values of Z, ω_{KL} is smaller as were the source geometries; consequently, the applied corrections for coincidence summing were quite small (<0.3%).

3.5. Results of Measurements of Relative K X-ray Intensities

Using the detection systems described, K x-ray intensities were measured for a variety of sources covering an extensive range in Z. The present experimental results on K_β/K_α ratios are presented in Table 3 together with the results for the $K_{\alpha_2}/K_{\alpha_1}$, $K'_{\beta_1}/K_{\alpha_1}$ and $K'_{\beta_2}/K_{\alpha_1}$ ratios at Z = 81, Z = 82 and Z = 96.

The Z = 96 measurements of $K'_{\beta_1}/K_{\alpha_1}$ and K_β/K_α ratios were corrected for a gamma ray at 122 keV which was hidden under the 122 keV K'_{β_1} x-ray group.† The intensity of this gamma ray is estimated to be 4.2%±1.0% of K'_{β_1}, using coincidence counting techniques.

The error in the K_β/K_α ratios reflects a 1 percent uncertainty in the ratio C_{K_i}/C_{K_j} and a maximum error of 1 percent in the ratio $\varepsilon_{K_j}/\varepsilon_{K_i}$. For x-ray groups separated by greater than 10 kev, the error in $\varepsilon_{K_j}/\varepsilon_{K_i}$ is approximately 1 percent per 10 keV.

The error in the intensity ratios $K_{\alpha_2}/K_{\alpha_1}$, $K'_{\beta_1}/K_{\alpha_1}$ and $K'_{\beta_2}/K_{\alpha_1}$ includes an uncertainty of approximately 3 percent due to a small amount of overlap of K_{α_2} and K_{α_1} and of K'_{β_1} and K'_{β_2}. At Z = 96 the detection efficiency

†W. D. Schmidt-Ott (private communication, 1971); details of this correction and the results from the Cf^{249} decay scheme study to be presented at Washington meeting of the American Physical Society, Apr. 26-29, 1971.

Table 3. Relative K X-ray Intensities from the Present Work

Nuclide	Daughter	Ratio	Measured Values		
			Ge(Li)-II	Ge(Li)-III	Si(Li)-I
$_{25}Mn^{54}$	$_{24}Cr^{54}$	K_β/K_α			0.1135±0.0023
$_{27}Co^{57}$	$_{26}Fe^{57}$	K_β/K_α			0.1283±0.0025
$_{34}Si^{75}$	$_{33}As^{75}$	K_β/K_α			0.1440±0.0029
$_{39}Y^{88}$	$_{38}Sr^{88}$	K_β/K_α	0.1745±0.0035		0.1720±0.0035
$_{48}Cd^{109}$	$_{47}Ag^{109}$	K_β/K_α	0.2100±0.0042	0.2143±0.0064	
$_{47}Ag^{110m}$	$_{47}Ag^{110}$	K_β/K_α	0.2100±0.0042		0.2130±0.0084
$_{53}I^{125}$	$_{52}Te^{125}$	K_β/K_α	0.2300±0.0046		
$_{55}Cs^{131}$	$_{54}Xe^{131}$	K_β/K_α	0.2345±0.0047		
$_{55}Cs^{137}$	$_{56}Ba^{137}$	K_β/K_α	0.2370±0.0048		
$_{58}Ce^{139}$	$_{57}La^{139}$	K_β/K_α	0.2435±0.0049		
$_{64}Gd^{157}$	$_{63}Eu^{153}$	K_β/K_α	0.2485±0.0050	0.2520±0.0101	
$_{66}Dy^{159}$	$_{65}Tb^{159}$	K_β/K_α	0.2485±0.0050	0.2499±0.0100	
$_{74}W^{181}$	$_{73}Ta^{181}$	K_β/K_α	0.2615±0.0052		
$_{79}Au^{195}$	$_{78}Pt^{195}$	K_β/K_α	0.2705±0.0054		

(continued)

Table 3. Relative K X-ray Intensities from the Present Work (Concluded)

Nuclide	Daughter	Ratio	Measured Values		
			Ge(Li)-II	Ge(Li)-III	Si(Li)-I
$_{80}Hg^{203}$	$_{81}Tl^{203}$	K_β/K_α	0.2795±0.0056		
$_{83}Bi^{207}$	$_{82}Pb^{207}$	K_β/K_α	0.2810±0.0056		
$_{96}Cf^{249}$	$_{94}Cm^{245}$	K_β/K_α		0.316±0.013	
$_{80}Hg^{203}$	$_{81}Tl^{203}$	$K_{\alpha_2}/K_{\alpha_1}$	0.580±0.030		
$_{80}Hg^{203}$		$K_{\beta_1'}/K_{\alpha_1}$	0.366±0.017		
$_{80}Hg^{203}$		$K_{\beta_2'}/K_{\alpha_1}$	0.101±0.005		
$_{83}Bi^{207}$	$_{82}Pb^{207}$	$K_{\alpha_2}/K_{\alpha_1}$	0.588±0.030		
$_{83}Bi^{207}$		$K_{\beta_1'}/K_{\alpha_1}$	0.363±0.017		
$_{83}Bi^{207}$		$K_{\beta_2'}/K_{\alpha_1}$	0.103±0.005		
$_{96}Cf^{249}$	$_{94}Cm^{245}$	$K_{\alpha_2}/K_{\alpha_1}$	0.626±0.006		
$_{96}Cf^{249}$		$K_{\beta_1'}/K_{\alpha_1}$	0.380±0.014		
$_{96}Cf^{249}$		$K_{\beta_2'}/K_{\alpha_1}$	0.133±0.010		

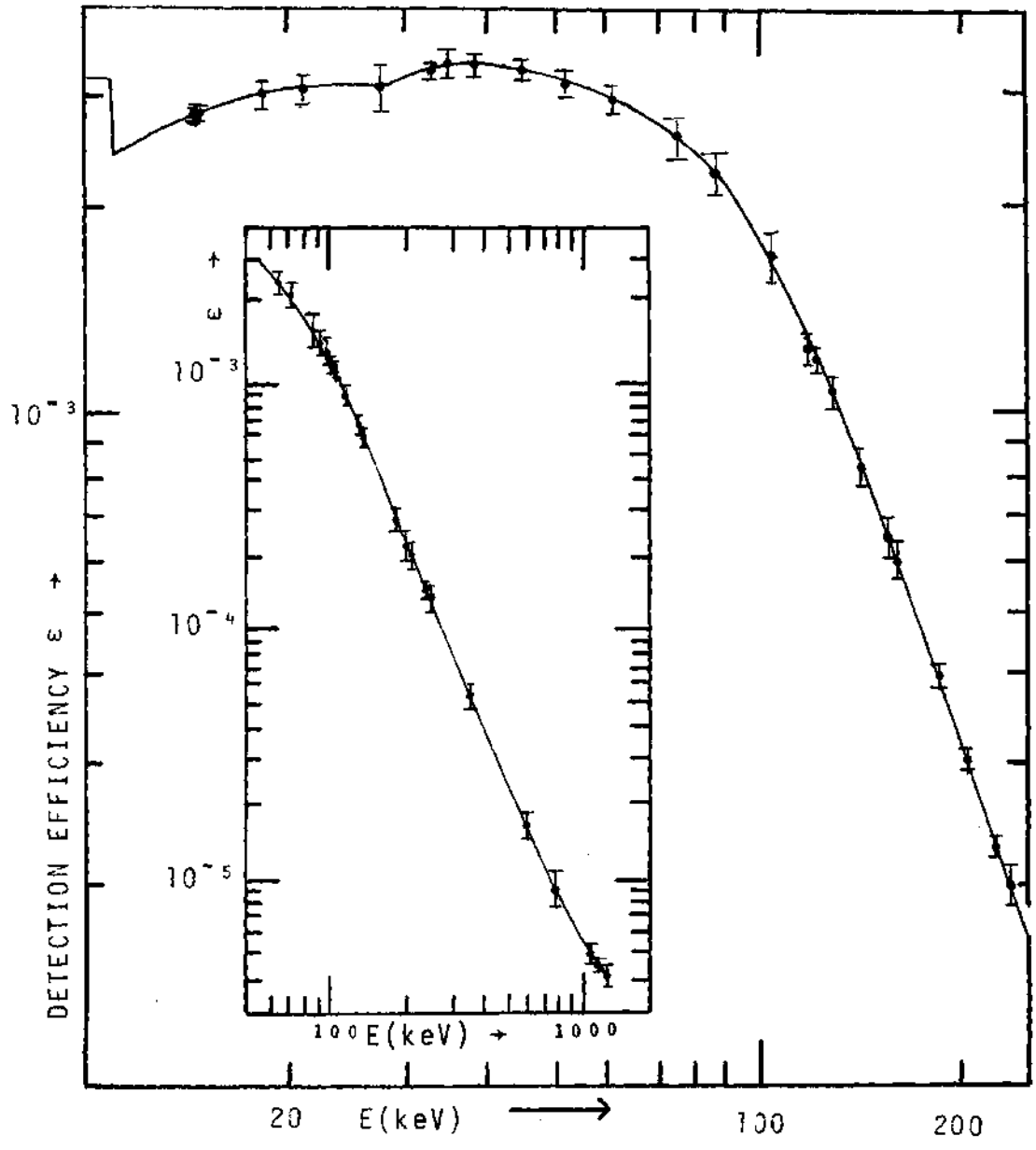

Fig. 10. Detection Efficiency Curve for Ge(Li)-III. (Change in slope at approximately 30 keV is due to aluminum collimation. Sec.3.3.1. Source to detector distance - 30 mm.)

curve (Fig. 10) is entirely dependent upon the experimental efficiency values. An error of 2 percent per 10 keV separation between the measured peaks was estimated.

CHAPTER IV

MEASUREMENT OF K-FLUORESCENCE YIELDS AT HIGH Z

The study of certain K x-ray intensity ratios, while giving information which may be compared directly to theoretical results, is void of any information concerning the absolute emission rates (transition probabilities). The rapid decay rates of the K-shell vacancies, 10^{-17} - 10^{-14} seconds, prohibits the measurement of transition rates by conventional timing techniques, as are often employed in the measurement of lifetimes of metastable nuclear states. The total rate of decay of a state is directly proportional to the natural width of the emitted K x-ray line (Eqn. 2-3); thus, in principle, the total decay rate of a state may be deduced from natural line width measurements, as has been done recently by Nelson, John and Saunders[31]. On the other hand, knowledge of the K-fluorescence yield and the total rate of emission of a particular state allows one to deduce the fraction of the decay process which goes by radiative or nonradiative decays.

For these reasons, the measurement of the K-fluorescence yield is valuable; studies at high Z are particularly important because

(1) Very few accurate measurements have been made in

this region.

(2) Of the few precision measurements made, none agree with the most recent theoretical values[5] or with the best semi-empirical predictions[93].

(3) Using the findings of Nelson, John and Saunders[31], an estimate of the nonradiative lifetime of the singly-ionized K shell may be made.

There are two direct experimental approaches for determining the K-shell fluorescence yield ω_K. Either the fraction of K vacancies filled radiatively is measured by K x-ray counting methods, or the fraction of K vacancies filled by nonradiative transitions is measured by K-Auger electron counting methods. A survey of experimental techniques for measuring to $\leq$1 percent accuracy K fluorescence yields at high Z is given below. The discussion is limited to techniques utilizing semiconductor x-ray detectors at high Z; a comprehensive discussion of published methods for measuring x-ray fluorescence yields will be given in the review of Bambynek, et al.[33].

4.1. Methods for the Measurement of K-fluorescence Yields at High Z Utilizing Semiconductor Detectors

Coincidence techniques can be employed to determine the number of K x rays coincident with a K vacancy by gating with K-conversion electrons[94] or with gamma rays[95,96]

which indicate the creation of a K vacancy, and counting the absolute emission rate of K x rays. Techniques based on gamma gating involve uncertainties associated with P_K, the probability of K-electron capture, or with the ratio $\frac{\alpha_K}{1 + \alpha_T}$, the fraction of transitions depopulating a nuclear level by internal conversion in the K shell. The application of the gamma gating technique to accurate measurements of the K-fluorescence yield is thus limited to nuclides in which P_K and the ratio $\frac{\alpha_K}{1 + \alpha_T}$ are well known. Cases in which this method has been developed are Mn^{54} (Bambynek[95]), using a 4π high-pressure proportional counter and I^{125} (Karttunen[96]) with a Ge(Li) coincidence experiment.

The technique which involves the counting of K x rays in coincidence with K-conversion electrons is suited to a wide variety of cases because of the many nuclides which undergo beta- or alpha-decay to an excited state in the daughter nucleus, which deexcites with K-shell conversion.

In the absence of K-K cascades, that is the production of K vacancies coincident with the ejected K conversion electron, the K-fluorescence yield, ω_K, is given by

$$\omega_K = \frac{C_{Kx}(eK)/\epsilon_{Kx}}{C_{eK}} \qquad (4\text{-}1)$$

The notation used here and in the following equations is ε_{Kx}, denoting the detection probability for the K x rays, and $C_{Kx}(eK)$, the counting rate of the K x-ray spectrum gated by K-conversion electrons. The quantity C_{eK} is the counting rate of K-conversion electrons in the coincidence gate. In the presence of K-K cascades, one must account for supplementary K-vacancy production, coincident K-electron capture, or internal conversion. Any of these may lead to significant corrections, whereas internal K-shell ionization by emitted beta or alpha particles is normally negligible.

The resolution of cooled Si(Li) or Ge(Li) detectors with thin entrance windows (<25 mg/cm^2) is adequate for resolving electron lines separated by more than 25 keV for electron energies greater than approximately 500 keV. Present state-of-the-art cooled Si(Li) detectors with entrance windows <5 mg/cm^2 are capable of resolving K and L conversion electrons above 500 keV for $Z \gtrsim 25$; thus K-fluorescence yields may be measured over an extended range in Z by application of this technique. Such a coincidence method has been used in the determination of ω_K at $Z = 33$ by J. Kyles, et al.[94] using a proportional counter and a thin NaI(Tl) for the gate and K x-ray detectors, respectively. In the above coincidence techniques, that is, either gating on K-conversion electrons or gating on gammas

which signal the creation of a K vacancy, the primary uncertainty is normally associated with the error in the detection efficiency of the K x-ray detector.

At high Z, where the K-fluorescence yield is large, a relatively crude measurement of the K-Auger electron yield, a_K, leads to an extremely accurate determination of ω_K, since

$$\omega_K = 1 - a_K \tag{4-2}$$

For example, in the high Z region where $\omega_K > 0.9$, a 10 percent measurement of a_K determines the value of ω_K to <1 percent accuracy.

The K-Auger yield a_K may in principle be determined by using coincidence techniques which involve the measurement of coincidences between K-Auger electrons and K-conversion electrons, i.e.

$$a_K = \frac{C_{KA}(eK)/\varepsilon_{KA}}{C_{eK}} \tag{4-3}$$

where $C_{KA}(eK)$ and ε_{KA} are the coincidence counting rates and efficiency of K-Auger electrons and C_{eK} is the K-conversion electron counting rate in the coincidence gate.

This method potentially should yield very accurate determinations of ω_K at high Z, but requires a

coincidence system composed of a "windowless" Auger electron detector. Applications of this method to the measurement of K-fluorescence yields have not been reported in the literature to date.

A new method, developed in the present investigation, does not require coincidences in order to signal creation of a K-vacancy but instead takes advantage of the capability of a windowless, cooled Si(Li) detector to measure in the singles mode K-Auger electrons and K x rays simultaneously. the K-fluorescence yield is found from

$$\omega_K = 1 - I_{KA}/(I_{KA} + I_{Kx}) \qquad (4\text{-}4)$$

where $I_{KA} = C_{KA}/\varepsilon_{KA}$ and $I_{Kx} = C_{Kx}/\varepsilon_{Kx}$ are the respective intensities of the K-Auger electrons and K-x rays. This method is particularly versatile since the manner in which the K vacancies are produced is unimportant and it can be used in the presence of K-K cascades; thus, electron-capture nuclides, as well as alpha- and beta-decaying nuclides, are suitable for measurement. Calibration of the electron and photon detection efficiencies may be made simultaneously by use of nuclides with gamma transitions below approximately 200 keV.

This method may also be applied directly to the determination of K-conversion coefficients since, for

example,

$$\alpha_K = I_{ek}/I_\gamma \qquad (4\text{-}5)$$

where I_{ek} and I_γ are the respective intensities of the K-conversion electron and its associated gamma ray, and α_K is the K internal conversion coefficient. Because of the relatively flat detection efficiency curve (Fig. 11) for electrons exhibited by the Si(Li) detector, the measurement of conversion coefficient ratios requires no large corrections for differing detection efficiencies. The major disadvantage of this method is the requirement of thin, uniform sources and of a windowless Si(Li) detector, in order to ensure essentially 100 percent electron transmission.

A discussion of the development and limitations of this method, followed by a description of its application to the determination of ω_K values at $Z = 78$ and $Z = 82$ follows.

4.2. Preliminary Investigation of a New Singles Method for Measuring ω_K at High Z With Room-temperature Windowless Si(Li) Detectors

The measurement of ω_K using a windowless Si(Li) detector may in principle be accomplished with a room-temperature semiconductor device. The advantage in using a

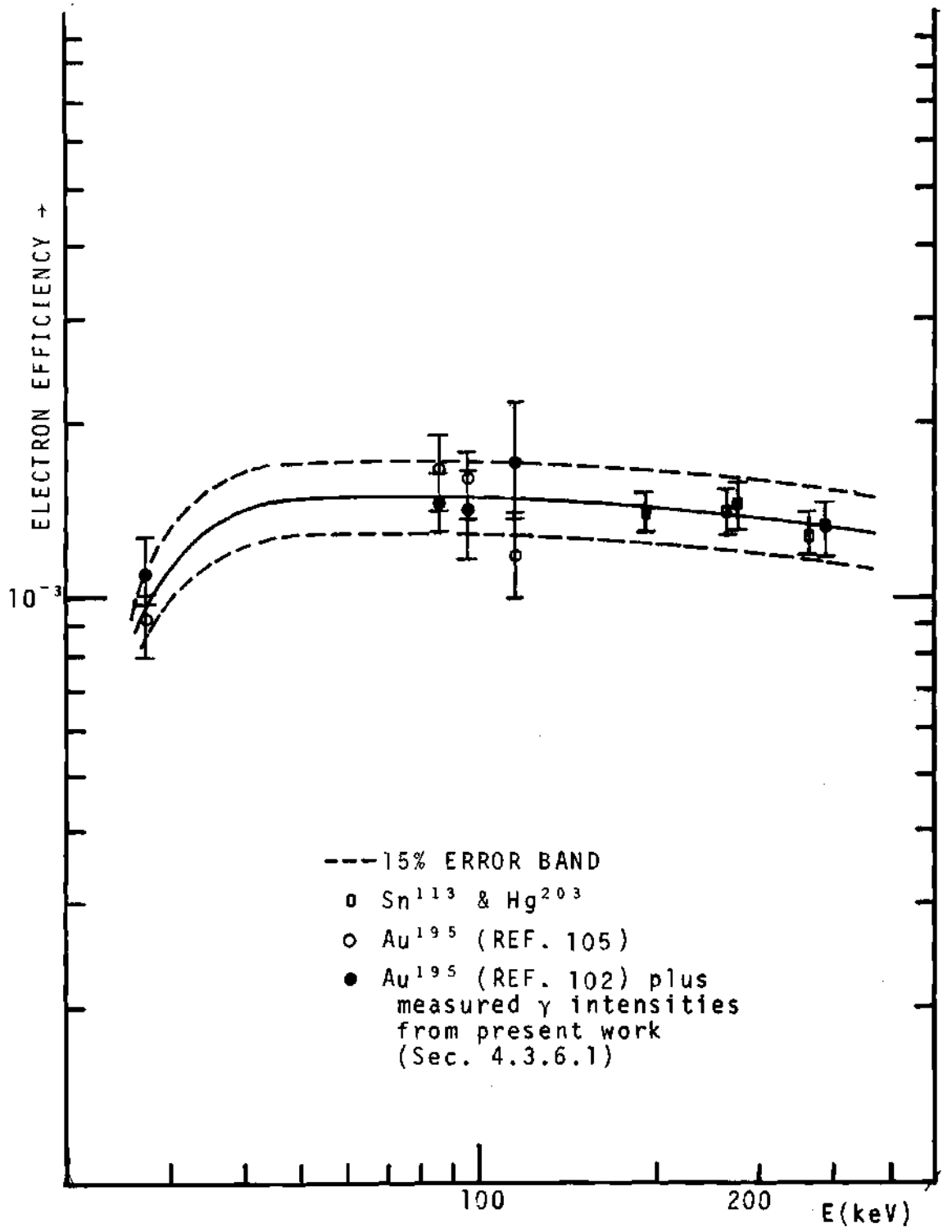

Fig. 11. Electron Efficiency Curve for Si(Li)-II. (Sharp decrease in efficiency at low energies is due to source self-absorption and finite window thickness of detector.)

room-temperature device is that the exposure of the detector to the atmosphere is not harmful, therefore alleviating the need for a sophisticated vacuum lock. Preliminary feasibility studies of this method were undertaken using a thin, room-temperature, surface barrier silicon detector; a 2 mm-thick room-temperature Si(Li) detector also was considered but was rejected for reasons detailed below.

The room-temperature, surface-barrier Si(Au) detector was a conventional, high resolution (13.7 keV FWHM at 100 keV) alpha detector (ORTEC 50-100) with a depletion depth of 100μ at a bias voltage of approximately 50 V, operated in a vacuum of 10^{-3} Torr. A TC-100-C tube-type preamplifier and a TC-200 main amplifier provided a uniform pulse with a risetime and a decay time of approximately 2 μsecs each, to the Nuclear Data (ND-180) 512-channel analyser. Drop-evaporated sources of Hg^{203}, Bi^{207}, Sn^{113}, Cs^{137}, Au^{195} and Ce^{141} were mounted in a vacuum (10^{-3} mm Hg) approximately 2 cm from the detector face. Three major disadvantages in the use of this particular type of detector for the measurement of ω_K at high Z were found. First, the detector was much too thin to stop the high-energy conversion electrons present in the decay of the above isotopes. Over a wide range in energy, ≈300 keV, the conversion electrons deposited only a portion of their energy, dependent upon the differential energy loss of the incident electrons

in the 100μ detector. This resulted in a broad peak between 30 and 100 keV, i.e. the thin detector acted as a dE/dx detector for high-energy conversion electrons. The broad energy peak, often an order of magnitude higher in intensity than the expected Auger electron peak intensity, prohibited accurate evaluation of the electron spectra in the energy region below 100 keV.

The second limitation associated with the use of a room-temperature detector of this type for low-energy electron spectroscopy (<100 keV) arises from the electronic noise of the detector-amplifier combination. In order to avoid paralysis of the ND-180 analyser the discriminator threshold (lower level discriminator) of the ND-180 had to be set at ≈3.0 × resolution (FWHM) at ≈100 keV. For the particular detector-amplifier combination used in these measurements, the resolution at 100 keV was 13.7 keV FWHM, consequently the discriminator threshold had to be maintained at approximately 40 keV. This effect seriously thwarted any attempt to determine the electron efficiency for low-energy electrons or to observe K-Auger electron spectrum below ≈45 keV (Z = 75).

The final limitation in the use of a thin, surface-barrier detector for this method is its particular insensitivity to photons of energies above approximately 15 keV, i.e. the intrinsic photon efficiency (excluding

solid angle) for a 100 μ (0.1 mm) thick Si detector is only 0.3 percent at 60 keV. Energy calibrations of the detector and absolute determinations of the K x-ray intensities (I_{Kx}) are therefore difficult.

Two of the above disadvantages of ω_K measurements with a room-temperature silicon detector can be avoided by use of a thick (>2 mm) silicon detector such as that used for electron spectroscopy. The range of 1 MeV electrons in silicon is less than 2 mm and thus even very high energy electrons deposit energy considerably above the K-Auger electron region. The intrinsic photon efficiency of a 2 mm silicon detector at 60 keV is approximately 7 percent; thus accurate energy calibration and K x-ray intensity measurements are feasible. The apparent limiting factor in the use of a thick detector of this type results from low-energy noise associated with the detector-amplifier combination. A typical 2 mm-thick, high-resolution room-temperature Si(Li) detector (ORTEC), combined with a TC-100-C preamplifier and TC-200 main amplifier, was low-level noise-limited at approximately 60 keV and thus was inadequate for the measurement of K-Auger electron spectra. The cooling of a detector of this type should, in principle, decrease the bulk leakage current and thus significantly minimize the noise. The manufacturer, however, recommends that this particular device not be cooled below 0° C

because of the different thermal coefficients of expansion of the silicon detector and its casing.

The availability at Emory University of a liquid nitrogen-cooled windowless Si(Li) x-ray detector permitted the measurement of the K-fluorescence yields at $Z = 78$ and $Z = 82$ by the present singles method. This device and its application to the measurement of ω_K are discussed in the remainder of the present chapter.

4.3. Application of a Cooled Windowless Si(Li) Detector to the Measurement of ω_K at High Z

Preliminary feasibility studies of the singles method described above for the measurement of K-fluorescence yields at high Z using a windowless silicon detector disclosed several important considerations. The onset of noise in room-temperature silicon detectors typically occurs in the K-Auger electron region, thus interfering with measurement of K-Auger electron spectra except at the very highest Z. The use of a thin detector (0.1 mm) in the presence of high energy conversion electrons gives rise to broad peaks, resulting from a fractional deposition of the total energy of the incident electrons. The efficiency of thin silicon detectors is very low for photons with energies above approximately 25 keV, thus absolute determinations of photon intensities is difficult. Thicker room-temperature silicon detectors typically have even greater noise limitations

than the thin surface-barrier detectors, hence are not suited for low-energy electron spectroscopy.

The use of a liquid nitrogen cooled, windowless Si(Li) detector avoids each of the above problems, thus is ideal for the measurement of high Z K-fluorescence yields. A description of such a system and its application to the measurement of the K-fluorescence yields, ω_K, at Z = 78 and Z = 82 follows.

4.3.1. Description of the Electron Detection System and Electronics

The detection apparatus, Fig. 12, used in this study consists of a conventional 2 mm × 30 mm^2 Si(Li) x-ray detector, Si(Li)-II, mounted within a liquid nitrogen-cooled, vacuum cryostat. A cooled FET, charge-sensitive preamplifier and active-filter main amplifier TC-200 provided a singly differentiated voltage pulse with rise and decay time of 2 μsec to the input of the TMC 1024-channel pulse height analyser. A 3-inch gate valve permits the internal mounting of radioactive sources at distances between 0.5 cm and 4 cm from the Si(Li) detector[97]. The detector photon resolution was measured to be 450 eV FWHM at 14.4 keV and 800 eV at 75 keV. The degradation of the incident electron energy in the thin Si-Au entrance window (≈0.2 mg/cm^2) resulted in an approximately 200 eV FWHM broadening of electron lines at 100 keV. A nominal

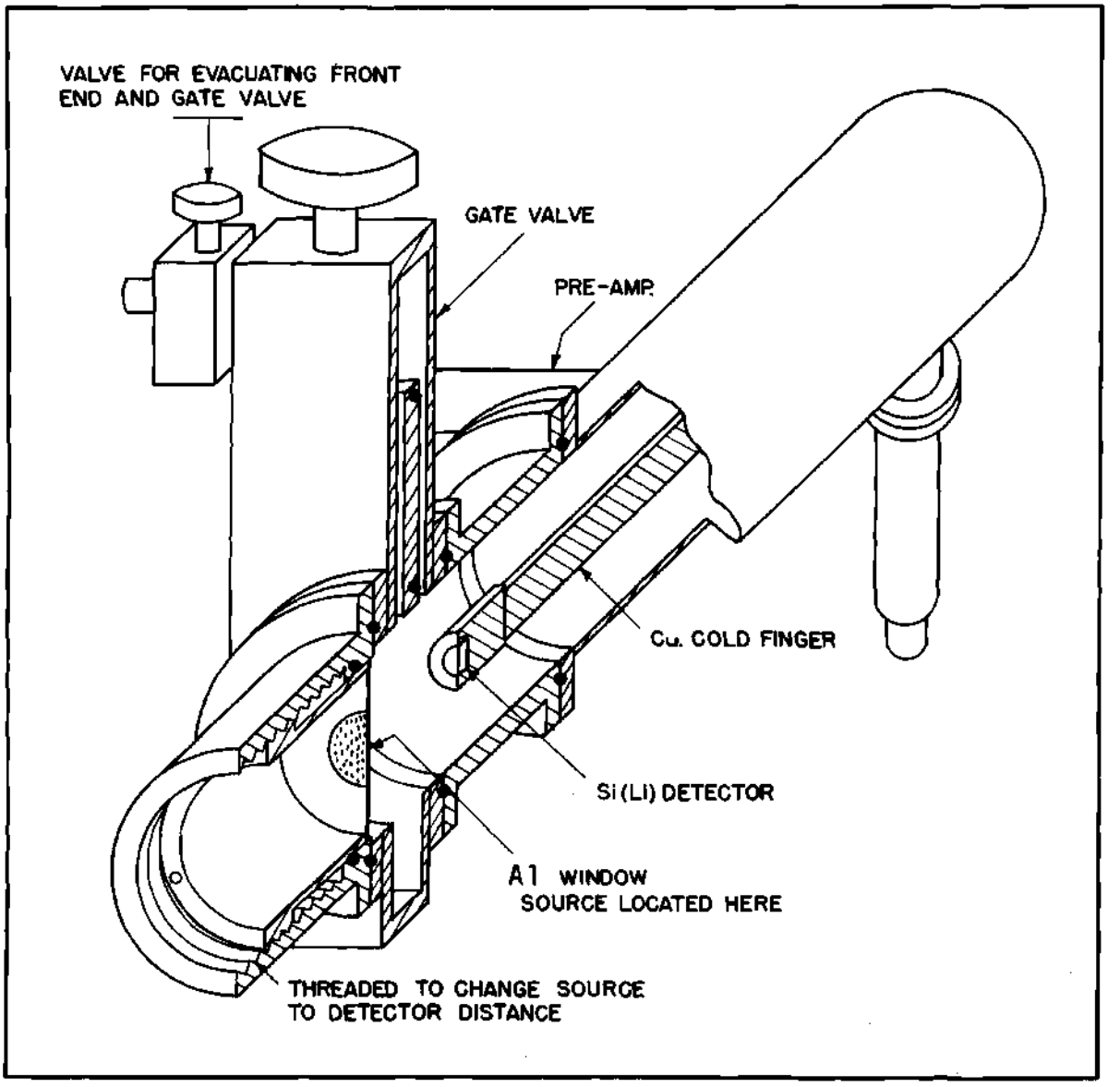

Fig. 12. Detection Apparatus Used in the Measurement of High Z ω_K

source thickness of $\simeq 0.3$ mg/cm^2 resulted in a further broadening of electron peaks of approximately 250 eV FWHM at 100 keV.

4.3.2. Preparation and Calibration of Radioactive Sources

The Au^{195} source and the sources used in the electron efficiency calibration of the Si(Li) detector were all prepared by drop evaporation of carrier-free solutions on 0.025 mm Mylar. The total amount of solids in each source was less than 50 μg and the average source thickness was restricted to less than 300 μg/cm^2. A microscope was used to examine each source to ensure that crystal formations which might significantly absorb the emitted electrons were absent. The Bi^{207} source, prepared for electron spectroscopy, was mounted on 0.005 mm Mylar and had an average thickness of 60 μg/cm^2.

The sources were generally fixed to the inside face of the 3 mm-thick aluminum entrance window at a distance of 4.0 cm from the face of the Si(Li) electron detector. Variations in the source-to-detector distance were no greater than 0.5 mm. However, the Bi^{207} source-mount was fixed to a 3 mm Lucite plate which in turn was fixed to the aluminum entrance window, in order to provide saturation backscattering for high-energy conversion electrons. A correction was made for this decreased source-to-detector distance relative to the calibration sources. There was

little effective change in the backscattering of the low-energy Auger electrons from Bi^{207} decay relative to the 0.025 mm Mylar-backed calibration sources.

In order to obtain the electron detection efficiency curve, Fig. 11, it was necessary to determine the electron emission rates of several sources having conversion electron lines in the energy region below 300 keV. The x-ray and gamma-ray emission rates of these calibration sources were measured with a Ge(Li) detector of accurately known photon detection efficiency (Fig. 10). The electron emission rates were then calculated using the conversion coefficients listed in Table 4.

4.3.3. Measurement and Interpretation of the Electron Spectra

A typical Bi^{207} spectrum taken with the windowless, cooled Si(Li) detector is shown in Fig. 13. The resolution is sufficient to resolve the K-LL and K-LX Auger electron groups. The low-intensity K-XY group in the energy region between the K_α and K_β x rays, was barely detectable. The K and L x rays provide an excellent means for energy calibration, allowing measurement of the degree of K-Auger electron energy degradation arising from source self-absorption and the finite thickness of the entrance window.

A typical Au^{195} spectrum is shown in Fig. 14 with and without filtration by a 390 mg/cm^2 Lucite absorber.

Table 4. Conversion Coefficients Used in the Calibration of Si(Li)-II

Nuclide	Gamma Energy (keV)	Shell	Electron Energy	Conversion Coefficients	
$_{80}Hg^{203}$	279.1 keV	K	193.6 keV	0.163±0.002[a]	
		L	263.2 keV	0.048±0.003[b]	
		M+N+ . . .	275.4 keV	0.014±0.001[b]	
$_{50}Sn^{113}$	393 keV	K	365 keV	0.438±0.008[c]	
		L+M+ . . .	389 keV	0.100±0.007[b]	
$_{79}Au^{195}$	30.8 keV	M+N+ . . .	27.5 keV	8.7 ±1.0	(7.6 ±1.1)
	98.8 keV	L	84.9 keV	0.82 ±0.07[d]	(0.92±0.09)[e]
	98.8 keV	M+N+ . . .	95.5 keV	0.247±0.021	(0.27±0.03)
	129.8 keV	L	126.8 keV	1.06 ±0.10	(0.73±0.13)

(a) From Ref. 98, Table 9, p. 565.
(b) From Ref. 98, 5% error assumed for K/L, and K/L+M . . .
(c) From Ref. 98, Table 9, p. 565.
(d) Measured values from Ref. 105.
(e) Values determined by normalizing to Hager and Selzer (Ref. 106) for L conversion coefficient for 98.8 gamma; other values in parenthesis determined using the measured relative intensities of Toburen. Nakai and Langley (Ref. 102) and measured gamma intensities in present work of 7.08±0.35, 100±3, and 7.64±0.38 for 30.8, 98.8 and 129.8 keV lines, respectively.

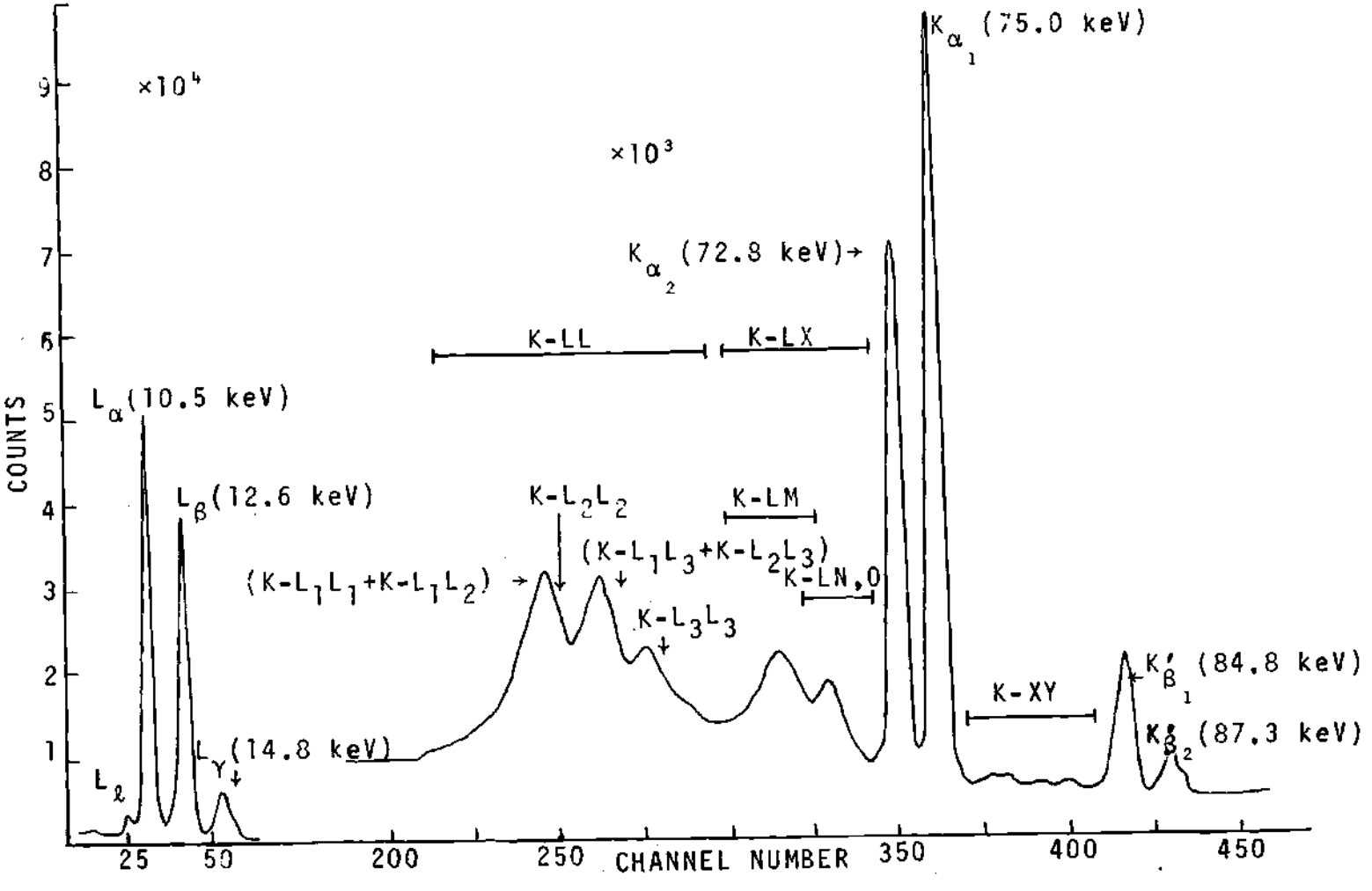

Fig. 13. Bi^{207} Electron and X-ray Spectrum With Si(Li)-II. (Composite spectra [electron and x-ray] permits a simple and accurate determination of quantities such as the K-fluorescence yields and internal conversion coefficients.)

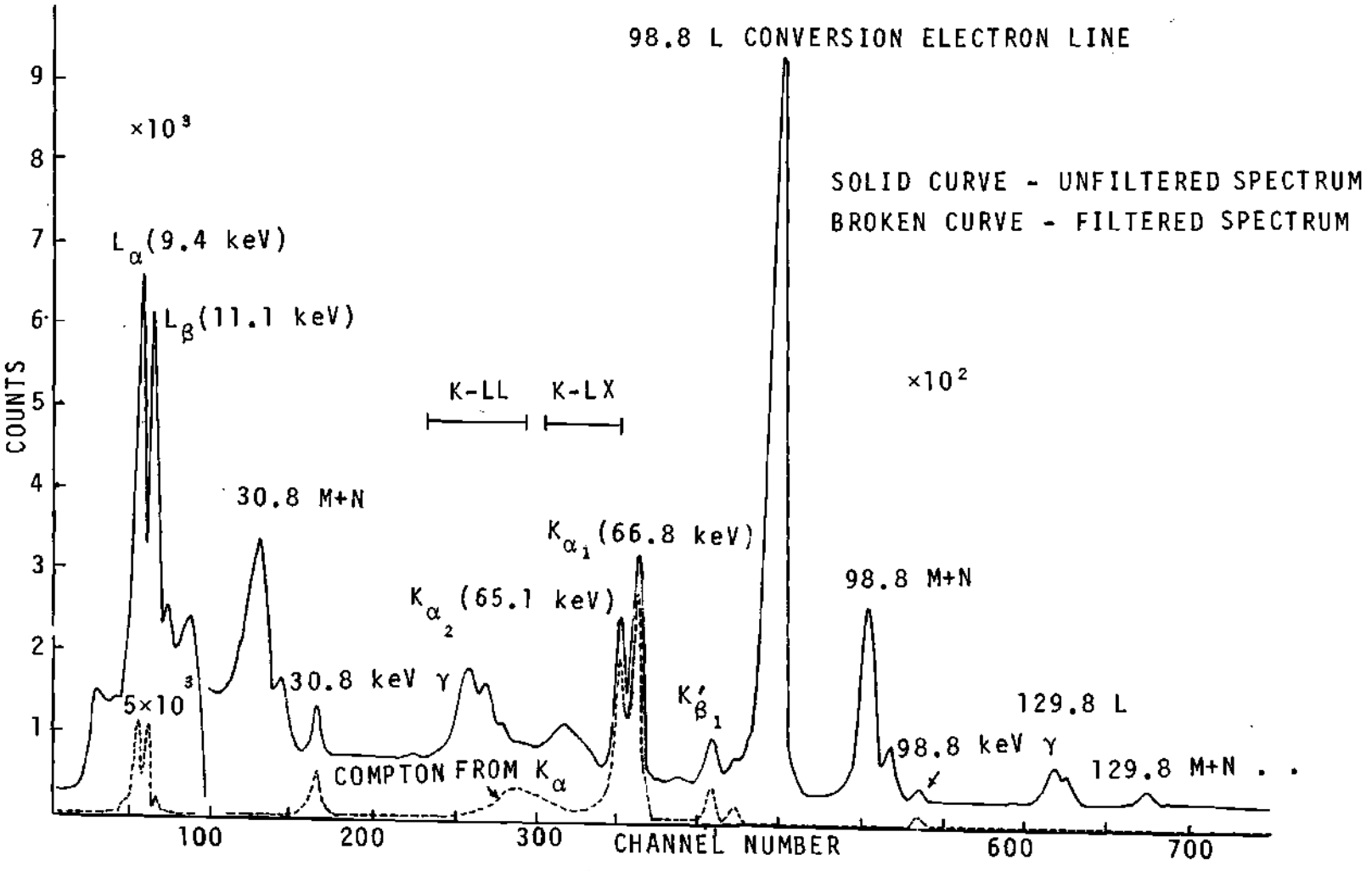

Fig. 14. Typical Au^{195} Spectra, Filtered and Unfiltered, Taken With Si(Li)-II. (Solid curve has been raised slightly to display photon peaks in filtered spectrum.)

The spectrum with filtration, normalized to the unfiltered K_α x-ray intensity, has a broad pronounced peak in the energy region between the K-LL and K-LX Auger electron groups. This peak results primarily from Compton scattering of the K_α x rays from the gate valve and from the inner face of the 3 mm-thick aluminum window. The magnitude of the correction of the K-Auger electron intensities for this effect was 21 percent for Au^{195} and 25 percent for Bi^{207} but could be accurately estimated from the filtered spectra (Sec. 4.3.6.1).

Integration of the K-Auger electron spectra (Figs. 13, 14) was done graphically, using a linear interpolation between the continuum on the left and right sides of the K-Auger electron groups. Integration of K x-ray groups and of isolated conversion electron groups was done numerically using a computer program which describes the continuum beneath the peaks in terms of step functions positioned at the centroids of the individual lines making up a particular multiplet. The height of each step function is proportional to the intensity of the line relative to the total intensity of the multiplet. In order to assure consistency between the graphical and the numerical methods of integration, the K_α x ray and the M + N + O . . . conversion group of unresolved lines of the 99 keV transition in Au^{195} decay were computed, using

both methods. Agreement in both cases was found to be better than 1 percent.

4.3.4. Consideration of Summing Effects Upon the Measured Counting Rates

The effects of chance summing (Sec. 3.4) are negligible due to distant geometry and low counting rates. The effects of coincidence summing (Sec. 3.4) are likewise negligible as seen by following this line of reasoning:

Consider for simplicity a decay scheme with two transitions in cascade which do nothing but make K vacancies. In the absence of summing the counting rates of K x rays and K-Auger electrons will be

$$C_{Kx} = 2N_0 \omega_K \varepsilon_{Kx} \tag{4-6}$$

and

$$C_{KA} = 2N_0 \ (1-\omega_K) \varepsilon_{KA} \tag{4-7}$$

respectively, where C_{Kx} and C_{KA} are the respective counting rates of the K x rays and K-Auger electrons; N_o is the disintegration rate (in this case 100% production efficiency of K vacancies assumed); ω_K is the K-fluorescence yield; and ε_{Kx} and ε_{KA} the respective detection efficiencies for K x rays and K-Auger electrons. Given a detected K x ray, the probability for summation and therefore loss of the count in the K x-ray peak, is:

$$P_{Kx-K} = \omega_K \varepsilon_{Kx} + (1-\omega_K)\varepsilon_{KA} \qquad (4\text{-}8)$$

where the first term gives the probability that the second event is a K x ray; the second the probability that it is a K-Auger electron.

However, the probability of summation following a detected K-Auger event, P_{KA-K}, is also given by the same expression:

$$P_{KA-K} = \omega_K \varepsilon_{Kx} + (1-\omega_K)\varepsilon_{KA} \qquad (4\text{-}9)$$

Clearly, the fractional loss from the main peaks due to summing is independent of the nature of the primary event, i.e. the fractional loss is identical for the K x rays and the K-Auger electrons. Since the expression (from Eqn. 4-4)

$$\omega_K = \frac{1}{1 + I_{KA}/I_{Kx}} \qquad (4\text{-}10)$$

involves only the intensity ratio I_{KA}/I_{Kx}, no correction is necessary, since

$$(I_{KA}/I_{Kx})_{\text{observed}} = \frac{\varepsilon_{Kx}}{\varepsilon_{KA}} \quad \frac{C_{KA}(1 - P_{KA-K})}{C_{Kx}(1 - P_{Kx-K})} = I_{KA}/I_{Kx} \qquad (4\text{-}11)$$

In the present measurements, the summing effect is

very small, since $\varepsilon_{KA} \approx 1.3\times10^{-3}$ and $\varepsilon_{Kx} \approx 7\times10^{-4}$. Thus, no sum peaks were observed.

The summing possibility that does not cancel completely arises from summing of K and L x rays (Sec. 3.3). However, the ratio of sum peaks/main peak is about 0.1%, completely negligible with relation to the approximate ±20% accuracy in I_{KA}/I_{Kx}.

4.3.5. Correction for Absorption in Source and Window

Because of finite source and window thickness, it is necessary to estimate the fraction of incident electrons which are sufficiently degraded in energy to appear in the degradation tail below the region of peak integration. The magnitude of this effect was evaluated in the following manner: the energy shift of the electron peaks was measured using the K and L x rays and gamma rays available in the decay for energy calibration. The energies of the conversion lines were computed using electron binding energies and gamma ray energies from Lederer, Hollander and Perlman[98]. The K-Auger electron energies were taken from Siegbahn[99]. A correction of 0.9 keV to each of the measured energy shifts was necessary, since the Si(Li) detector operated at -900 V bias, i.e. the Si(Li) detector face was 900 volts beneath ground.

The equivalent Si thickness which would produce the measured energy degradation for each conversion line was

then determined using the relativistic Bethe-Bloch[99] expression for the mean energy loss per centimeter of path:

$$-\frac{\overline{dE}}{dx} = 0.153\,\frac{\rho Z}{A}\,\beta^{-2}\left[\ln\frac{E(E+m_0c^2)^2\beta^2}{2I^2m_0c^2} + (1-\beta^2) - (2\sqrt{1-\beta^2} - 1 + \beta^2)\ln 2 + \frac{1}{8}(1-\sqrt{1-\beta^2})^2\right] \text{MeV/cm} \qquad (4\text{-}12)$$

where $\rho(\text{Si}) = 2.33$ g/cm^3; $Z/A\ (\text{Si}) = 0.5$; $\beta = v/c$; E = kinetic energy of electrons; $m_0c^2 = 0.511$ MeV; $I_{(\text{Si})} = 157$ eV.

Since the actual measured quantity, the energy shift of the channel corresponding to maximum peak height indicates most probable energy loss rather than the calculated mean energy loss, a slight correction was necessary using the Landau[100] distribution which describes the integral probability for an energy loss to exceed the most probable energy loss. The correction to the equivalent Si thickness ranged from 9.5 percent at 100 keV to 12 percent at 20 keV. The corrected equivalent Si thickness of the source-plus-detector window found in this manner was 0.48 mg/cm^2 and 0.43 mg/cm^2 for Au^{195} and Bi^{207}, respectively. By interpolating the results of Lane and Zaffarano[101] for transmission of monoenergetic incident electrons through aluminized Formvar films, a transmission greater than 95 percent for 50 keV electrons through an equivalent Si

thickness of 0.5 mg/cm^2 is predicted. In the present work not all of the degradation tail is included in the total peak integration, as was the case in the Lane and Zaffarano study; thus, an estimate of the fraction of electrons excluded from the integration is necessary. For monoenergetic electrons with an initial energy of 50 keV, the fraction of electrons present in the degradation tail beneath the lower limit of integration in this work is predicted by the Landau[100] distribution to be less than 5 percent.

The combined results of the Lane and Zaffarano[101] findings and the Landau[100] predictions can be used to deduce the shape of the intrinsic electron efficiency curve. Accepting an equivalent Si thickness of 0.48 mg/cm^2 the intrinsic electron efficiency at 25 keV (excluding solid angle) is predicted to be 70 percent, rising rather abruptly to 90 percent at 35 keV and then increasing very slowly to 100 percent at higher energies. These predictions agreed within experimental uncertainty with the present findings in the energy region between 25 and 300 keV.

4.3.6. Evaluation of the Experimental Results and Error Analysis

The K-fluorescence yield, ω_K, is computed in this experiment directly from measured K-Auger electron

intensities, I_{KA}, and measured K x-ray intensities, I_{Kx}:

$$\omega_K = 1 - \frac{I_{KA}}{I_{KA} + I_{Kx}} = 1 - \frac{C_{KA}/\varepsilon_{KA}}{C_{KA}/\varepsilon_{KA} + C_{Kx}/\varepsilon_{Kx}} \qquad (4\text{-}13)$$

where C_{KA} and C_{Kx} are the measured K-Auger electron and K x-ray counting rates, respectively. The quantities ε_{KA} and ε_{Kx} are the mean K-Auger electron and K x-ray detection probabilities, respectively. The magnitude of these quantities and the associated errors are given in Table 5. A discussion of each of the quantities in Eqn. 4-13 follows below.

4.3.6.1. Determination of the K-Auger Electron Intensity. The total K-Auger electron counting rate, C_{KA}, for Au^{195} is given by:

$$C_{KA} = [C'_{KA} - C_S - C_{eK(129)}] \; [1 + R] \qquad (4\text{-}14)$$

where C'_{KA} is the total measured uncorrected Auger count; C_S is the counting rate associated with Compton scattering; $C_{eK(129)}$ is the counting rate in the Au^{195} K-Auger electron spectrum due to unresolved K-conversion electrons from the 129-keV transition in Au^{195} decay; and $R = \frac{\text{K-XY}}{\text{K-LL} + \text{K-LX} + \text{K-XY}}$ is the ratio of the K-XY Auger electron group intensity to the total K-Auger electron intensity. The equivalent

Table 5. Experimental Data from K-fluorescence Yields Measurements

	Au^{195}	Bi^{207}
C'_{KA} (sec^{-1})	0.4518±0.0151	10.94±0.25
C_S (sec^{-1})	0.0972±0.0026	2.742±0.063
$C_{eK(129)}$ (sec^{-1})	0.0362±0.0036	—
R	0.059±0.006	0.059±0.006
ε_{KA}	$1.44\ 10^{-3}$±0.216×10^{-3}	†1.48×10^{-3}±0.222×10^{-3}
C_{KA} (sec^{-1})	0.3372±0.0215	8.69±0.30
I_{KA} (sec^{-1})	234.3±47.9	5862±998
I_{KX} (Si) (sec^{-1})	6708±335	2.002×10^4±1002
I_{KX} (Ge) (sec^{-1})	7036±275	—
ω_K	0.967±0.008	0.972±0.008

†A 14.3% correction was made to both the electron and photon efficiencies owing to a decreased source-to-detector distance (see Sec. 4.3.1).

expression for the total K-Auger electron counting rate in the Bi^{207} measurements is the same as Eqn. 4-14 except that $C_{eK(129)} = 0$.

The quantity C'_{KA} was determined by graphical integration of the K-Auger electron spectrum in which the continuum was described by a linear interpolation between the low- and high-energy sides of the K-Auger electron multiplet. Because of the relatively flat continuum above and below the K-Auger electron multiplet, and because there is a minimal amount of tailing from the electron peaks, the error in the graphical integration is approximately 2 percent. The error in the counting statistics associated with the gross counting rate, C'_{KA}, of the K-Auger electron spectra from Bi^{207} and Au^{195} decay was 0.25 percent and 1.23 percent, respectively, where the assigned error represents twice the standard deviation, i.e. 95.5 percent confidence limit.

The ratio of the Compton scattering rate, C_S, to the K_α x-ray counting rate was determined from Au^{195} and Bi^{207} spectra filtered with 10 mg/cm^2 Mylar. The correction for Compton scattering of K_α x rays (Fig. 14) into the K-Auger electron energy region was found to be 21.5 and 25.1 percent for Au^{195} and Bi^{207}, respectively. The error in the above corrections is statistical in origin and was added quadratically with the statistical error in

the gross K-Auger electron counting rate.

The 50.4 keV K-conversion electron associated with the 129 keV transition in Au^{195} decay is not resolved from the K-Auger electron spectra and thus must be subtracted from C'_{KA}. The results of Toburen, Nakai and Langley[102] were used to estimate the ratio of the intensity of this line, $C_{eK(129)}$ to the total intensity of the unresolved K-Auger electron group:

$$\frac{C_{eK(129)}}{C_{eK(129)} + C'_{KA} - C_S} = 0.10 \pm 0.01 \qquad (4\text{-}15)$$

A final correction is necessary in order to account for the K-XY electrons, not estimated in this work. The ratio R (Eqn. 4-14) was found to be 0.059 ± 0.002 by Nall, Baird and Haynes[103] for $Z = 80$. Because of the slow variation[104] of R with Z and the relative insensitivity of ω_K to rather large (percentage) changes in R, a value of $R = 0.059 \pm 0.006$ was used in the determination of ω_K for both Bi^{207} and Au^{195}.

In order to find the intensity I_{KA} of the K-Auger electrons from the measurement of the corrected counting rate C_{KA}, it is necessary to evaluate the electron detection efficiency ε_{KA} of the Si(Li) detector. The mean K-Auger electron detection efficiency was obtained by calibrating a set of conversion electron sources. In

the energy region where source and window absorption are significant, the experimental results of Lane and Zaffarano were employed[101] to show that the electron efficiency decreases rapidly with decreasing energy below approximately 35 keV, due to increased absorption of the emitted electrons in the source and detector window. Above approximately 40 keV the effects of source and window absorption are small and can be predicted accurately using Lane and Zaffarano[101] results and the theoretical Landau[100] distribution described above. In the case of Au^{195} decay, conversion electrons with energies above and below the K-Auger electron energy region provide an internal calibration for the efficiency. The mean source thickness in the Bi^{207} source, deduced from the K-Auger electron energy degradation, was found to be less than in the case of the Au^{195} source; thus, the source and window absorption are assumed to be minor effects which are easily handled using the results of Lane and Zaffarano[101].

The gamma-ray emission rates for calibration sources of Au^{195}, Sn^{113}, and Hg^{203} were measured using a Ge(Li) detector whose efficiency is accurately known [Ge(Li)-III]. The total uncertainty in this calibration does not exceed 3 percent. The internal conversion coefficients, necessary to predict the conversion electron emission rate, have errors which range from approximately 2 percent for the

K-conversion coefficients of Hg^{203} and Sn^{113} to 10-15 percent for the conversion coefficients associated with the main transitions in Au^{195} decay at 30.8 keV, 98.8 keV and 129.1 keV. The error bars shown in Fig. 11 were obtained by linearly adding the errors in the internal conversion coefficients to the errors in the gamma-ray emission rates and the electron peak integrations, 3 percent and 2 percent, respectively. Both the conversion coefficients of Fink[105] and the relative electron intensities of Toburen, Nakai and Langley[102] were used to obtain the two sets of efficiency points plotted in Fig. 11 for the Au^{195} transitions. Using the latter results, the experimental relative electron intensities were normalized to the theoretical total L conversion coefficient of the 99 keV transition[106]. The error in each of the efficiency points found in this manner reflects a 5 percent uncertainty in the theoretical L conversion coefficient, in addition to the experimental uncertainties (≈5%), and in the relative electron intensities given by Toburen, Nakai and Langley[102] (2 - 10%).

The total estimated error of 15 percent in the mean K-Auger electron efficiency is represented in Fig. 11 by the two dashed curves above and below the solid efficiency curve which was used to obtain the K-Auger electron intensity I_{KA} from the corrected counting rate C_{KA}, since $I_{KA} = C_{KA}/\epsilon_{KA}$.

4.3.6.2. Determination of the K X-ray Intensity.

The total K x-ray intensity, I_{Kx}, in Au^{195} decay was measured with an accurately calibrated Ge(Li) detector in a standard geometry [Ge(Li)-III], in addition to the measurements with the Si(Li) electron detector. After correction for K x-ray detection efficiency, ε_{Kx}, the intensity I_{Kx} as measured by the standard Ge(Li) detection system had an uncertainty of approximately four percent, which includes the errors in the Ge(Li) calibration (2.5%), statistics (0.2%), geometry error (0.5%), peak integration (0.5%) and half-life correction (0.2%). The uncertainty of the Si(Li) measurement of the Au^{195} K x-ray intensity was approximately 5 percent. An average of these two measurements was used in the determination of the final results for ω_K at Z = 78.

The Bi^{207} source was measured only with the Si(Li) detector and in a slightly different geometry from that used for Au^{195}, being mounted on a 3-mm Lucite plate which was fixed to the inside of the aluminum window. The increase in the solid angle due to this geometry increased the overall detection efficiency by 14.3 percent. The error in the calibration of the photon efficiency of the Si(Li) electron detector was approximately 5 percent, and the error in source placement, 1 percent, yielded a total error in the Bi^{207} K x-ray intensity of 6 percent.

4.3.6.3. Final Results and Error Propogation. Table 5 summarizes the measured quantities and their respective errors involved in the measurement of ω_K for $Z = 78$ and 82 from Au^{195} and Bi^{207} decays, respectively. The error associated with the reported values of ω_K were computed under the assumption that the respective errors in C_{Kx}, C_{KA}, ε_{Kx} and ε_{KA} combined in such a fashion as to give maximum and minimum values of the measured values of ω_K. This leads to a small amount of asymmetry in the error, thus the average of the upper and lower bounds of the computed errors was assumed.

CHAPTER V

COMPARISON OF PRESENT RESULTS WITH EXPERIMENT AND THEORY

5.1. Relative K X-ray Transition Probabilities

5.1.1. Comparison of the Relative K X-ray Intensities With Experiment

Recent measurements of the K_β/K_α, $K_{\alpha_2}/K_{\alpha_1}$, $K'_{\beta_1}/K_{\alpha_1}$ and $K'_{\beta_2}/K_{\alpha_1}$ ratios have been made, in addition to the earlier work of Beckman[16] and Williams[15]. Because of improved methods and instrumentation, the recent results are the more reliable; therefore, the details of the older work are not dealt with here.† The results of the present measurements of the K_β/K_α intensity ratio are listed in Table 6, in addition to the interpolated values for each Z not measured. Fig. 15 compares the present results with other experimental measurements and it can be seen that the present results are in reasonable agreement with the other experimental work.

The measurements of the $K_{\alpha_2}/K_{\alpha_1}$, $K'_{\beta_1}/K_{\alpha_1}$ and $K'_{\beta_2}/K_{\alpha_1}$ ratios at Z = 81, 82 and 96 are compared to other recent experimental measurements in Table 7 where, also,

†An account of the earlier measurements is given by the present author in Ref. 26, in addition to a graphical comparison of the results.

Table 6. Final Results for Measured Intensity Ratio - K_β/K_α

Z	K_β/K_α	Z	K_β/K_α	Z	K_β/K_α
17	0.020 ±0.015[a]	44	0.2018	71	0.2572
18	0.0382[b]	45	0.2055	72	0.2593
19	0.0538	46	0.2091	73	0.2615±0.0052
20	0.0690	47	0.2110±0.0042	74	0.2632
21	0.0828	48	0.2155	75	0.2653
22	0.0945	49	0.2192	76	0.2671
23	0.1053	50	0.2226	77	0.2693
24	0.1135±0.0023[c]	51	0.2254	78	0.2705±0.0054
25	0.1219	52	0.2300±0.0046	79	0.2734
26	0.1283±0.0025	53	0.2319	80	0.2755
27	0.1317	54	0.2345±0.0047	81	0.2795±0.0056
28	0.1328	55	0.2367	82	0.2810±0.0056
29	0.1339	56	0.2370±0.0048	83	0.284
30	0.1352	57	0.2435±0.0049	84	0.286
31	0.1371	58	0.2420	85	0.289
32	0.1395	59	0.2433	86	0.291
33	0.1440±0.0029	60	0.2442	87	0.293
34	0.1511	61	0.2452	88	0.296
35	0.1573	62	0.2459	89	0.298
36	0.1634	63	0.2485±0.0050	90	0.301
37	0.1682	64	0.2481	91	0.303
38	0.1732±0.0035	65	0.2485±0.0050	92	0.306
39	0.1791	66	0.2502	93	0.308
40	0.1838	67	0.2511	94	0.311
41	0.1886	68	0.2521	95	0.314
42	0.1930	69	0.2535	96	0.316±0.013[d]
43	0.1973	70	0.2550±0.0051		

[a] Value from proportional counter measurement (J. P. Renier, H. Genz, K. W. D. Ledingham and R. W. Fink, Phys. Rev. 166 [1968] 935.)

[b] From interpolation of Curve C, Fig. 16.

[c] Measured values from present work.

[d] Corrected for 122 keV gamma hidden beneath K'_{β_1}; see footnote p. 70.

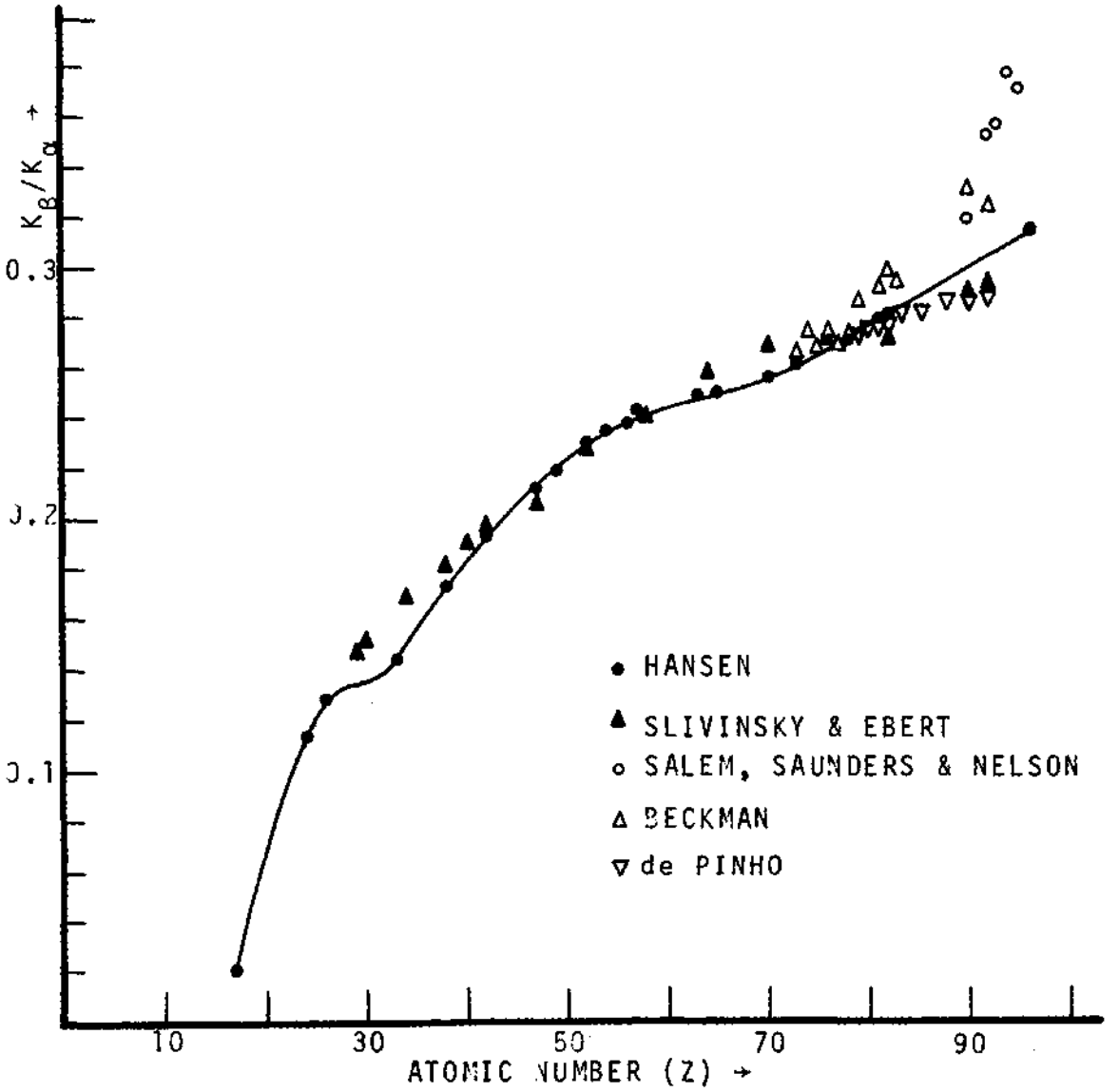

Fig. 15. Measured K_β/K_α Intensity Ratios Compared With Other Experimental Work. (Solid curve is drawn through present experimental values.)

Table 7. Intensity Ratios $K_{\alpha_2}/K_{\alpha_1}$, $K'_{\beta_1}/K_{\alpha_1}$ and $K'_{\beta_2}/K_{\alpha_1}$ Compared With Experiment and Theory

Z	Ratio	Present Work	Nelson, Salem[a] and Saunders	Theory[b]
81	$K_{\alpha_2}/K_{\alpha_1}$	0.580±0.030	0.592±0.006	0.593
	$K'_{\beta_1}/K_{\alpha_1}$	0.366±0.017	0.344±0.003	0.333
	$K'_{\beta_2}/K_{\alpha_1}$	0.101±0.005	0.102±0.005	0.095
82	$K_{\alpha_2}/K_{\alpha_1}$	0.588±0.030	0.595±0.006	0.596
	$K'_{\beta_1}/K_{\alpha_1}$	0.363±0.017	0.346±0.004	0.334
	$K'_{\beta_2}/K_{\alpha_1}$	0.103±0.005	0.103±0.005	0.097
96	$K_{\alpha_2}/K_{\alpha_1}$	0.626±0.006	0.638±0.006	0.640
	$K'_{\beta_1}/K_{\alpha_1}$	0.380±0.014[c]	0.370±0.004	0.357
	$K'_{\beta_2}/K_{\alpha_1}$	0.133±0.005	0.130±0.007	0.124

[a] From the review of Nelson, Salem and Saunders (to be published in Atomic Data). Errors estimated by same workers from scatter in experimental data.

[b] Relativistic Hartree-Fock-Slater (Refs. 2 and 3).

[c] Corrected for 122 keV gamma hidden beneath K'_{β_1}; see footnote p. 70.

the recent relativistic Hartree-Fock-Slater calculations of Scofield[2] and of Rosner and Bhalla[3] are presented for comparison.

Aside from the present work, the most complete study of the K_β/K_α ratios performed to date has been carried out by Slivinsky and Ebert[23] who measured twenty-two K_β/K_α ratios in the region of atomic number from 29 to 92. Rather good general agreement for the K_β/K_α ratio (<5%) is found between the Slivinsky and Ebert results and the present results from medium-low to high Z. At low Z, their values are some 7 percent higher than those measured in the present work. The primary K vacancies in the Slivinsky and Ebert work were produced by exciting pure metal and oxide samples mounted on thin Mylar placed at a 45° angle to a primary bremsstrahlung beam from a 150 kV x-ray machine. A highly collimated (0.15 cm-diameter pinhole) Ge(Li) spectrometer with a resolution of 650 eV FWHM was placed at a 90° angle to the bremsstrahlung beam and 25 cm from the fluorescer. Air attenuation was corrected for when the data were analysed. The low energy efficiency of the detector was measured using an x-ray machine and a variety of fluorescer foils. Absolute intensities of the x-ray lines were measured using a thin NaI(Tl) monitor. The major uncertainty in the work of Slivinsky and Ebert was associated with unfolding the K_α and K_β peaks. They

estimate this source of error to be approximately 5 percent. In the present work the low Z points were measured with a Si(Li) detector with a resolution of 260 eV at 6.4 keV, thus spectrum stripping, even at Z = 24 ($E_{K_\beta} - E_{K_\alpha}$ = 0.6 keV) presented no undue difficulties.

Six isolated measurements of K_β/K_α have been made by Mistry and Quarles[107] who produced K vacancies by ionization with electrons obtained from a 150 keV linear accelerator. The x rays were analysed with a 5 mm-thick Ge(Li) detector (450 eV FWHM at 6.4 keV). The major source of error in this experiment was associated with the subtraction of the continuum from beneath the x-ray peaks. The continuum in this experiment was large owing to the large production of bremsstrahlung by the electron beam. The measured values of the K_β/K_α intensity ratio are in reasonable agreement with the present work in all cases except Z = 66 where the value found in the present work is 6 percent lower than that found by Mistry and Quarles.

de Pinho[108] and Salem, Saunders and Nelson[109] have reported high Z K_β/K_α ratios. The dePinho results are in good general agreement, although slightly lower than the present work; whereas the Salem, Saunders and Nelson values are significantly higher than those measured in the present work. de Pinho created K vacancies by external conversion of the 662 keV photons from Cs^{137} decay (Ba^{137m});

radioactive sources were also used for a few cases; observation of the K x rays was with a Ge(Li) detector. Salem, Saunders and Nelson created K vacancies using gamma rays from a 500-curie Ta^{182} source and observed the K x rays with a Ge(Li) detector. The results of these two studies are also included in Fig. 15.

5.1.2. Comparison of the Measured Relative K X-ray Intensities With Theory

The K_β/K_α intensity ratios measured in the present work are compared in Fig. 16 with relativistic calculations by Babushkin[29]. The three theoretical curves correspond to unscreened (Curve A), empirically screened (Curve B) and Burns' Screened hydrogenic calculations (Curve D). Curves A and B are seen to be only poor approximations to the experimental findings, with the empirically screened hydrogenic calculation obviously overestimating the effective nuclear charge, i.e. the empirical screening constants for the M and higher shells are too small. The third curve (Curve D) is in reasonable agreement with the experimental results. The screening constants in this case have been derived by Burns[59] from a comparison of wave functions of the screened hydrogenic type with Hartree-Fock wave functions.

In Fig. 17, an additional comparison of the calculated values of K_β/K_α of Babushkin, using the Burns'

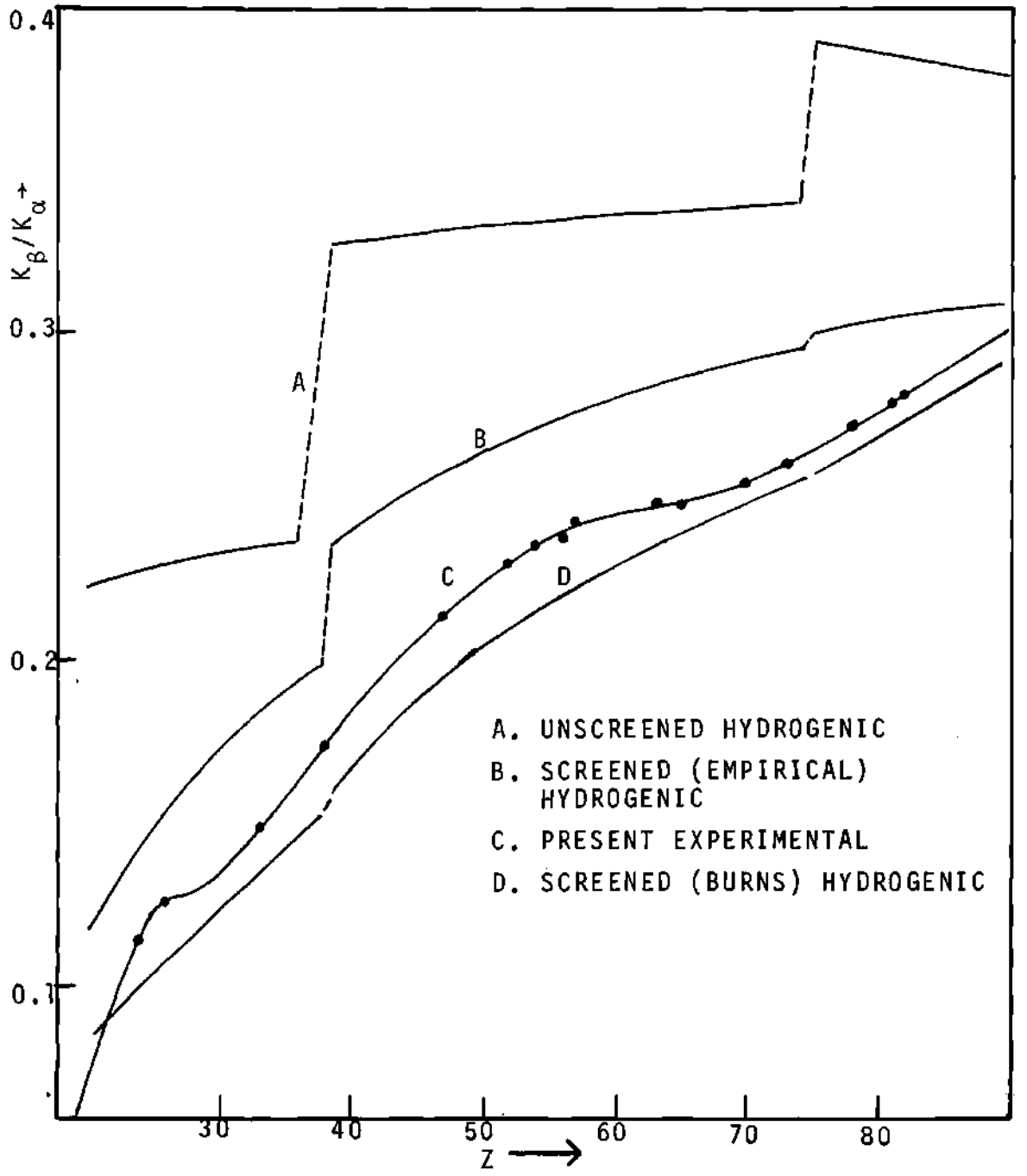

Fig. 16. Present K_β/K_α Results Compared With The Theoretical Work Of Babushkin. (See Sec. 5.1.2 for a discussion of this figure.)

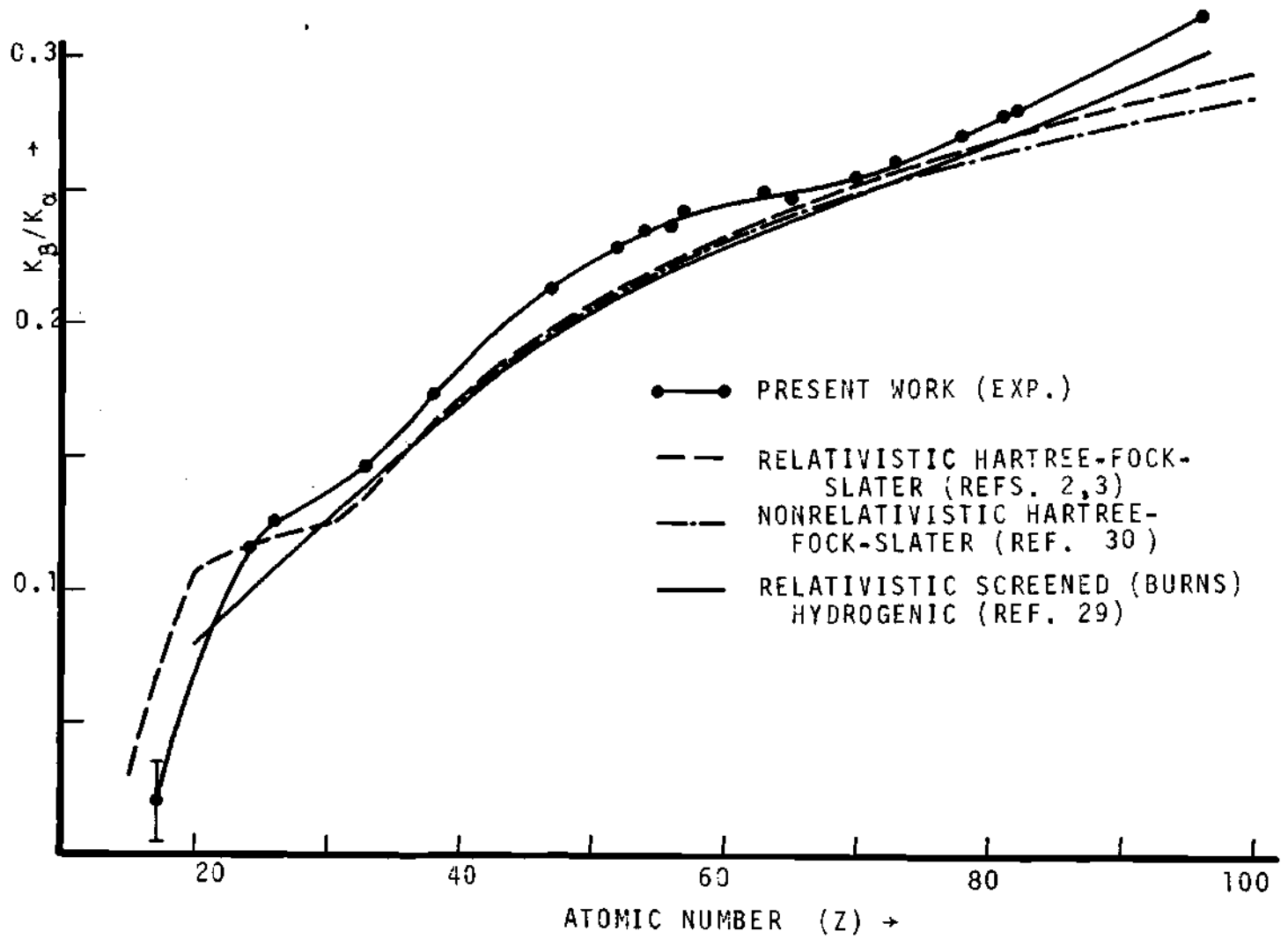

Fig. 17. Comparison of Theoretical Predictions in Best Agreement With Experimental Findings

screening recipe is made with the recent relativistic calculations by Scofield[2] and by Rosner and Bhalla[3], employing the Relativistic Hartree-Fock-Slater (RHFS) model; Manson and Kennedy[30] have calculated the K_β/K_α ratios using the nonrelativistic Hartree-Fock-Slater (HFS) model and the results are included in Fig. 17. The present experimental findings are included as an aid in depicting the overall agreement of experimental work with the most recent theoretical calculations.

A smooth curve was joined between the atomic numbers $Z = 31$ and $Z = 40$ and between $Z = 49$ and $Z = 75$ for Curve A in Fig. 16. In the work by Babushkin[29], the effects of the 4p and 5p shells are not included until $Z = 40$ and 75, respectively. The 4p and 5p shells begin to fill at $Z = 31$ and 49, respectively, thus explaining the major discontinuities in Curves A and B at $Z = 40$ and 75, seen in Fig. 16.

The RHFS calculations by Scofield and by Rosner and Bhalla predict identical K_β/K_α ratios provided one compensates for the contribution of the 5p electrons which were neglected in the Rosner and Bhalla calculation. Using the results of Scofield, the present author applied this correction, the magnitude of which is 4.4% of K_β at $Z = 92$, 2.3% at $Z = 56$ and zero for $Z \leq 48$.

It is interesting to note the remarkable agreement

between the theoretical calculations over almost the entire range in Z, particularly when one considers the basically different theoretical approaches involved in the various calculations. Relativistic effects upon the K_β/K_α transition rates are seen to be only moderately important, even at high Z. A comparison of the absolute transition probability of the 2p-1s transition, which is particularly sensitive to relativistic effects, shows that the nonrelativistic value is only 10 percent higher than the relativistic value, even at Z = 100. In addition, the contribution of higher multipole radiations (M_1, E_2 . . .) has been shown by Scofield to be only of the order of 1 percent at Z = 92; thus, the electric dipole approximation certainly seems justified in the work of Babushkin[29] and of Manson and Kennedy[30].

The fact that the Babushkin calculations (solid curve, Fig. 17) implicitly involve a rigorous exchange correction, i.e. the screening constants are derived from Hartree-Fock wave functions (whereas the HFS calculations employ the Slater approximation for the exchange effect) may attest to the fact that the Slater exchange approximation does not introduce undue error in the calculated relative K x-ray transition probabilities, at least in the region of Z where agreement is good. On the other hand, the divergence of the two methods of theoretical calculation at high Z

may also imply a worsening of the exchange approximation in the HFS calculations. As pointed out by Slater[110],

> . . . for very small and very large values of r, the approximation (Slater) behaves rather badly and thus inteferes rather seriously with the eigenvalues of the K electrons on one hand, the outer most ones on the other hand.

In the low Z region, certain dissimilarities in the two above-mentioned calculations appear. The HFS calculations predict a plateau in the K_β/K_α ratio between $Z = 21$ and $Z = 30$, corresponding to the filling of the 3d shell, whereas the Babushkin calculation predicts a continuous decrease in the K_β/K_α ratio with decreasing Z in this region. The experimental results on the other hand tend to indicate a plateau shifted somewhat to higher Z and terminating at approximately $Z = 30$.

All of the above-mentioned theoretical calculations treat only free atoms, whereas the measured results were made in solids, which suggests that agreement at low Z should not necessarily be expected. The experimental results actually lie lower than the theoretically predicted results below $Z = 24$, possibly due to the nonparticipation of one or several 3p electrons which may be totally ionized in the solid or involved in chemical bonding.

The extrapolation of such ideas, i.e. chemical effects, to higher Z in order to account for discrepancies between experiment and theory is hardly justified,

considering on the one hand the probably small influence[59] of the outer shell electrons upon the 3p and 4p electrons from which the major contributions of K_β arise, and on the other hand the magnitude of the discrepancies (3 to 8 percent).

5.2. K-fluorescence Yield Measurements at Z = 78 and 82

5.2.1. Comparison With Other Experimental Work

A comparison of the present measured values of ω_K with previous experimental work is made in Table 8. The present values are in disagreement with the measurements by Broyles, Thomas and Haynes (BTH)[111] and Nall, Baird and Haynes (NBH)[103] but agree within the estimated error limits with Park and Christmas[112] at Z = 80. Aside from these few values in the Z range, $78 \leq Z \leq 82$, a few precision values in the medium-high Z region indicate that the fluorescence yield may be somewhat higher than found by NBH and BTH, notably[113] $\omega_K(Z = 66) = 0.943 \pm 0.007$ and $\omega_K(Z = 55) = 0.898 \pm 0.005$.

The β-spectrometer measurements by BTH and by NBH involved a comparison of the K-Auger electron intensity to the intensity of K-conversion electrons associated with the primary K-vacancy production. The precision of the former measurement (BTH) is lower than the latter measurement due primarily to poorer resolution and also to the presence of radioactive contaminants in the Au^{198} source used in the

Table 8. Present ω_K Results Compared with Experiment and Theory

Z	ω_K					
	Present	NBH[103]	TBH[111]	Park & Christmas[112]	Semi-empirical[93]	Theory[5]
78	0.967±0.008					
80	0.969(5)±0.008[(a)]	0.952±0.003	0.946±0.008	0.97±0.01(7)	0.964(7)±0.004	0.966[(b)]
82	0.972±0.008					

[(a)] Average of present measured values of ω_K at Z = 78 and Z = 82.

[(b)] A correction is made to this value in Sec. 5.2.2 in order to account for K-Auger electron transitions not included in the calculation.

measurements. The present method of determination basically differs from these measurements in that it does not require knowledge of the means of vacancy creation. In addition, in the present method, since the Auger electron and x-ray data are collected simultaneously, the present measurements are not subject to error in time normalization. On the other hand, both methods may be subject to error due to electron loss in source or window or in corrections for K-Auger electron components not measured. The evaluation of the magnitude of electron loss in source and window has been given in Sec. 4.3.5 and an estimation of the K-XY group intensity not measured in the present work given in Sec. 4.3.6.1.

The measurements by Park[112] of the K-fluorescence yield at $Z = 80$ involved the determination of the intensity ratio $R_{A\beta}$ of the K-Auger electrons to the beta particles as measured by a high-resolution magnetic spectrometer, and the intensity ratio $R_{X\beta}$ of the K x rays to the beta particles as measured by NaI(Tl) detectors and the $4\pi\beta$-γ coincidence method. The fluorescence yield is then determined from

$$\omega_K = \frac{R_{X\beta}}{R_{X\beta} + R_{X\gamma}} \qquad (5\text{-}1)$$

The precision of this value of ω_K was limited by an

abnormally large amount of tailing in the electron spectrum, prohibiting an accurate determination of the K-Auger electron intensity.

The present values are also compared in Table 6 with values calculated from the semi-empirical formula given in Eqn. 2-15. A thorough study of all of the reported values of ω_K was made by Bambynek[93] and the most reliable values used to calculate the fluorescence yield with Eqn. 2-15. The present measured values of ω_K are in good agreement with these semi-empirically determined values.

5.2.2. Comparison of the K-fluorescence Yield Measurements With Theory

An accurate theoretical calculation of the K-fluorescence yield at high Z is particularly difficult because of two requirements: (1) the Auger transition probability must be calculated relativistically as the magnitude of the relativistic effects upon all the absolute K-Auger electron intensities is large and (2) all of the K-Auger electron and K x-ray transitions must be accounted for explicitly or else corrections must be applied for contributions from transitions not calculated.

Recently, a very extensive relativistic calculation of the K-Auger electron intensities has been carried out and K-fluorescence yields at high Z calculated[5]. In this work, only the K-LL and K-LM Auger groups were

accounted for, thus the calculated values of ω_K should be systematically low.

Bhalla[114] has estimated that the effect on ω_K of including only the K-LL and K-LM Auger transitions is approximately 0.3% at $Z = 80$, i.e. the calculated values are 0.3% too high. The present author, using the experimental results of Toburen, Nakai and Langley for the relative K-Auger electron intensities at $Z = 78$, also found the effect to be small (0.3% ± 0.2%). The corrected theoretical value[5] for $\omega_K(Z = 80) = 0.963$ is to be compared to the computed value measured in the present experimental work of $\omega_K(Z = 80) = 0.969(5) \pm 0.008$ which represents an average of those values measured at $Z = 78$ and $Z = 82$.

An estimate of the nonradiative width at $Z = 80$ may be made from the average of the results for ω_K at $Z = 78$ and $Z = 82$ provided one knows the total width defined by Eqn. 2-4.

$$\Gamma_K = \Gamma_{KR} + \Gamma_{KN} \qquad (2\text{-}4)$$

The measurement of the natural line width of K_{α_2} and K_{α_1} by Nelson, John and Saunders[31] are in good agreement with the theoretical predictions of Scofield[2] for the radiative width Γ_{KR}, thus using Scofield's value for $\Gamma_{KR} = 51.7$ eV at $Z = 80$ and Eqn. 2-5:

$$\Gamma_K = \frac{\Gamma_{KR}}{\Gamma_{KN} + \Gamma_{KR}} \qquad (2\text{-}5)$$

the measured nonradiative width at $Z = 80$ is found to be $\Gamma_{KN} = 1.63$ eV $\pm$ 0.41 eV (2σ) for $Z = 80$.

In summary, the present measured results at $Z = 78$ and $Z = 82$ agree within the experimental error found by Bhalla, Ramsdale and Rosner[5]. In addition, the present experimental results are also in agreement with the semi-empirical findings of Bambynek[33] but are not in agreement with the lower values of ω_K found by Broyles, Thomas and Haynes[111] and Nall, Baird and Haynes[102].

CHAPTER VI

CONCLUSIONS AND RECOMMENDATIONS

In the present investigation of the inner shell atomic transition probabilities, the K x-ray intensity ratios and high Z fluorescence yields have been measured in order to provide a rigorous test for recent theoretical predictions. The accuracy of the most sophisticated predictions has been sufficiently high to place very strict requirements upon the experimental measurements, with regard to the uncertainties which could be tolerated. This, on the one hand, led to the detailed study of the detection efficiencies of semiconductor detectors (Sec. 3.3) and, on the other hand, required the development of new methods for measuring the K-fluorescence yields (Sec. 4.1).

6.1. Conclusions

As the result of the current investigation of the K x-ray intensity ratios and K-fluorescence yields at high Z, the following conclusions can be drawn:

(1) The experimental measurements of the relative K x-ray intensities indicate that most refined present-day theoretical predictions [2,3,29,30], although in good agreement with each other, exhibit systematic discrepancies

with experimentally measured K_β/K_α intensity ratios. The magnitude of these discrepancies is smallest in the regions following the closing of the 3d shell and the closing of the 4f shell. The largest discrepancies exist at $Z < 24$, at the beginning of the rare-earth series, and at high Z. (Sec. 5.1.2)

(2) The general discrepancy of 3 - 12 percent from medium Z to high Z suggests, in a general sense, that the theoretical screening of M and higher shells is overestimated. This cannot be accounted for in terms of chemical effects of outer shell electrons, considering the negligible effects[59] of these electrons upon the deep-lying p levels (i.e. 3p, 4p) which account for major contributions to K_β. (Sec. 5.1)

(3) The discrepancies in the K_β/K_α ratio at low Z are probably related to chemical bonding effects and to ionization of the 3p electrons. (Sec. 5.1)

(4) The general agreement between the theoretical predictions in the medium-low to medium-high Z region may imply that the Slater exchange approximation introduces very little error into the Hartree-Fock-Slater calculations, at least throughout this region of Z. (Sec. 5.1)

(5) The divergence of the RHFS predictions and the predictions using relativistic Burns' Screened hydrogenic wave functions may imply a worsening of the Slater exchange

approximation. (Sec. 5.1)

(6) The measured[31] natural line widths of K_{α_2} and K_{α_1} at high Z appear to be in excellent agreement with the RHFS predictions. Within the experimental uncertainties of that experiment and the present study of the K_β/K_α ratios, this agreement indicates that the absolute K_β transition probabilities are theoretically underestimated.

(7) Relativistic effects upon the K_β/K_α ratios are small, even at high Z, as are the contributions other than electric dipole radiation; thus additional theoretical investigations of these relative transition probabilities may be carried out in the electric dipole approximation, using the more manageable nonrelativistic wave functions. (Fig. 17)

(8) Recent theoretical predictions of the K-fluorescence yields are found to agree with the present experimental results at $Z = 78$ and $Z = 82$. The measured values of ω_K constitute a test for the total nonradiative transition probability, assuming the experimental findings for the natural line widths of K_{α_2} and K_{α_1} substantiate the fact that the total radiative transition probability at high Z is as given by the RHFS calculations. Therefore, within the limits of experimental error ($\simeq$20%) the calculated nonradiative transition probabilities are in agreement with experimental findings at $Z = 78$ and

Z = 82. (Sec. 5.2)

(9) The present measured values of ω_K are in good agreement with the semi-empirical formula, Eqn. 2-14, in contrast with previous precision measurements of ω_K at Z = 78 and Z = 82. (Table 8)

(10) Because of the many factors affecting the efficiency of semiconductor detectors below 100 keV, no two detectors will ordinarily have identical efficiency curves, even if their nominal dimensions are the same. (Fig. 3)

(11) In the region of the germanium K binding energy (11.1 keV), where sharp discontinuities occur in the efficiency of Ge(Li) detectors, Si(Li) detectors are more suited to accurate efficiency calibration than are Ge(Li) detectors. (Sec. 3.3.3)

(12) For energies between approximately 3 and 100 keV, and as qualified by the previous conclusion (11), certain guidelines may be established for the accuracy to which both Ge(Li) and Si(Li) detectors may be efficiency-calibrated:

(a) Accuracies in the relative efficiencies of 1 percent per 10 keV are attainable for narrow energy regions.

(b) The overall error in the relative efficiency can be kept as small as 2% to 5% by

careful experimental efficiency calibration

(c) Accuracies in the absolute efficiency of approximately 1 percent plus the uncertainty in the relative efficiency can be attained but only by use of accurate standardization sources.

6.2. Recommendations for Further Work

(1) A systematic experimental study of the K-fluorescence yield should be made at high Z using thin sources and the semiconductor detector technique employed in the present work. This would provide an excellent test of the total nonradiative transition probability in a region of Z where the Auger transition rates are so strongly influenced by relativistic effects.

(2) An experimental investigation of the chemical effects at low Z upon the relative intensity ratios, using very high-resolution, semiconductor detectors should be made. This would establish limitations of the free atom approximation for inner-shell transition rates.

(3) Theoretical estimates of the magnitude of relativistic effects on the K-LN and higher Auger electron transitions would be valuable. This would be particularly useful for deciding the suitability at very high Z of extensive nonrelativistic calculations of these higher transitions.

(4) Measurement of the relative intensity of the weak line K_{α_3} (1s-2s) should be possible with high resolution, curved crystal spectrometers or suitable coincidence techniques. As pointed out by Scofield[2], the existence of this transition is due to retardation and relativistic effects, and the intensity is sensitive to mixtures of other angular momentum states.

(5) An investigation of the relative L x-ray transition probabilities with high-resolution, curved-crystal spectrometers should provide additional tests for the theoretical predictions.

APPENDICES

APPENDIX A

CALCULATION OF THE K X-RAY ESCAPE PROBABILITY

The formula given by Eqn. 3-10 and graphically displayed in Fig. 8 was derived under the assumption that incident radiation is normal to the front surface of a cylindrical germanium detector (Fig. 18).

The fraction of incident gammas producing K vacancies between x and x + dx is given by:

$$\frac{dI_\gamma}{I_\gamma} = e^{-\mu_\gamma x}\mu(K)\,dx \qquad (1)$$

where I_γ is the incident intensity of the gamma; μ_γ is the total attenuation coefficient of the gamma ray in germanium; $\mu(K)$ is the K-shell photoelectric attenuation coefficient of the gamma ray in germanium, found by subtraction of the L and higher shell contributions to the total photoelectric attenuation coefficient.

Assuming a K vacancy at position X (Fig. 18), the probability of K x-ray escape from the <u>front</u> surface of the detector is given by:

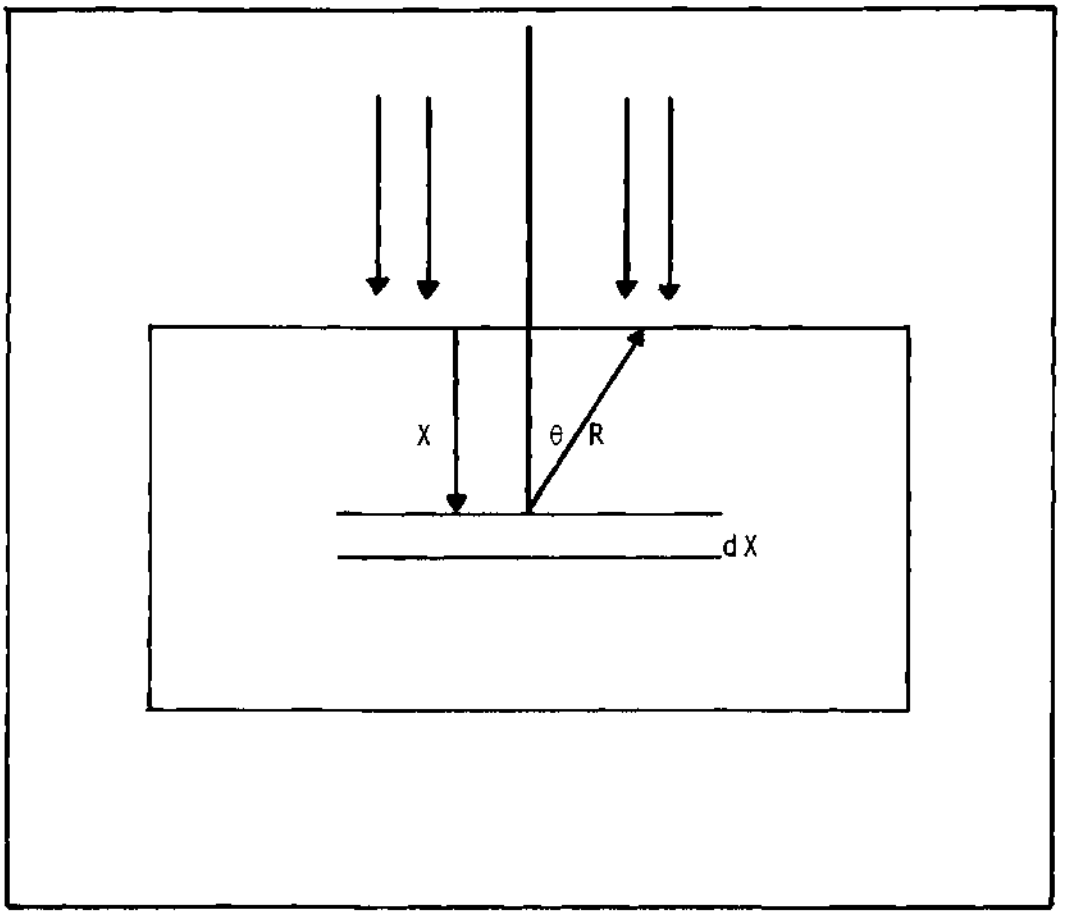

Fig. 18. Assumed Geometry For Escaping K X Rays

$$\frac{\omega_K}{2} e^{-\mu_K R} \tag{2}$$

where ω_K is the K-fluorescence yield of Ge, $\omega_K(Ge) = 0.57 \pm 0.003$ [87], μ_K is the total attenuation coefficient of the escaping K x rays in germanium and $R = x \sec\theta$ (Fig. 18). The differential solid angle into which the fluorescent K x ray is emitted is given by:

$$d\Omega/4\pi = \frac{\sin\theta d\theta d\phi}{4\pi} \tag{3}$$

Therefore, the fraction of K x rays escaping in the solid angle $d\Omega$ is determined by:

$$\frac{dI_e}{I_\gamma} = \frac{e^{-\mu_\gamma x} \mu(K) dx \quad \omega_K \; e^{-\mu_K x \sec\theta} \sin\theta d\theta}{2} \tag{4}$$

where the integration over ϕ has been carried out.

Substituting $Z = \sec\theta$

$$dZ = \frac{-1}{\cos^2\theta}(-\sin\theta)d\theta \tag{5}$$

and $dZ/Z^2 = \sin\theta d\theta$ into the above integrand where

$$\int_0^{\pi/2} d\theta = \int_1^{\infty} dZ \qquad (6)$$

Then the fraction of K x rays escaping per incident gamma into the solid angle defined by R and ϕ is given by:

$$dI_e/I_\gamma = \frac{e^{-\mu_\gamma x} \mu(K)\, dx\; e^{-\mu_K xZ}\; dZ}{2Z} \qquad (7)$$

Thus the probability of K x-ray escape is given by:

$$dI_e/I = \int_0^{\infty} e^{-\mu_\gamma x} \mu(K)\; dx \int_1^{\infty} \frac{\omega_K}{2Z^2} e^{-\mu_K xZ}\; dZ \qquad (8)$$

which is found to be equal to

$$\frac{\mu(K)\,\omega_K}{2\mu_\gamma} \left[1 + \frac{\mu_K}{\mu_\gamma} \ln \left(\frac{\mu_K}{\mu_K + \mu_\gamma} \right) \right] \qquad (9)$$

Setting $K_\alpha = \frac{K_\alpha}{K_\beta + K_\alpha} = \frac{1}{1 + K_\beta/K_\alpha}$ and $K_\beta = \frac{K_\beta/K_\alpha}{1 + K_\beta/K_\alpha}$; the ratio of the escape peak to the incident γ intensity is:

$$\frac{I_e}{I_\gamma} = \frac{\mu(K)\,\omega_K}{2\mu_\gamma} K_\alpha \left[1 + \frac{\mu_{K_\alpha}}{\mu_\gamma} \ell n \left(\frac{\mu_{K_\alpha}}{\mu_{K_\alpha} + \mu_\gamma} \right) \right] \qquad (10)$$

$$+ \frac{\mu(K)\,\omega_K}{2\mu_\gamma} K_\beta \left[1 + \frac{\mu_{K_\beta}}{\mu_\gamma} \ell n \left(\frac{\mu_{K_\beta}}{\mu_{K_\beta} + \mu_\gamma} \right) \right]$$

where μ_{K_α} and μ_{K_β} are the total attenuation coefficients in germanium for the germanium K_α and K_β x rays with μ_{K_α} = 32.4 cm^2/gm; μ_{K_β} = 26.6 cm^2/gm; and K_α = 0.878 and K_β = 0.122 (Chapter V).

$$\frac{I_e}{I_\gamma} = 0.2503 \frac{\mu(K)}{\mu_\gamma} \left[1 + \frac{34.2}{\mu_\gamma} \ell n \left(\frac{34.2}{34.2 + \mu_\gamma} \right) \right] \qquad (11)$$

$$+ 0.0348 \frac{\mu(K)}{\mu_\gamma} \left[1 + \frac{26.6}{\mu_\gamma} \ell n \left(\frac{26.6}{26.6 + \mu_\gamma} \right) \right]$$

which is the expression from which the theoretical values for Fig. 8 were calculated

The escape probability in silicon is found in an identical manner as described here but is less significant owing to the smaller value of the K-fluorescence yield.

APPENDIX B

EFFECT OF SHADOW COLLIMATION ON RELATIVE DETECTION EFFICIENCY

The inspection of Ge(Li)-II with a narrow, collimated beam (Sec. 3.2) revealed an arch-shaped p-i junction as depicted in Fig. 3. The effects of this type of collimation on the relative efficiency were unknown but the experimental efficiency values suggested that these effects might be large (Fig. 3).

The general behavior of the relative efficiency was studied after the following determination of the general equation for the relative efficiency for this type of geometry (Fig. 19).

The differential probability for a photon normal to the front surface of the detector to interact in a ring defined by y and $y + dy$ at a depth defined by x and dx is given by:

$$dP(y,x) = \frac{e^{-\mu x}\, \mu dx\, (2\pi y\, dy)}{\pi y_1^2} \qquad (1)$$

where μ is the linear attenuation coefficient (cm^{-1}) and y and x are described in Fig. 19.

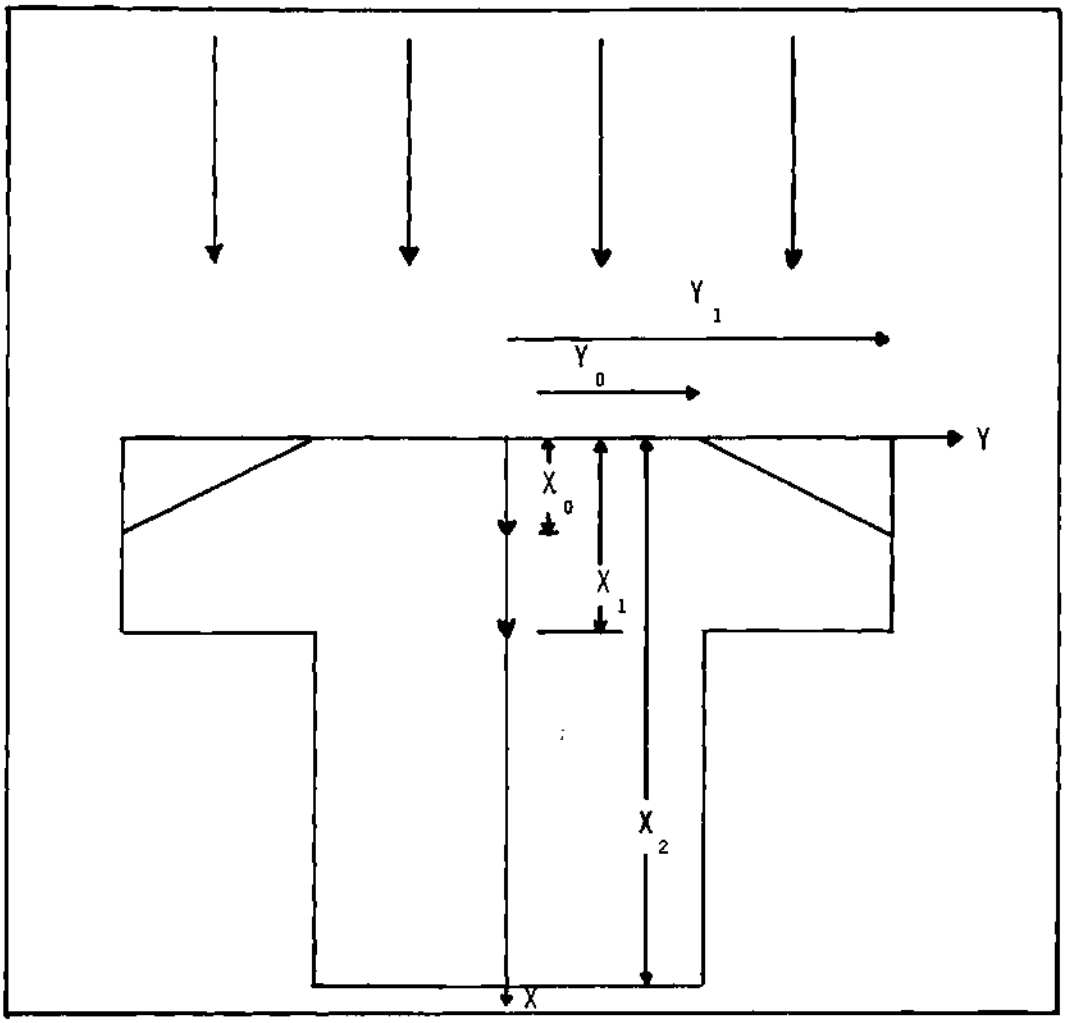

Fig. 19. Geometry Used In Calculating The Effects Of Shadow Collimation On The Relative Efficiency

The integral probability for a photon normal to the detector surface defined by y_1 to interact in the dead triangular ring defined by x_0, y_0 and y_1 is given by:

$$P = \frac{2\pi\mu \int_{y=y_0}^{y_1} \int_{x=0}^{Sx_0} e^{-\mu x}\, y\, dy\, dx}{\pi y_1^2} \qquad (2)$$

where S is defined as $\frac{y - y_0}{y_1 - y_0}$. On the other hand, the probability that a photon will interact in the ring defined by Y_0, y_1 and x_1 is given by:

$$\frac{\pi(y_1^2 - y_0^2)}{\pi y_1^2} (1 - e^{-\mu x_1}) \qquad (3)$$

Therefore the probability that a photon normal to the detector surface will interact in the sensitive region defined by y_0, y_1, x_0 and x_1 is found by subtracting Eqn. 2 from Eqn. 3.

$$\text{Setting } I = 2\pi\mu \int_{y_0}^{y_1} \int_{x=0}^{Sx_0} e^{-\mu x_0} y\, dy\, dx \qquad (4)$$

one finds that

$$\varepsilon_2 \equiv I = \frac{2}{a^2 y_1^2}\left[(ay_0 + 1) - e^{-a(y_1 - y_0)}(ay_1 + 1)\right] - \frac{(y_1^2 - y_0^2)e^{-\mu x}}{y_1^2} \tag{5}$$

where ε_2 is the detection probability for a photon normal to the detector defined by y_0 and y_1.

In order to study the effect of this expression on the total relative efficiency, ε_R, one must compare it to the efficiency of the right-circular cylinder defined by y_0 and x_2. The relative detection efficiency of this segment of the detector is given by:

$$\varepsilon_1 = \frac{\pi y_0^2}{\pi y_1^2}\varepsilon_R' \tag{6}$$

where ε_R' is the relative detection efficiency for photons normal upon the area defined by Y_0. Therefore, the total relative detection efficiency is given by adding expression (5) to expression (6), i.e., $\varepsilon_R = \varepsilon_1 + \varepsilon_2$.

Shadow collimation of this type for Ge(Li)-II gives rise to the large rise in efficiency at approximately 40 keV (see Fig. 9).

BIBLIOGRAPHY[†]

1. M. P. Auger, J. Phys. radium 6, 205 (1925).

2. J. H. Scofield, Phys. Rev. 179, 9 (1969).

3. H. R. Rosner and C. P. Bhalla, Z. Physik 231, 347 (1970).

4. D. J. Ramsdale, thesis, Kansas State University, 1969 (unpublished).

5. C. P. Bhalla, D. J. Ramsdale and H. R. Rosner, Phys. Lett. (Netherlands).

6. W. C. Röntgen, Sitz. ber. Wurzburg Phys. Med. Ges. (1895); Ann. Physik 64, 1 (1898); translation by A. Stanton in Science 3, 227 and 726 (1896).

7. H. Haga and C. H. Wind, Ann. chim. et phys. 68, 884 (1899).

8. C. G. Barkla, Proc. Roy. Soc. (London) A77, 247 (1906).

9. H. G. J. Moseley, Phil. Mag. 26, 1024 (1913).

10. N. Bohr, Phil. Mag. 26, 1024 (1913).

11. W. Heisenberg, Z. Physik 33, 879 (1925).

12. E. Schrödinger, Ann. Physik 79, 734 (1926).

13. P. A. M. Dirac, Proc. Roy. Soc. (London) A109, 642 (1925).

14. H. T. Meyer, Wiss. Veroffn. Siemens-Konzern 7, 108 (1929).

15. J. H. Williams, Phys. Rev. 44, 146 (1933).

16. O. Beckman, Arkiv Fysik 9, 495 (1955).

[†]Abbreviations used herein follow the form employed by the American Institute of Physics Style Manual, published by the Publication Board, 2nd edition, 1959.

BIBLIOGRAPHY (Continued)

17. D. Coster and R. Kronig, Physica 2, 13 (1935).

18. L. Pincherle, Nuevo Cimento 12, 18 (1935).

19. E. H. S. Burhop, Proc. Roy. Soc. (London) A148, 272 (1935).

20. E. H. S. Burhop, The Auger Effect and Other Radiationless Transitions (Cambridge Univ. Press, New York, 1952).

21. J. S. Hansen, H. U. Freund and R. W. Fink, Proc. Int. Conf. in Radioactivity in Nuclear Spectroscopy, Nashville, Tenn. (Gordon and Breach Publ., New York, 1969).

22. G. C. Nelson and B. G. Saunders, Phys. Rev. 188, 108 (1969).

23. V. W. Slivinsky and P. J. Ebert, Phys. Lett. 29A, 463 (1969).

24. P. J. Ebert and V. W. Slivinsky, Phys. Rev. 188, 1 (1969).

25. S. I. Salem and J. P. Johnson, Phys. Lett. 30A, 163 (1969).

26. J. S. Hansen, H. U. Freund and R. W. Fink, Nucl. Phys. A142, 343 (1970).

27. P. Richard, Y. I. Bonner, T. Furata and I. L. Morgan, Phys. Rev. A1, 1044 (1970).

28. J. S. Hansen, H. U. Freund and R. W. Fink, Nucl. Phys A 153, 465 (1971).

29. F. A. Babushkin, Acta Phys. Polon. 25, 749 (1964).

30. S. T. Manson and D. J. Kennedy, private communication, (1971).

31. G. C. Nelson, W. John and B. G. Saunders, Phys. Rev. 187 (1969); Addendum to be published in Phys. Rev. (Preprint No. UCRL-71856 Add. 1).

32. R. W. Fink, R. C. Jopson, Hans Mark and C. D. Swift, Rev. Mod. Phys. 38, 513 (1966).

BIBLIOGRAPHY (Continued)

33. W. Bambynek, B. Crasemann, R. W. Fink, H. U. Freund, Hans Mark, R. E. Price, P. V. Rao and C. D. Swift, (to be published in Rev. Mod. Phys.)

34. M. A. Blohkin, The Physics of X-rays (Publishing House of Technical-Theoretical Literature, Moscow, 1957) 44.

35. R. L. Graham, I. Bergström and F. Brown, Nucl. Phys. 39, 107 (1962).

36. O. Hornfeldt, A. Fahlman and C. Nordling, Arkiv Fysik 23, 155 (1962).

37. E. Karttunen, thesis, Georgia Institute of Technology, Atlanta, Georgia (1971) (unpublished).

38. K. A. Richardson, D. S. McKay, W. R. Greenwood and T. H. Foss, Science 167, 516 (1970).

39. J. L. Eisberg, Fundamentals of Modern Physics (John Wiley and Sons, Inc. New York, 1961) 291.

40. A. S. Davydov, Quantum Mechanics (Addison-Wesley Publ. Co. Inc., Reading, Mass., 1968) 309 ff.

41. B. B. Kinsey, Can. J. Res. A26, 404 (1948).

42. W. Heitler, The Quantum Theory of Radiation (Oxford Univ. Press, Oxford, 1954) Chap. 6.

43. S.A. Moszkowski, "Theory of Multipole Radiation", in Alpha, Beta, Gamma-Ray Spectroscopy, edited by K. Siegbahn (North Holland Pub. Co., Amsterdam, 1965) Ch. XV.

44. E. Fermi, Rev. Mod. Phys. 4, 87 (1932).

45. M. E. Rose, Relativistic Electron Theory (John Wiley and Sons, Inc., New York, 1961).

46. H. A. Bethe and E. E. Salpeter, Quantum Mechanics of One and Two Electron Atoms (Springer - Verlag, Berlin, 1957).

47. W. S. C. Chang, Principles of Quantum Electronics (Addison-Wesley Pub. Co., Reading, Mass., 1969) 179.

BIBLIOGRAPHY (Continued)

48. H. Eyring, J. Walter and G. F. Kimball, Quantum Chemistry (John Wiley and Sons, Inc., New York, 1944) 115.

49. A. Messiah, Quantum Mechanics Volume II (North Holland Pub. Co., Amsterdam, 1965) 1043.

50. R. D. Evans, The Atomic Nucleus (McGraw-Hill Book Co., New York, 1955) 213.

51. F. A. Babushkin, Opt. i Spektroskopiya 19, 3 (1965), [(Engl. trans. Opt. Spectry. [USSR] 19, 1 (1965).]

52. E.J.Callan, Bull. Am. Phys. Soc. 7, N. 416 (1962).

53. V. O. Kostroun, M. H. Chen and B. Crasemann, (in press).

54. H. S. W. Massey and E. H. S. Burhop, Proc. Cambr. Phil. Soc. 32 461 (1936).

55. W. Laskar, J. Phys. radium 16 644 (1955).

56. W. Laskar, Ann. Phys. (Paris) 13, 258 (1958).

57. W. B. Payne and J. S. Levinger, Phys. Rev. 101 1020 (1956).

58. G. R. Taylor and W. B. Payne, Phys. Rev. 118 1549 (1960).

59. G. Burns, J. Chem. Phys. 41 1521 (1964).

60. F. Herman and S. Skillman, Atomic Structure Calculations (Prentiss-Hall, Inc., Englewood Cliffs, N. J., 1963).

61. D. Liebermann, J. T. Waber and D. T. Cromer, Phys. Rev. 137A, 27 (1965).

62. F. A. Babushkin, Zh. Eksp. Teor. Fiz. 48, 5611(1965) [Sov. Phys. JETP 21, 372(1965)]

63. G. Wentzel, Z. Physik 43, 524 (1927).

64. W. Gordon, Z. Phys. 48 180 (1928); see also C. P. Bhalla, Phys. Rev. 157, 1136 (1967).

BIBLIOGRAPHY (Continues)

65. W. Melhorn, The Auger Effect, (Univ. of Neb. Press, Lincoln, Neb., 1969).

66. H. S. W. Massey and E. H. S. Burhop, Proc. Roy. Soc. (london) A153, 661 (1936).

67. J. C. Slater, Phys. Rev. 36, 57 (1930).

68. H. N. Russell and F. A. Saunders, Astrophys. J. 61, 38 (1925).

69. W. N. Asaad, Proc. Roy. Soc. (London) A249, 555 (1959).

70. D. R. Hartree, Phys. Rev. 109, 840 (1958).

71. W. N. Asaad, Nucl. Phys. 44, 399 (1963); Nucl. Phys. 66, 494 (1965).

72. W. Melhorn and W. N. Asaad, Z. Physik 191, 231 (1966).

73. C. P. Bhalla, Phys. Rev. A2, 722 (1970).

74. C. P. Bhalla, J. Phys. B.: Atom. Molec. Phys. 3, L29 (1970).

75. C. P. Bhalla, H. R. Rosner and D. J. Ramsdale, J. Phys. B: Atom. Molec. Phys. 3, 1232 (1970).

76. C. P. Bhalla and D. J. Ramsdale, Z. Physik 239, 95 (1970).

77. E. H. S. Burhop, J. Phys. radium 16, 625 (1955); also J. Laberrigue and P. Radvany, J. Phys. radium 17, 944 (1956); Compte. Rend. 242, 901 (1956); and M. A. Listengarten, Izv. Akad. Nauk. USSR, Ser. Fiz. 24, 1041 (1960) [Bull. Acad. Sci. USSR, Phys. 24 1050, 1960)].

78. C. Geffrion and G. Nadeau, Air Force Off. of Sci. Res. Rept. TR-59-145 (1959) (unpublished).

79. E. J. Callan, Aer. Res. Lab., Wright Patterson AFB, Ohio, (unpublished) Prelim. rept. given in Ref. 52.

BIBLIOGRAPHY (Continued)

80. M. A. Listengarten, Izv. Acad. Nauk. SSSR, Fiz. 26, 182 (1962) [Bull. Acad. Sci. USSR, Phys. Colombia Tech. Transl. 26, 1-2 (1962)]; Izv. Akad. Nauk SSSR, Colombia Tech. Transl. 25, 803 (1961).

81. W. N. Asaad, Proc. Roy. Soc. (London) A249, 555 (1959).

82. A. H. Wapstra, G. J. Nijgh and R. van Lieshout, Nucl. Spectroscopy Tables, (North Holland Pub. Co., Amsterdam, 1959).

83. E. J. McGuire, U.S.A.E.C. Report, Sandia Lab., Albuquerque, N. Mex. (unpiblished).

84. H. U. Freund, J. S. Hansen, E. Karttunen and R. W. Fink, Proc. Int. Conf. of Radioactivity in Nuclear Spectroscopy, Nashville, Tenn. (Gordon and Breach Publ., New York, 1969).

85. R. E. Wood, J. M. Palms and P. V. Rao, Phys. Rev. 187, 1497 (1969).

86. W. J. Veigle, E. Briggs, B. Bracewell, M. Donaldson, X-ray Cross Section Compilation (Report No. KN-798-69-2 (R)m 1969), unpublished.)

87. J. Pahor, A. Kodrie, M. Hribar, A. Moljk, Z. Physik 221, 490 (1969).

88. W. J. Price, Nuclear Radiation Detection (McGraw-Hill Book Co., New York, 1964).

89. J. M. Freeman and J. G. Jenkin, Nucl. Instr. and Meth. 43, 269 (1966).

90. N. V. Castro de Faria and J. A. Lévesque, Nucl. Instr. and Meth. 46, 325 (1967).

91. J. H. Hubbell "Photon Cross Sections, Attenuation Coefficients and Energy Absorption Coefficients", Nat. Stand. Ref. Sec. Nat. Bur. Stand. (U.S.) 29, (1959).

92. D. M. Walker, thesis, Georgia Institute of Technology, Atlanta, Ga., (1969) (unpublished).

93. W. Bambynek, private communication to R. W. Fink (1970).

BIBLIOGRAPHY (Continued)

94. J. Kyles, J. C. McGeorge, F. Shaikh and J. Byrne, Nucl. Phys. A150, 143 (1970).

95. W. Bambynek, Z. Physik 206, 66 (1967).

96. E. Karttunen, Nucl. Phys. A131, 343 (1969).

97. R. E. Wood, P. Venugopala Rao, O. H. Puckett and J. M. Palms, to be published in Nucl. Instr. and Meth.

98. C. M. Lederer, J. M. Hollander and I. Perlman, Table of Isotopes, 6th ed. (John Wiley and Sons, Inc., New York, 1967).

99. K. Siegbahn, editor, Alpha, Beta and Gamma Spectroscopy, (North Holland Publ. Co., Amsterdam, 1964).

100. D. ter Haar, editor, Collected Papers of L. D. Landau, Sci. Publishers, New York, 1965); p. 417; L. Landau, J. Phys. USSR 8, 201 (1944).

101. R. O. Lane and D. J. Zaffarano, U.S.A.E.C. Rept. No. ISC-439 (1953)(unpublished).

102. L. H. Toburen, M. Y. Nakai and R. A. Langley, (Oak Ridge National Laboratory Rept. No. ORNL-TN-1988) (1967) (unpublished).

103. J. C. Nall, Q. L. Baird and S. K. Haynes, Phys. Rev. 118, 1278 (1960).

104. J. Byrne and N. Howarth, J. Phys. B: Atom. Molec. Phys., 3, (1970).

105. T. Fink and N. Benczer-Koller, Nucl. Phys. A138, 337 (1969).

106. R. S. Hager and E. C. Seltzer, International Conversion Tables, Part I: K, L, M Shell Conversion Coefficients, Calt-63-60, AEC Research and Development Report, Calif. Inst. of Tech., Pasadena, Calif., (1967).

107. V. D. Mistry and C. A. Quarles, Texas Christian Univ. preprint, Ft. Worth, Tex. (to be published in Nucl. Phys.)

BIBLIOGRAPHY (Concluded)

108. A.G. dePinho, Phys. Rev. Abstracts 2, N. 2, 2 (1971).

109. S. I. Salem, B. G. Saunders, G. C. Nelson, Bull. Am. Phys. Soc. 14, n. 12, 1180 (1969).

110. J. C. Slater, Quantum Theory of Atomic Structure, Vol. II (McGraw-Hill Book Co., Inc., New York, 1960) p. 15.

111. C. Broyles, D. Thomas and S. K. Haynes, Phys. Rev. 89, 715 (1953).

112. J. J. H. Park and P. Christmas, Can. J. Phys. 45, 2620 (1967).

113. R. L. Graham and J. S. Merritt, Can. J. Phys. 39, 1058 (1961); R. L. Graham, F. Brown, G. T. Ewan and J. Uhler, Can. J. Phys. 39, 1086 (1961).

114. C. P. Bhalla, private communication to R. W. Fink (1971).

VITA

John Steven Hansen was born December 29, 1940, in Louisville, Kentucky. Most of his youth was spent in Baton Rouge, Louisiana, where he graduated from Baton Rouge High School and from Louisiana State University (B. S., Physics, 1965). In 1966, Mr. Hansen entered Georgia Tech, School of Nuclear Engineering, and recieved his M.S. from that School in 1967.

Mr. Hansen worked as a health physicist for the Louisiana Board of Nuclear Energy in 1965 and 1966, just prior to entering graduate school. His program at Georgia Tech has been supported in part by U. S. Public Health Service funds, Georgia Tech Graduate Research funds and a U. S. Atomic Energy Commission Traineeship. His publications include:

J. S. Hansen, H. U. Freund and R. W. Fink, "Relative X-ray Intensities in the K Shell", Proc. Int. Conf. of Radioactivity in Nuclear Spectroscopy, Nashville, Tenn. (Gordon and Breach Publishers, New York) 1969.

J. S. Hansen, H. U. Freund and R. W. Fink, "Relative Transition Probabilities to the K Shell", Nucl. Phys. A142, No. 2 (1970).

J. S. Hansen, H. U. Freund and R. W. Fink, "Relative K X-ray Transition Probabilities at Z = 96 from Cf^{249} Decay", Nucl. Phys. A153, (1970)

J. S. Hansen, J. C. McGeorge, R. W. Fink (Ga. Tech) and P. V. Rao, R. W. Wood, J. M. Palms (Emory Univ.), "A New Method for Measuring High Z K-fluorescence Yields Using a Cooled Si(Li) Electron Detector", to be published in 1971.

Mr. Hansen is married to the former Cora Phillips of Mendenhall, Mississippi. He belongs to the American Physical Society and the Health Physics Society. After completing the requirements for his degree, he will remain temporarily with Georgia Tech in a postdoctoral capacity to develop research projects already in progress.